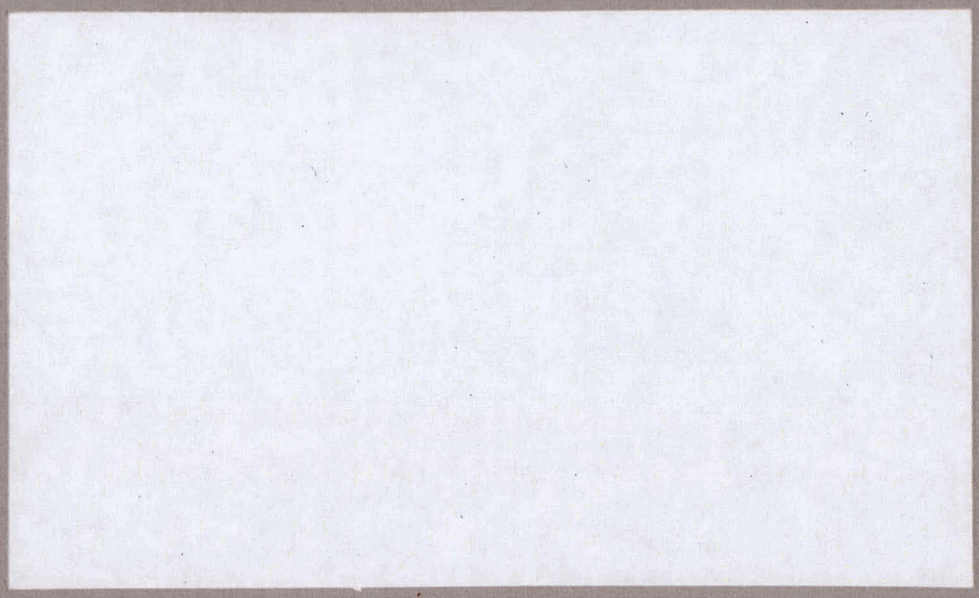

ALLIS-CHALMERS

ATOMIC ENERGY DIVISION

DISCLAIMER

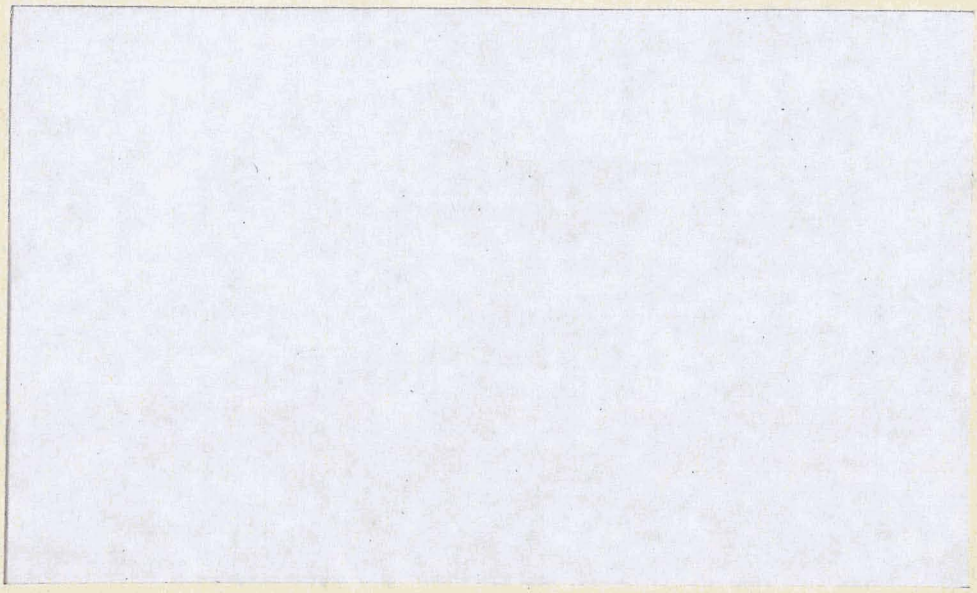

ACNP-63013
JOINT US/EURATOM RESEARCH
and DEVELOPMENT PROGRAM

JOINT US/EURATOM R&D PROGRAM
AT(11-1)-1186

Steam Separation Technology Under the Euratom Program

QUARTERLY PROGRESS REPORT
JANUARY 1, 1963 – MARCH 31, 1963

Prepared for the

U. S. ATOMIC ENERGY COMMISSION
Under the US/EURATOM Agreement

ALLIS-CHALMERS
ATOMIC ENERGY DIVISION
MILWAUKEE 1, WISCONSIN
U.S.A.

April 10, 1963

TABLE OF CONTENTS

TABLE OF CONTENTS (Continued)

TABLE OF CONTENTS (Continued)

LIST OF ILLUSTRATIONS

LIST OF ILLUSTRATIONS (Continued)

LIST OF ILLUSTRATIONS (Continued)

PROJECT STATEMENT

The United States and the European Atomic Energy Community (EURATOM), on May 29 and June 18, 1958, signed an agreement which provides a basis for cooperation in programs for the advancement of the peaceful applications of atomic energy. This agreement, in part, provides for the establishment of a Joint U.S-Euratom research and development program which is aimed at reactors to be constructed in Europe under the Joint Program.

The work described in this report represents the Joint U.S.-Euratom effort which is in keeping with the spirit of cooperation in contributing to the common good by the sharing of scientific and technical information and minimizing the duplication of effort by the limited pool of technical talent available in Western Europe and the United States.

1.0 ABSTRACT

Technical Progress During Report Period

The activities this quarter have centered about the following areas:

1. Development of Centrifugal Type Downflow Separators

For purposes of analysis and experiment the separator has been divided into the inlet nozzle, separating zone, and outlet nozzle. The analysis and experiments performed has resulted in a new outlet design, a method of determining separating length, and a more effective inlet nozzle. The results, gathered from the above, have caused a reduction in pressure loss from 5 ft of water for the reference design to 1.5 ft of water for the new design at a flow rate of 1400 gpm.

This quarter has brought about completion of outlet and separator zone investigations and continuation of the inlet nozzle investigations.

2. Investigation of Carryunder in a Natural Separation System

A reactor core riser and downcomer region has been mocked-up in the large air-water tank. Void fraction in the downcomer region has been measured as a function of water velocity, water temperature, inlet gas flow rate, and riser geometry. Results show that the void fraction in the downcomer is essentially zero until a threshold downcomer velocity is reached. The void fraction then rises rapidly with increasing water velocity to approximately 11 per cent and then appears to remain constant. Test data from this experiment is being correlated using a dimensional analysis technique. An

initial prediction equation has been developed and is reported this quarter.

3. Steam-Water Facility

The steam-water facility is scheduled for operation April 15, 1963

2.0 PRINCIPAL INVESTIGATORS

The following investigators have been active on the program this Quarter.

Frank Currier	William Meyer
Ronald Grenda	John Wilson
William Littleton	Howard Yant

3.0 STATEMENT OF THE PROBLEM

Program activities this quarter have been divided into the following categories:

3.1 Air-Water Tank Tests

The purpose of this series of tests is to provide data on a number of above-core methods of reducing carryunder. To date this effort has been concentrated on obtaining the effects of riser geometry.

3.1.1 Reduced Flow Area Riser

A relatively simple method of reducing steam carryunder may be accomplished by reducing the flow area of the riser, which results in an increased downcomer flow area. Testing this quarter has been aimed at evaluating the effect of certain system variables. These include straight length of riser, static height of water above the riser, water recirculation rate (downcomer velocity), quantity of air introduced into the system, and the system temperature. Computer programs have been developed to reduce the data and to correlate the data in terms of dimensionless groups consisting of system variables. The results of this effort are described in Section 4.1.

3.2 Centrifugal Separator Tests

The purpose of these tests is to improve the pressure drop, flow capacity, and efficiency of the centrifugal steam separator. Testing of the outlet nozzle is directed toward developing an outlet which will terminate the

the separating vortex without excessive carryunder or pressure drop. Analysis of the outlet nozzle has been facilitated through the use of a computer program describing the water flow patterns.

Testing of the inlet nozzle has commenced. This testing is directed toward improving the inlet nozzle performance through reduction of pressure drop and increase of nozzle coefficient.

The required minimum separating length for the separator depends on the separator inlet velocity and other fluid parameters. A computer program for analysis of the separating zone was refined to give a better prediction of air-water test results as well as for steam water testing in the future.

3.3 Loop Design and Construction

3.3.1 Air Water Facility

The work outlined for this quarter were modifications to the necked-down riser configuration in the air-water tank test equipment, and the construction of discharge nozzles, of various lengths and flow areas, for the centrifugal separator test.

The results of this effort are described in Section 4.3.1.

3.3.2 Steam-Water Facility

The work outlined for this quarter included expediting pressure vessel fabrication, completing structural changes necessary for vessel installation, and installation of the vessel. Included also in this quarter was the acquiring of control and test equipment for operation of the loop.

The results of this effort are described in Section 4.3.2.

4.0 DESCRIPTION OF WORK AND ANALYSIS OF TEST RESULTS

This section will present the scope of the experimental program, and the design of the test facilities.

4.1 Air-Water Tank Tests

4.1.1 Test Objective

The main objective of this test is to determine what effect a necked-down riser above a simulated core will have on the amount of carry-under. Refer to Figure 1.

4.1.2 Description of the Test Apparatus

Figure 1-A gives a general view of the air-water tank facility. Water before entering the air-water tank is pumped through an orifice plate, located in the discharge line. The orifice plate is used to measure the recirculating flow rate. Air is injected into the water downstream of the orifice plate forming an air-water mixture. This mixture then passes into the air-water tank, and rises through the test section to the interface. At the interface the greatest part of the air is released. The remaining mixture then enters the downcomer area, where differential pressure readings determine the percentage by volume of the voids. From the downcomer area the mixture flows into the larger outer tank, and again a portion of air that has been carried under is separated from the water. Leaving the tank by way of the pump suction line, the mixture enters the air collector tank, where the remaining air is removed from the water. The water then returns to the pump completing the circuit.

Flow deflectors made from perforated plate are placed at the top of the riser. This minimizes any steam channeling and gives a more even distribution of the bubbles emanating from the top of the riser. The location of these plates above the riser can also be adjusted to determine the effect (if any) upon the carryunder.

Differential pressure measurements made to determine the void fraction at the different points in the system are made with D.P. cells having a range of 0 to 20 in. or 0 to 25 in. of water. The cells when set at 20 per cent of full scale, can accurately measure differential pressure from 0 to 4 in. and 0 to 5 in. of water. The corresponding deflection of the manometers connected to the air side of the cells is 6.1 to 31 inches of mercury.

4.1.3 Variations in Test Parameters

In order to establish a complete understanding of the problem, it is necessary to vary geometric parameters as well as fluid and gas properties in the investigation. A schematic diagram of the test section depicting the test parameters is shown in Figure 1.

Presently, diameters D1, D2, and D3 (Fig. 1) are 32.0 in., 15.5 in., and 29.5 in., respectively. The tests on the D2 riser have been completed. These tests include variations in riser height (H1) from 6.0 in. to 24.0 in. in six inch increments, or H1 to D2 ratios from approximately 0.4 to 1.5.

At each riser height the following parameters were varied:

A. Loop Temperature

1. Test run at 85 ± 10 F
2. Test run at 150 ± 10 F

B. Static water level (H3):

1. Test run at 0 in.
2. Test run at 6 in.
3. Test run at 12 in.
4. Test run at 18 in.
5. Test run at 24 in. (With the riser (H1) extended to 24.0 in., this run was not possible due to reaching height limitations of the system.)

C. Air Flow:

From 30 cfm to 200 cfm through the orifice.

The air expands when it contacts the water, and the test range for air flow becomes 45 cfm to approximately 300 cfm through the riser.

D. Water Flow:

At each air flow the water flow is varied from approximately 400 gpm to 2000 gpm. The maximum recirculation rate is somewhat determined by physical limitations of the loop. This results in superficial water velocities, in the necked down portion of the downcomer, of 0.214 ft/sec to 1.07 ft/sec.

4.1.4 Typical Test Run

4.1.4.1 Pre-Run Procedure and Checks

Since the diameters D1, D2, and D3 (Fig. 1) are fixed for this system it is only necessary to set the riser length H1 to the

desired length. After this has been accomplished the test section is filled to the predetermined static water level (H3). Air pressure is then applied to the differential pressure cells and all manometer lines purged to remove any air that may be trapped in the lines.

At startup a friction run is made to determine the single phase pressure drop across the void fraction manometers located in the lower region. The water flow (with no air added to the system) is progressively increased and the appropriate manometer readings recorded for each flow. By subtracting these manometer readings from the readings recorded when air is added to the system, the true void fraction for each point is established. This is automatically accomplished by the data reduction program at the time the data is processed.

4.1.4.2 Startup and Data Recording

After completion of the friction run, the water flow is set at approximately 400 gpm. Air is introduced to the system allowing approximately 30 or 40 cfm to proceed into the feed line and hence to the riser. The following data is then recorded:

A. Run number

B. Water flow manometer, inches of mercury

C. Air pressure upstream of the air-flow orifice plate, psi

D. Air-flow manometer, inches of water

E. System temperature, ^{o}F

F. Void fraction manometers, inches of mercury

G. Dynamic head (true water level) (H2), inches

H. Riser Length (H1), inches

I. Static water level, inches

The water flow is then increased to maximum flow (approximately 2000 gpm) by increments of approximately 150 gpm. After the maximum flow readings have been taken, the water flow is again reduced to approximately 400 gpm, and the air flow is increased for the next run. The above cycle is continued until maximum air and water flow conditions have been reached.

4.1.4.3 Shutdown and Geometry Change

After the maximum flow conditions have been reached the air and water flows to the test section are terminated. Water may now be added to or drained from the loop depending upon the next static level (H3) and/or riser length (H1) to be tested (Fig. 1).

4.1.4.4 Elevated Temperature Test

In order to investigate the effects of fluid and gas properties it is necessary to vary the temperature of the system. The test data for the heated condition (Temp. $\approx$ 150 F) are taken in the same way as for the cool condition (Temp. $\approx$ 85 F).

The loop is heated by three sources. One, a small steam generator that injects saturated steam at 270 F into the main tank. The second source is electrical strip heaters located on the pump suction line. One or both of these sources of heat may be needed for any particular run. The third source of heat is pump work

which is small in comparison to the two main sources.

To heat the loop a flow of approximately 1000 gpm is allowed to circulate through the loop with all heat sources operating. To reach a test temperature of 150 F may require as much as 5 hours of heating time, depending on the initial loop temperature. It has been found that once the test temperature is attained it becomes quite stable even with the addition of rather large quantities of 75 F air.

After the loop is heated, the manometer lines are purged and test parameters checked before commencing the test run.

4.1.5 Test Results and Discussion

4.1.5.1 Computer Programs for Data Reduction

Figure 2 illustrates the IBM 1620 FORTRAN STATEMENT print-out of the computer program used to reduce the test data. Actual readings, such as manometer deflection and temperatures, taken during a run are the input for the program which has as an output the meaningful test variables under investigation. Figure 3 shows the flow diagram for this program.

Figures 2 and 3 show that a dimensional analysis is also incorporated into the program. A thorough discussion of this part of the program is presented in Section 4.1.5.5.

4.1.5.2 Effect of Air Flow and Temperature on Carryunder

Figures 5 and 6 present typical runs indicating the effect of air flow and loop temperature on the void fraction. Downcomer void fraction (% by volume) is plotted as a function of recirculation rate. The downcomer velocity is the superficial water velocity that exists in the upper region of the downcomer (Fig. 1).

Curves of Figures 5 and 6 both show a sharp increase in the void fraction after a critical downcomer velocity has been reached. At velocities lower than critical, the void fraction remains essentially zero. For the test run taken at a water temperature of 90 F, the void fraction is somewhat a function of the air flow through the riser. However, this dependency on air flow seems to vanish once a certain air flow is reached. Thus, it appears that there has been a change in flow regime, and for the higher air flows the mixture does indeed act more as a two phase mixture.

As the temperature of the system is increased to 150 F changes of some magnitude occur in the liquid and vapor properties, further complicating the problem. By comparing Figure 5 to Figure 6, the following observations may be made:

1. It appears that the carryunder is not now as strong a function of air flow. Since the viscosity of the water has decreased by approximately 40 per cent, a two phase flow regime has been reached even for the low air flow.
2. The carryunder, in general, is lower than the 90 F test run for a given air and water flow. The change in a number of

the mixture properties resulting in higher lift forces and lower drag forces on the bubble are probably responsible for this.

3. The velocity at which carryunder starts is lower for the heated condition. This also appears to be the result of a change in flow regime. However, since a reactor designed to operate below this velocity would require excessively large downcomer areas the location of this point does not seem to be of further interest.

4.1.5.3 Effect of Riser Length on Carryunder

Figures 7 and 8 present typical cross plots to show the effect of riser length (H1 in Figure 1) on the carryunder. Once again the downcomer velocity is the superficial water velocity that exists in the upper region of the downcomer. Tests using the straight length of the riser equal to zero have not been conducted as of this report's publication date. However, Figure 7 shows that there is little effect for a riser length (H1) less than the riser diameter D2 (15.5 inches for these tests). This figure also shows no measurable effect for an increase in riser length once the ratio of length to diameter of the riser has become greater than one. Figure 8 also shows this effect.

Once again it is possible that because of a change in flow regime the very sharp decrease in voids at a length to diameter ratio of one is not as noticeable as in Figure 7. However, for runs with H1 (18 inches and 23 inches) the points are quite close, indicating

that the effect of riser length has been maximized. Curves for other constant air flows exhibit these same tendencies.

4.1.5.4 Effect of Initial Water Level

Figure 9 presents a cross plot of data indicating the effect of initial water level in the system. Data are for a constant riser length of 6 in. and a constant air flow of 123 cfm. In all cases H3 is measured from the top of the riser (Figure 1).

Once again the curve (Figure 9) exhibits the characteristic break in the void fraction. It appears that the initial water level in the system has essentially no effect on the voids. However, the true water level in the system is proportional to initial water level, and therefore, it must be considered from other standpoints in the overall reactor design concept.

4.1.5.5 Correlation Procedure

One of the ultimate goals of this investigation is to correlate steam-water and air-water downcomer void characteristics in terms of basic fluid and geometric parameters.

4.1.5.5.1 Parameters

The following variables (16) have been considered in a dimensional analysis of the present air-water tank test facility:

Variable	Symbol	Unit	Basic Dimension
Diameter	D1	Ft	L
Diameter	D2	Ft	L
Diameter	D3	Ft	L
Length of Riser	H1	Ft	L
Dynamic Head	H2	Ft	L
Static Head	H3	Ft	L
Quantity Air	QG	Ft^3/sec	L^3/T
Quantity Water	QF	Ft^3/sec	L^3/T
Density of Air	ρg	lb/Ft^3	M/L^3
Density of Water	ρf	lb/Ft^3	M/L^3
Viscosity Air	μg	lb/Ft-sec	M/LT
Viscosity Water	μf	lb/sec^2	M/LT
Surface Tension	σ	lb/sec^2	M/T^2
Gravitational Acceleration	g	Ft/sec^2	L/T^2
Downcomer Velocity	V	Ft/sec	L/T
Void Fraction	α	------	-----

According to the Buckingham PI theorem, the above 16 variables result in 13 independent dimensionless parameters. The dimensionless parameters which are presently being used for analysis are those shown in the Program 23, of Figure 2 and Section 4.1.5.5.2.

Figure 10 illustrates the basic line of attack which is presently being used to correlate the data into a general prediction equation.

The present thought is that this prediction equation is of the general form:

$$\alpha = k \times \prod_{n=2}^{13} P(n)^{E(n)} \qquad (1)$$

However, there is some reason to believe that the general form of the equation is semi-log, e.g.

$$\alpha = k \times \exp\left(\prod_{n=2}^{13} P(n)^{E(n)}\right) \qquad (2)$$

A thorough investigation of the above two prediction equations has not as yet been completed. This will be a gradual development depending upon the attainment of suitable data. The computer programs have been developed and a preliminary analysis of the air-water tank data above 1200 gpm has been made according to Equation 1. Some of these results and the mathematical technique involved is explained in the next two sections.

4.1.5.5.2 Mathematical Formulation

The input to computer program 029(Figures 10, 11, and 12) is the dimensionless parameters as calculated and punched in program 023. Basically, program 029 is designed to do two operations;

1. Formulate equations from parameters (log-log or semi-log analysis)
2. Calculate a least square fit for all data points, resulting in a system of linear equations.

For log-log analysis (Eq. 1), the equations are formulated as:

$$E(2)\ln P(2)+E(3)\ln P(3)+\ldots+E(13)\ln P(13) = \ln k-\ln P(1) \quad (3)$$

where from Program 023:

P(1) = (α), Void Fraction

P(2) = ($\rho g/\rho f-\rho g$), Density Ratio

P(3) = (H2-H3/H2), Dynamic and Static Head Relation

P(4) = (H1/H2), Riser Length/Dynamic Head

P(5) = (D1/H2)

P(6) = (D2/H2) Diameters/Dynamic Head

P(7) = (D3/H2)

P(8) = ($\mu f/\mu g$), Viscosity Ratio

P(9) = ($\rho f D_{HYD} V/\mu f$) Reynolds Number (Fluid)

P(10) = V^2/g H1), Froude Number

P(11) = ($\rho f\ V^2$ H1/σ), Weber Number

P(12) = ($\rho g Qg/H1\mu g$), Reynolds Number (gas)

P(13) = (Qf/Qg), Quantity Flow Ratio

E(N) = Calculated Exponents

k = Constant

These parameters are subject to change, for some interrelationships and/or singularities may be found. As yet they have only been preliminarily tested to the extent shown in Section 4.1.5.5.3.

For semi-log analysis, the equations are formulated as:

From Eq. 2

$$\ln \alpha = \ln k + \prod_{n=2}^{13} P(n)^{E(n)} \qquad (4)$$

which leads to

$$E(2)\ln P(2)+E(3)\ln P(3)+\ldots+E(13)\ln P(13) = \ln(\ln\alpha-\ln k) \qquad (5)$$

Equation No. 5 has not as yet been tested, but the program (029) is ready for use. The main drawback which is encountered is the computer time necessary for a complete analysis.

To continue, the above equations either log-log or semi-log are then processed in a least square method as explained in Reference 2. Having many more equations than unknowns, the over-determined system is reduced to a set of linear equations which when solved yield the best exponents. The resulting set of linear equations punched out from 029 is solved as a determinant in program 017 (Fig. 13 and 14) by the Jordan method of elimination. Program 017 is the only program which was not written by the authors. It is a standardized determinant Program written by IBM personnel.

If an exponent is predetermined; for example, if a value is assigned to it before the least square fit is computed, Program 029 will multiply the exponent by the corresponding logarithm and adjust the constant vector on the right hand

side of Equation 3 or 5. Also of interest is the fact that Program 029 is capable of handling 5 separate constants (k) for each run.

After program 017 has solved the determinant yielding 5 solutions for the five constant vectors, the resulting solutions (exponents) are manually punched and applied to the corresponding parameters in the verification program 025, Figures 15, 16, and 17. This program is essentially Equation 1 or 2 depending upon which one is applicable.

4.1.5.5.3 Preliminary Results

Figure 14 illustrates the five solutions as printed from Program 017 for the five constants tested. The first constant (k = 0.00005) was chosen for the verification.

Consequently, solving from Program 029

$$\alpha_{CALC.} = 0.00005 \times \left[\left[\frac{\rho_g}{\rho_f - \rho_g}\right]^{+.38} \times \left[\frac{H2-H3}{H2}\right]^{-.692} \times \left[\frac{H1}{H2}\right]^{.505} \times \left[\frac{D1}{H2}\right]^{.0} \times \left[\frac{D2}{H2}\right]^{.0} \times \left[\frac{D3}{H2}\right]^{.0} \times \left[\frac{\mu_f}{\mu_g}\right]^{.603} \times \left[\frac{\rho_f D_{HYD} V_{DC}}{\mu_f}\right]^{.73} \times \left[\frac{V_{DC}^2}{g H1}\right]^{.52} \times \left[\frac{\rho_f V_{DC}^2 H1}{\sigma}\right]^{-.73} \times \left[\frac{\rho_g Q_g}{H1 \mu_g}\right]^{-1.} \left[\frac{Q_f}{Q_g}\right]^{-1.}\right]^{-1.}$$

where:

0.00005 = k

0.38 = E2

-0.692 = E3

0.505 = E4

0.0 = E5

0.0 = E6

0.0 = E7

0.6026 = E8

0.73 = E9

0.52 = E10

-0.73 = E11

-1.02 = E12

-1.01 = E13

P(N) - See Section 4.1.5.5.2

Parameters 5, 6, 7, in the diameter ratios, were "forced" to zero in Program 029 because the diameters have not as yet been varied. As can be seen, some of the parameters have nearly the same exponents or only vary by a sign. This may lead to some cancellations or revisions in parameters after further investigation.

The above exponents and parameters are involuted and multiplied in Program 025 resulting in an error curve, Figure 18. The residuals or standard deviation of the least square analysis has not as yet been programmed.

This will be a necessary step in order that the relative worth of the prediction can be measured and will be added to Program 025 in the near future.

The print-out from Program 025 is shown in Figure 17. The first column, the run number, is made up of a number and a letter(s). The different letters designate a change in independent variables, e.g., static water level (H3) and/or riser length (H1). The numbers are in order of increasing air and water flow. Columns 2 and 3 are self-explanatory and column 4 is the following equation:

$$X\text{-}COOR = (P_1^{E1}\ P_2^{E2}\ \ldots\ P_{13}^{E13}) \qquad (7)$$

The above analysis, as stated previously, is preliminary and is sighted mainly as an example of the correlation procedure to be followed. The present correlation is limited because the diameter terms were not considered.

As more test data becomes available both from the air-water facility and the steam-water facility, this analysis will become more useful to reactor design.

4.2 Centrifugal Separator Program

During this quarter, all separator testing has been done using the same 10 in. diameter separator chassis described in the previous quarterly report and as shown in Figure 19. The greatest part of the testing has been directed

toward improving the outlet nozzle performance. As a result of this work, it is felt that knowledge of outlet performance has been advanced to the point where testing of it should be suspended, and future attention directed toward investigation of the inlet nozzle.

Toward the end of this quarter, testing commenced on a series of inlet nozzles. These tests have already led to a reduction in inlet nozzle pressure drop through refinement of the inlet. These tests will also increase our knowledge of the mechanics of void separation. This is true since the inlet flow patterns have considerable effect on the separating zone of the centrifugal separator. Further work on the inlet nozzle may reduce even further the pressure drop in the separator.

4.2.1 Outlet Nozzle Development

Testing and refinement of the outlet nozzle is directed toward developing an outlet which will terminate the separating vortex without excessive carryunder or excessive pressure drop. Testing of the conically shaped outlets was continued. The testing was continued until an improvement in pressure drop reached a point of diminishing returns and further refinement was judged to be unprofitable until better inlet nozzles could be developed.

In addition to the conical outlets, two other designs were tested briefly. The first utilized annular discharge opening while the second used turning vanes in an attempted recovery of the rotational velocity component. Both of these outlets exhibited good nozzle coefficients, but the overall performance could not be raised to a

point where they were comparable to that of the cone shaped outlet nozzles. These nozzles are described in more detail in Sections 4.2.1.2 and 4.2.1.3.

4.2.1.1 Testing and Analysis of Conical Shaped Outlet Nozzles

The outlet nozzle series of models 17 through 20 (Ref. 1) operated as predicted, although pressure drop was higher than that for models of similar open area in the model series 11 through 14. For the operating range of 2000 to 2400 GPM, the pressure drop was 5 to 10 per cent higher for the series 17 through 20. Water flow patterns determined with the pitot-static yaw tube verified the water flow pitch angles predicted in the computer analysis of the cone-type outlet.

In order to further reduce outlet nozzle pressure drop, another outlet was fabricated. This outlet again had six trapezoidal outlet openings. The opening size was increased so the new series had approximately 1.5 times the open area as the previous series of models 17 through 20. The new outlet openings were shaped to produce constant axial velocity, as described in the computer program of Fig. 48 (Ref. 1) when equipped with the 7 in. diameter outlet disk. This disk gives outlet openings, trapezoidal in shape, 24 in. long, with upper base length of 3.00 in. and a lower base length of 2.00 in. See Figures 20 and 21. The series was tested with 5, 6, 7, and 8 in. outlet disks being described as models 25 through 28, respectively.

This series of outlets was tested with the model 2 inlet. The outlets showed an improvement in pressure drop over both of the previous series. See Figure 22. The greatest improvement was in the cases with 200 CFM air added to the loop. Here, the series of models 25 through 28 showed an improvement of 20 per cent over series 17 - 20 and an improvement of 10 per cent over series 11 - 14. At lower air flow rates the pressure drop was improved by 10 to 15 per cent over the two series of conical outlets previously tested.

Carryunder is essentially the same for all three series of outlets. This is added proof that all void separation is occurring in the separator chassis and that any outlet of this type that does not disturb the vortex pattern will exhibit similar carryunder properties.

Traverses of the outlet series 25 through 28 with the pitot-static yaw tube showed reasonable agreement between test and predicted pitch angles. However, a large dead-zone was discovered above the outlet disk. Visual observation of the dead-zone confirmed yaw-tube indications. In the case of outlet model 27, with the 7 in. disk, the zone was cone-shaped with a base of 5 in. diameter at the disk, tapering to 2 in. diameter at a point 11 in. higher. See Figure 23. Within this region axial velocities were negligible, although rotational velocities continued. The zone also existed for smaller outlet disks of this series, being roughly proportional

to the outlet disk diameter. It apparently existed, to a much lesser degree in the outlet series of models 17 through 20. This zone of low axial velocities is thought to be similar to the hydrocone effect common to conditions of water flow at right angles to a flat plate.

With the discovery of this dead zone, the computer program describing the outlet nozzle was re-evaluated. The term 'arem' which approximates the cross sectional area of the nozzle was modified to give a better description in view of the known flow, pattern and was changed to

```
AREM=((DS-(A*DDINC))**2-(A*(DD/T))**2)/DS**2
```

As a result of this change the calculated axial velocity for this outlet with the 7 in. disk now shows a 40 per cent decrease along the length of the outlet. Pitch angles were also brought to even closer agreement with the test data.

As mentioned previously, the hydrocone effect was more obvious in the 25 - 28 outlet series than the 17 - 20 series. Higher axial velocities and higher outlet exit velocities in the earlier series are probably responsible for the smaller dead zone in those models. Although the hydrocone did not appear to be disturbing the function of the outlet, an attempt was made to break it up. This was done by removing the outlet disk and replacing it with a hoop of the same diameter. Results with the first such model were encouraging, so a series of 3 hoops were made having diameters

of 8, 7, and 6 in. The opening at the bottom of the outlet cone increases outlet area slightly, but major effect desired is the disruption of the dead zone.

Below are listed the models and dimensions of the 24 in. outlets.

MODEL	24 In. OUTLETS DISK DIAMETER	OUTLET AREA
26	6 in.	2.25 ft^2
27	7	2.50
28	8	2.75
	HOOP DIAMETER	
31	6 in.	2.45 ft^2
30	7	2.77
29	8	3.10

Pressure drop for the new series of models 29 through 31 showed an overall improvement of 15 per cent over the series of models 25 through 28. See Figure 24. This is proportionally greater than the outlet area increase for these models. The improvement is attributed to the improved flow pattern as much as the outlet area increase. Carryunder was improved slightly through the operating range and carryunder break points were extended 100 GPM.

Visual inspection and a series of traverses with the pitot-static yaw tube showed that the dead zone in the lower part of the outlet had been dispersed. See Figure 25. Analysis of the yaw tube data

shows that the tangential velocity components are higher than for the disk type outlets, at the same time; the axial velocities do not die out in the lower part of the nozzle as they did previously. The improved flow patterns allow more efficient use of the outlet area in the lower section of the outlet nozzle and the pressure drop across the outlet is reduced.

The computer analysis of the outlet was modified again to describe the flow pattern through the outlets of series 29 - 31. The change was made in the 'arem' term which describes the cross sectional area of the outlet and was changed to

```
AREM=((DS-A*DDINC))**2)/DS**2
```

Calculated values and yaw tube test data are within 5° of agreement for the 0 in. and 15 in. probe locations. Probe readings at the 6 in. location are consistently 10 to 14 degrees higher than calculated values. Cause of the discrepancy has not been established.

After the hoops were tested at the bottom of the 24 in. outlet, it was decided to test shorter outlet nozzles and find their effect on separator performance. The possibility of using shorter outlets would be of considerable value in reactors where axial space is at a premium. To begin this test, an 18 in. outlet nozzle was fabricated. This nozzle had six trapezoidal openings. In order to ease comparison to models tested previously, the trapezoidal bases

were made to the same dimensions as the series 29 through 31. Thus, the 7 in. hoop gave an upper base of 3 in. and a lower base of 2 in. A series of hoops varying in diameter from 8 in. to 5 in. was used in conjunction with the model 2 inlet. This series of outlets is identified as models 35 through 38.

Below are listed the models and dimensions of the 18 in. outlets.

18 In OUTLETS

Model	Disk Diameter	Outlet Area
35	8 in.	2.41 ft^2
36	7	2.15
37	6	1.89
38	5	1.64

In general, the pressure drop across the 18 in. outlet nozzles was slightly lower than that for the 24 in. outlet nozzle for the equivalent outlet area. However, the pressure drop break point and the maximum flow for the 18 in. nozzle was reduced by approximately 100 GPM. See Figure 27. The carryunder characteristics for both outlet nozzles were approximately the same. The pitot-static yaw tube traverse angles showed very close agreement with those from the computer program. The majority of the angles were within two degrees of the computer analysis.

Because of the success with the 18 in. long outlet nozzle, a 12 in. long outlet was fabricated. Once again the outlet openings were sized to be 3 in. at the upper base and 2 in. at the lower base

when using the 7 in. hoop. The same series of hoops was used at the bottom of the outlet. This series is identified as models 39 through 42 (Fig. 21 and 26). Below are listed the models and dimensions of the 12 in. outlets.

12 In. OUTLETS

Model	Disk Diameter	Outlet Area
39	8 in.	1.72 ft^2
40	7	1.50
41	6	1.32
42	5	1.13

The pressure drop across this nozzle shows a slight improvement over the 18 in. and 24 in. outlet nozzles. See Figure 28. The break point and the maximum flow were approximately the same as for the 18 in. outlet. The pitot-static yaw tube traverse angles are fairly close to those from the computer program. However, they do not agree as well as those from the 18 in. outlet as the usual deviation is 3 to 6 degrees, with some variances as high as 13 degrees from the predicted angle. The carryunder characteristics of this nozzle were comparable to those of the 18 and 24 in. models.

In general, the shorter outlet appears to have slightly better pressure drop when compared to a long outlet of similar outlet area. However, this comparison usually compares the short nozzle with 7 in. or 8 in. hoop with the long nozzle with the 5 or 6 in. hoop. When

the longer outlet is equipped with the same hoop as the short outlet the longer outlet has more open area and thus a lower overall pressure drop. The maximum flow for the 24 in. outlet was also 100 GPM higher than for the shorter outlets. Still a pressure drop for the shorter outlet is by no means prohibitive since it did not exceed 2.1 ft of water for an operating range up to 2300 GPM.

4.2.1.2 Disk Type Outlets

The function of any outlet nozzle is to contain the separating vortex, preventing it from becoming unstable and causing large amounts of carryunder. At the same time the outlet should have as low a pressure drop as possible. The conically shaped outlets with long, narrow openings can be built with enough outlet area to reduce pressure drop to acceptable levels, but so far they have always had a low outlet coefficients. Presumably this low outlet coefficient is caused by the rotational component of flow which causes the fluid to 'see' a smaller outlet area than exists. That is, the projected area of the outlet opening is less than the true area.

It is assumed that an annular or cylindrical shaped opening would have a better projected area than the slits used with the conical outlets. An outlet was fabricated to test this assumption. The outlet was formed by suspending a flat disk on hangars below the separator chassis. The resultant opening was cylindrical in

shape. The cross sectional area could be changed by raising and lowering the plate. Below are listed the models and dimensions of the disk type outlets.

Disk Type Outlet Nozzle Dimensions

Model	Outlet Area
21	1.00 ft^2
22	1.50
23	.50

The three models of the outlet were tested for varying air and water flow rates. These outlets had lower pressure drops and higher outlet coefficients than the conical outlets of comparable outlet area. Model 22 had pressure drop roughly equivalent to that for the conical model 29 which had twice the outlet opening. However, the disk type outlets did not have good carryunder properties. The vortex whipped around above the disk, collapsing at times and trapping pockets of carryunder. At flow rates of 2000 GPM and above, where the vortex entered the outlet, carryunder was approximately twice that for the conical outlets. The disk type outlet was rejected as unsuitable for a high capacity separator because of the high carryunder.

4.2.1.3 Turning Vane Outlet

Another type of outlet model was built to use turning vanes to recover the tangential velocity component of flow (Fig. 29). This outlet had the same cross-sectional area as the 10 in. diameter

separator, approximately 0.50 sq. ft. The leading edges of the turning vanes were inclined at 45 degrees as indicated by yaw tube data on pitch angles for the lower portion of the separating length. The outlet coefficient for this model was higher than 0.50 sq. ft. However, because the open area was only 0.50 sq. ft., the pressure drop was prohibitive. There is no way to increase the outlet area for this type of nozzle without increasing the diameter. That approach would lead to an ungainly separator which would be difficult to install in a reactor downcomer, so no further models of this type were tested.

4.2.2 Separating Length Analysis

The separating zone is the portion of the separator between the bottom of the inlet nozzle and the top of the outlet nozzle. In this region, the last of the gas bubbles are forced by centrifugal force from the periphery of the separator into the central vortex (Fig. 19). A computer program was developed last quarter to determine the axial distance traveled by a bubble in moving from the wall to the vortex. The equations used in the program are based on basic fluid, gas and geometric parameters so the calculational technique can be applied to various diameter separators as well as to gases and fluids having different properties. The primary output of this program is the minimum length of separating zone required in order to be assured that bubbles at the periphery are forced into the vortex.

The separating length calculation developed for the previous quarterly (Ref. 1), was developed using equations for Peebles' Region

4 (Ref. 3) where:

$$V = .825\left[\frac{NG^4}{g}\right]^{.083}\left[\frac{\gamma g_c}{P_1}\right]^{.25}$$

$$NG = 8\ vt^2\left[\frac{(\rho_1-\rho_2)}{3r\rho_1}\right]$$

The lower limit for region 4 is described by the equation:

$$V = .663\left[\frac{\gamma g_c}{P_1}\right]^{.75}\left[\frac{1}{r_b}\right]$$

At bubble velocities below the region 4 minimum the equation for region 3 prevails:

$$V = 1.146\left[\frac{NG^4}{g}\right]^{.167}\left[\frac{\gamma g_c}{r_b \cdot \rho_1}\right]^{.50}$$

γ = Surface tension (lbF/Ft)

P_1 = Density of Water (lb_m/Ft^3)

P_2 = Density of Vapor (lb_m/Ft^3)

r_b = Bubble Radius (Ft)

V = Radial velocity of bubble Ft/sec

The limiting minimum velocity for region 4 is inversely proportional to the bubble radius. The smaller the bubble radius, the higher the minimum limit for region 4 conditions.

Thus, with all other variables unchanged, the bubble size will determine whether the bubble velocity is described by equations for region 3 or region 4. An equation to describe the bubble diameter was derived

previously and is described in ACNP-62006. The equation is:

$$D_b = (.30)\ (3.47)\sqrt{\frac{\gamma}{P_1 - P_2}}$$

The factor 0.30 in the equation is an arbitrary size reduction factor indicating the reduction in size from stationary fluid conditions to the moving fluid conditions in the separator.

This equation predicts a bubble diameter of $\approx$ .10 in. at 175 F water temperature.

Further investigation of the bubble velocity equation using the predicted bubble size indicated that the calculated bubble velocity often fell below the minimum for region 4, and was more exactly described by the velocity equation for region 3. The computer program was revised to calculate the region 4 velocity, the region 3 velocity, and the lower limit of region; and then to choose the region governing the particular case and print the proper velocity, noting whether it is in region 3 or region 4 (Fig. 30-A and B).

The calculated bubble velocity in region 3 is sensitive to bubble size, while region 4 is not, except for the calculation of the region 4 minimum velocity. To demonstrate this fact the separating length program was run for a series of bubble diameters ranging by 0.033 in. to either side of the predicted 0.100 bubble for 175 F water. (See Fig. 31-A and B). The smaller bubble sizes fall into region 3 and the larger into

region 4 as shown in the following:

TABLE 1

10 In. Diameter Separator, 2000 GPM, Inlet Velocity 9.75 Ft/Sec.

Bubble Diam. In.	Bubble Velocity Ft/Sec	Region Number	Separating Length Ft.
0.066	1.92	3	1.35
0.083	1.72	3	1.51
0.100	1.57	3	1.66
0.117	1.46	4	1.79
0.133	1.46	4	1.79

If the inlet velocity is reduced, the separating forces are also reduced, and bubble velocity decreases. As a result, the required separating length is increased as shown in the following table.

TABLE 2

10 In. Diameter Separator, 2000 GPM, Inlet Velocity 8.00 Ft/Sec.

Bubble Diam. In.	Bubble Velocity Ft/Sec	Region Number	Separating Length Ft
0.066	1.80	3	1.45
0.083	1.61	3	1.62
0.100	1.47	3	1.77
0.117	1.36	3	1.92
0.133	1.28	4	2.04

For complete print out of separating length calculations, see Figures 31-A and B.

In cases where the flow regime was changed from region 4 to region 3, the calculated bubble velocity increased slightly. For the 9.75 ft/sec., inlet velocity of the model 2 inlet at 176 F, the calculated bubble velocity increased from 1.46 ft/sec to 1.57 ft/sec. This reduces the calculated separating length from 1.79 ft to 1.66 ft, or by less than 8 per cent.

The listings show that by doubling the bubble size in the calculation, the separating length is increased by a factor of approximately 40 per cent from that for the 0.066 in. bubble. The change in separating length is thus approximately 20 per cent for a bubble size change of 0.033 in. larger or smaller than the predicted 0.100 in. bubble. This 20 per cent variance represents a change in predicted separating length of 3 in. or less for the inlet velocities considered. A variance of this magnitude is difficult to detect with the short separating length of the present separator.

The present separator with the model 2 inlet shows good agreement between calculated and actual separating length. We would then assume that this agreement at least partially verifies the present bubble size estimate. If future inlet nozzles give lower inlet velocities than those at present, the separating length should be increased. In this case, disparities between calculated and actual separating length would be more obvious if they do exist.

4.2.3 Inlet Nozzle Development

The function of the inlet nozzle is to introduce the voided mixture to the separator. The inlet mixture must enter the separator at a rate

of speed great enough to form the separating vortex at the operating range of the separator. If the inlet velocity is too low the vortex will not form. If the inlet velocity is unnecessarily high, a very strong vortex will form, but at the expense of a high pressure drop across the inlet. Thus the sizing of the inlet nozzle is a compromise between pressure drop and required inlet velocity.

Testing of inlets commenced in mid-February. To date, four scroll shaped inlet configurations have been tested and analyzed. While none of these models can be considered to have optimum performance, the pressure drop, nozzle coefficients, and velocity profiles serve as guides to be used in improving the inlet.

4.2.3.1 Inlet Nozzle Experiments

The air-water test procedure for a given inlet nozzle was the same as that used for testing outlets. The separator was tested at inlet submergences of 0.75 ft and 2.75 ft of water. The separator was tested for the flow range from no flow to the maximum flow as dictated by pressure drop or carryunder. The separator was tested at the air flow rates of 60, 120, and 200 cfm free air. During the air-water testing, the loop temperature was maintained at temperatures above 165 F. For brevity, analysis of air-water test data will be confined to the condition of 200 cfm air added to the loop. A highly voided inlet mixture gives the most severe condition of operation.

The computer program for data reduction was essentially unchanged

from the procedure used for testing outlet nozzles. However, emphasis now switched to inlet pressure drop, inlet coefficient, and the position of the vortex in the separator.

In addition to air-water testing, the inlet nozzle area was extensively probed at several levels with the pitot-static yaw tube. This information was very useful in determining the velocity profiles in the separator and determining the effect of design changes to the inlet.

In order to show the interrelation of the inlet and the outlet nozzle, all of the inlets were tested with the same outlet. Outlet model 30 was one of the better performing outlet shapes and has been used in the testing of all inlets.

All of the inlet nozzles tested were of the scroll shaped type. The variables from model to model were the width at the nozzle throat, and at the mouth. As the throat width was varied, the length from mouth to throat varied in some cases as did the inlet length to width ratio as shown in the table below.

Table of Inlet Dimensions

Model No.	Mouth	Throat	Length : Width (horizontal plane)	Throat Area
2	1.50 in.	1.25 in.	4 : 1	0.83 Ft^2
3	3.25	1.25	4 : 1	0.83
4	3.25	0.75	10 : 1	0.50
5	3.25	1.75	3 : 1	1.17

4.2.3.2 Inlet Nozzle Analysis

The first inlet extensively tested was model 2 which was used throughout the testing of outlet nozzles (Fig. 32). While the performance of this inlet was considered adequate, the pressure drop was excessive, and the inlet coefficient was not particularly good.

Inlet coefficient is defined by the following expression:

$$C = \frac{Q'}{A\sqrt{2gh}}$$

Where:

Q' = (CFM water + CFM vapor carryunder + CFM vapor exhaust flow)/60

A = Inlet cross sectional area

h = Inlet drop in ft of flowing fluid

g = Acceleration due to gravity

Performance of Model 2 Inlet Nozzle

Run	Water Flow GPM	Vapor Flow CFM	Total CFS	*Effective Length	Pressure Drop-Ft Water	Nozzle Coef. "C" Corrected for Eff. Length
569	1000	128	4.37	100%	0.6	0.59
568	1500	221	7.04	100%	1.4	0.60
564	2000	354	10.36	100%	2.6	0.63
565	2200	350	10.72	100%	3.4	0.59
567	2500	351	11.40	58%	6.2	0.80
					Ave.	0.60

*Effective Length: At high water flow rates, the inlet nozzle pressure drop is great enough that the water level in the separator is lower than the top of the inlet nozzle. During these conditions, the effective inlet area is restricted to that part of the inlet below the water level in the separator. For the purpose of analysis, the inlet coefficient is corrected to give the coefficient for this reduced inlet area. The correction is not applied to the inlet nozzle pressure drop, as that reading is indicative of the true separator performance.

The inlet nozzle was probed with the pitot-static yaw tube on both sides of the vortex core at three elevations along the axial length of the inlet. These elevations were 1 ft, 3 ft, and 5 ft above the bottom of the inlet, which was 8 ft from top to bottom. The tangential velocities recorded with the probe show a velocity increase toward the center of the separator roughly equivalent to the equation $Vr^{0.3} = C$ (Fig. 33). Indicated velocity at the 5 ft level is considerably less than at the other two levels. This effect was most pronounced for the inlets tested which had relatively low nozzle coefficient.

As listed previously, the model 2 inlet had a length to width ratio of 4:1 and a convergence of 0.25 in. over the length of the inlet. It was assumed that the inlet coefficient and pressure drop could be reduced for the same width of throat by increasing the mouth dimension of the inlet. The model 3 inlet was fabricated with the same 1.25 in. throat and a mouth of 3.25 in. (Fig. 34). The inlet was tested for the same range of conditions as the model 2 inlet.

Performance of Model 3 Inlet Nozzle

Run	Water Flow GPM	Vapor Flow CFM	Total CFS	Effective Length	Pressure Drop-Ft Water	Nozzle Coef. "C" Corr. for Eff. Length
975	1000	129	4.38	100%	0.5	0.65
974	1500	298	8.31	100%	1.3	0.68
971	2000	275	9.06	100%	2.3	0.63
972	2200	387	10.91	94%	3.4	0.64
973	2400	392	11.88	72%	5.6	0.70
					Ave.	0.66

The listing shows that the increase in the mouth area of the inlet did cause an improvement in inlet coefficient, of 0.06, but the increase is by no means large.

This inlet was probed with the pitot-static yaw tube for the same three elevations as the model 2 inlet. The inlet velocities in model 3 were much closer to a common value than those for the model 2 inlet. At the same time, the pattern of velocity increase toward the center of the separator was improved over those for the model 2 inlet for the 1 and 3 ft levels of the inlet (Fig. 35). One would expect improved flow patterns to lead to a slightly shorter separating length for the model 3 inlet than the model 2.

The model 2 and model 3 inlets both had length to width ratios of approximately 4:1, and produced almost equivalent pressure drops. It was decided that an inlet should be tested which had a greater L/W ratio. To determine the effect of this parameter, the model 4 inlet was fabricated with a 0.75 in. throat and the same 3.25 in. mouth (Fig. 36). The inlet had a length in the horizontal plane of approximately 7.5 in. which has a L/W ratio of 10:1. It was expected that this inlet would have a higher pressure drop, because of the reduced cross-sectional area, but that it would have an improved inlet coefficient because of the L/W ratio.

Performance of Model 4 Inlet Nozzle

Run	Water Flow GPM	Vapor Flow CFM	Total CFS	Effective Length	Pressure Drop-Ft Water	Nozzle Coef. "C" Corrected for Eff. Length
1006	1000	129	4.38	100%	0.8	0.85
1005	1500	288	8.05	100%	2.0	0.90
1002	1700	370	9.97	100%	2.4	0.98
1003	2000	373	10.69	85%	4.1	0.99
1004	2200	356	10.83	69%	6.7	1.01
					Ave.	.95

The increased length to width ratio of the model 4 inlet nozzle produces a considerable increase in the nozzle coefficient. The coefficient values above 0.95 appear optimistic. However, small errors in pressure drop or vortex height readings would be the most likely source of error in data. Nevertheless, it appears that the increase in L/W is the best means of improving the inlet coefficient.

The model 4 inlet was probed with the pitot-static yaw tube at the same elevations as the previous inlets. The inlet velocities were higher than for previous inlets because of the reduced inlet area. This increase in velocity did not reduce the pattern of velocity increase which remained at approximately $Vr^{0.3} = C$ for the 1 and 3 ft levels. The inlet velocity at the 5 ft level was proportionally better than for the model 2 inlet, though, axial velocity distribution was not so compact as for the model 3 inlet (Fig. 37).

The inlet of model 4 produced higher velocities in the vortex for a given water flow rate and thus formed a larger vortex core, with a reduced separating length. Because of the reduced cross sectional area at the throat, the inlet nozzle pressure drop was high, and judged to be excessive for any separator model except perhaps one designed for less than 1500 gpm. Nevertheless, the high inlet coefficient is attractive.

The model 5 inlet nozzle was fabricated to test the effect of a relatively low length to width ratio in the horizontal plane. This nozzle had a 1.75 in. throat and the 3.25 in. mouth (Fig. 38). The length of the nozzle was approximately 5.5 in. giving a L/W ratio of approximately 3:1. This nozzle was expected to give a relatively low pressure drop because of the large inlet area, but to have a poor inlet coefficient because of the low L/W ratio.

Performance of Model 5 Inlet Nozzle

Run	Water Flow GPM	Vapor Flow CFM	Total CFS	Effective Length	Pressure Drop-Ft Water	Nozzle Coeff. "C" Corrected for Eff. Length
1045	1000	105	3.98	100%	0.5	0.44
1044	1500	288	8.14	100%	1.1	0.52
1040	2000	402	11.15	100%	2.0	0.52
1041	2200	401	11.60	95%	3.0	0.49
1042	2400	392	11.90	75%	4.7	0.52
1043	2600	384	12.20	70%	5.3	0.56
					Ave.	0.51

As expected, the coefficient for the model 5 inlet nozzle was the lowest of the present series of inlets. The low coefficient is attributed to the low L/W ratio. Pressure drop for this inlet was the lowest of the series because of the relatively high cross sectional area of the throat section.

The separator was traversed with the yaw tube at the same elevations as the previous inlets (Fig. 34). While the fluid velocities at the 1 ft and 3 ft levels were almost equal. The velocities at the 5 ft level were reduced considerably as in the case of the model 2 inlet. The water flow pattern also showed a much lower rate of velocity increase toward the center of the separator. For this inlet the expression $Vr^{0.15} = C$ describes the pattern at the 1 ft and 3 ft levels.

The reduced pressure drop of this inlet allows an extension of the operating range of the separator of approximately 200 gpm over the model 2 and 3 inlets previously tested. However, the poor inlet coefficient and water flow patterns indicate that the inlet performance should be improved. An overall graph of pressure drop is shown in Figure 40.

4.2.4 Separator Performance

During the present quarter, the separator chassis has been tested using six series of outlets and four inlet nozzles. The series of 24 in. long outlet models 29 through 31 showed the best pressure drop and carryunder

characteristics of the nozzles tested with the model 2 inlet. The model 30 outlet, with a 7 in. outlet hoop was chosen for testing with the series of inlet nozzles.

Pressure drop and carryunder curves are shown for the inlet models 3, 4, and 5 equipped with the model 30 outlet nozzle. See Figures 41 through 44. The curves in Figures 36 - 39 are shown for an air flow rate of 200 cfm air to the test loop. This produces approximately 400 cfm voids when the air has become saturated. The pressure drop curves for the inlet nozzles show the effect of changing the cross sectional area from one model to another. The outlet drop curves show the effect of the tangential velocity component on outlet nozzle pressure drop. Model 5-30 with the lowest inlet velocity had the lowest outlet drop, while model 4-30 with the highest inlet velocity also had the highest pressure drop across the outlet nozzle.

The model 5 inlet nozzle extends the capacity of the separator by approximately 200 gpm with no unfavorable effect on carryunder. It is assumed that further modification to improve the inlet coefficient will lower the pressure drop without increasing carryunder.

4.3 Loop Design and Construction

4.3.1 Air-Water Facility

The air-water facility was modified to obtain proper operation by locating the air-injection point and installing a perforated pipe to distribute the air entering across the diameter of the pipe.

A valve was installed in the discharge line to facilitate the isolation of the air-water tank test from the centrifugal separator test.

A filter system was installed to remove corrosion impurities from the circulating water.

A flanged extension section 3 ft high was added to the outer tank of the test section to permit testing with deeper submergence and higher air flows.

The centrifugal separator was modified to allow testing with velocity probes.

The centrifugal separator was equipped with discharge nozzles of 18 in. and 12 in. lengths without bottom plate. The inlet nozzle was modified to allow the throat area to vary from 1-3/4 to 3/4 in.

4.3.2 Steam-Water Facility

The high pressure vessel was fabricated and hydrostatically tested in the A-C West Allis Works. It was completed on March 7, 1963 and shipped to the installation site on March 8, 1963. The structural steel work was completed before the arrival of the vessel. The vessel erection was completed March 12, 1963 (Fig. 45).

Installation of the piping and controls is proceeding.

The control instrument panel has been completed and will be delivered to the site. The entire facility should be completely fabricated, insulated and ready for use April 15, 1963.

The test section for the first phase of testing has been completed and will be installed when the operation of the test loop has been tested.

5.0 PLANS FOR FUTURE WORK

5.1 Air-Water Tank Test

The testing of the necked-down riser will continue with a considerable amount of time devoted to the correlation procedure as explained in Section 4.1.5.5.2.

There are plans to test the characteristics of a spiral vane in the straight section of the necked-down riser. There are also plans to cut the riser down as shown in Figure 46, and to test a different diameter necked-down riser. This will result in velocities, in the upper region of the downcomer, greater than 2.0 ft per second.

In addition to the above, the system will be converted so that the amount of carryunder can be collected and measured. This will then mean that the downcomer slip ratio (ratio of gas velocity to fluid velocity) can be calculated. Since the slip ratio is independent of geometry, the amount of carryunder (cfm of air) can then be calculated for all previous test runs.

5.2 Air-Water Column

Testing of the centrifugal separator will continue. The scroll shaped inlets will be refined to improve pressure drop and nozzle coefficient. Following these improvements, the separator will be tested with multiple inlet nozzles. Another separator is being fabricated which will use a series of louvers instead of the usual inlet nozzle, and is scheduled for testing in the coming quarter. This should complete the test schedule

on the 10 in. diam downcomer separators. Following the testing of the 10 in. diam models, an 8 in. diam separator will be tested to determine the effect of separator diameter on separator capacity and performance. (Further tests of downcomer separators will be made in the Steam-Water Loop as referred to in Ref. 1). Testing of upcomer type separators will also commence during the coming quarter as scheduled.

6.0 SUMMARY AND CONCLUSIONS

6.1 Development of Centrifugal Type Downflow Type Separators

For the purpose of analysis, the separator has been divided into the inlet nozzle, separating zone and outlet nozzle as shown in Figure 19. Analysis and testing of the outlet nozzle and separating zone has been completed. The outlet nozzle flow characteristics were analyzed by two methods. The first method used a computer program to determine the velocities and flow direction of the mixture within the nozzle. The second method was the analysis of the overall performance, which consisted of measuring pressure drop and carryunder in the air-water loop. The result of both methods of investigation have led to what appears to be an optimum outlet nozzle design.

The separating zone has also been analyzed by writing a computer program to determine the axial distance traveled by a gas bubble while moving from the wall of the separator to the central vortex. The analytical approach was confirmed by experiment. The results of this effort is a calculational technique, which although is more amenable to computer solution can be accomplished by hand calculations, to determine the length of the separation zone required. Tables 1 and 2 of this report show values to be applied to an air-water system.

An investigation of the improved inlet nozzles is underway. Results so far have led to considerable reduction in pressure drop in this region.

Applying the results obtained to date under this program has resulted in reduction of total pressure drop through the separator at 1400 gpm from

5 ft of water for the reference design to 1.5 ft of water for the best model to date. Performance characteristics for the best separator developed to date is shown in Figures 43 and 44.

6.2 Investigation of Carryunder in a Natural Separation System

This investigation is being carried out in the air-water tank. A reactor core riser and downcomer region have been mocked up, and the void friction in the downcomer was measured as a function of water velocity, water temperature, inlet gas flow rate, and riser geometry. Results show that the void fraction in the downcomer is essential zero until a threshold water velocity is reached in the downcomer. The void fraction then rises rapidly with increasing water velocity to approximate 11 per cent and then appears to remain constant; see Figure 5. Initial investigation of the effect of riser geometry upon carryunder shows that the height of the risers straight section above the cone has considerable effect upon carryunder.

A semi-empirical correlation of the 400 pieces of data obtained thus far is underway using a dimensional analysis technique. The constant and exponents applied to the various dimensionless terms are determined by computer analysis of the data. This technique will be extended to include data from the steam-water loop when it is available. Equation 6 represents this work in its present form.

6.3 Steam-Water Loop Design Construction

The pressure vessel fabrication and testing was completed and the vessel is now installed. Prefabricated piping is being installed to connect the

vessel to the Wisconsin Electric Power Company's boiler and condenser. The loop should be ready for operation April 15, 1963.

6.4 Proposal

Figure 47 shows progress to date as compared to proposed progress.

REFERENCES

1. Steam Separation Technology Under the Euratom Program Quarterly Progress Report, October-December, ACNP-62033, 1962.

2. Advanced Engineering Mathematics, Wylie, C.R., Jr., 2nd Edition, Mc-Graw-Hill Book Company, Inc., New York, 1960, Page 175-179.

3. Peebles, F. N., "The Motion of Gas Bubbles in the HRE Reactor" ORNL-1171, 1952.

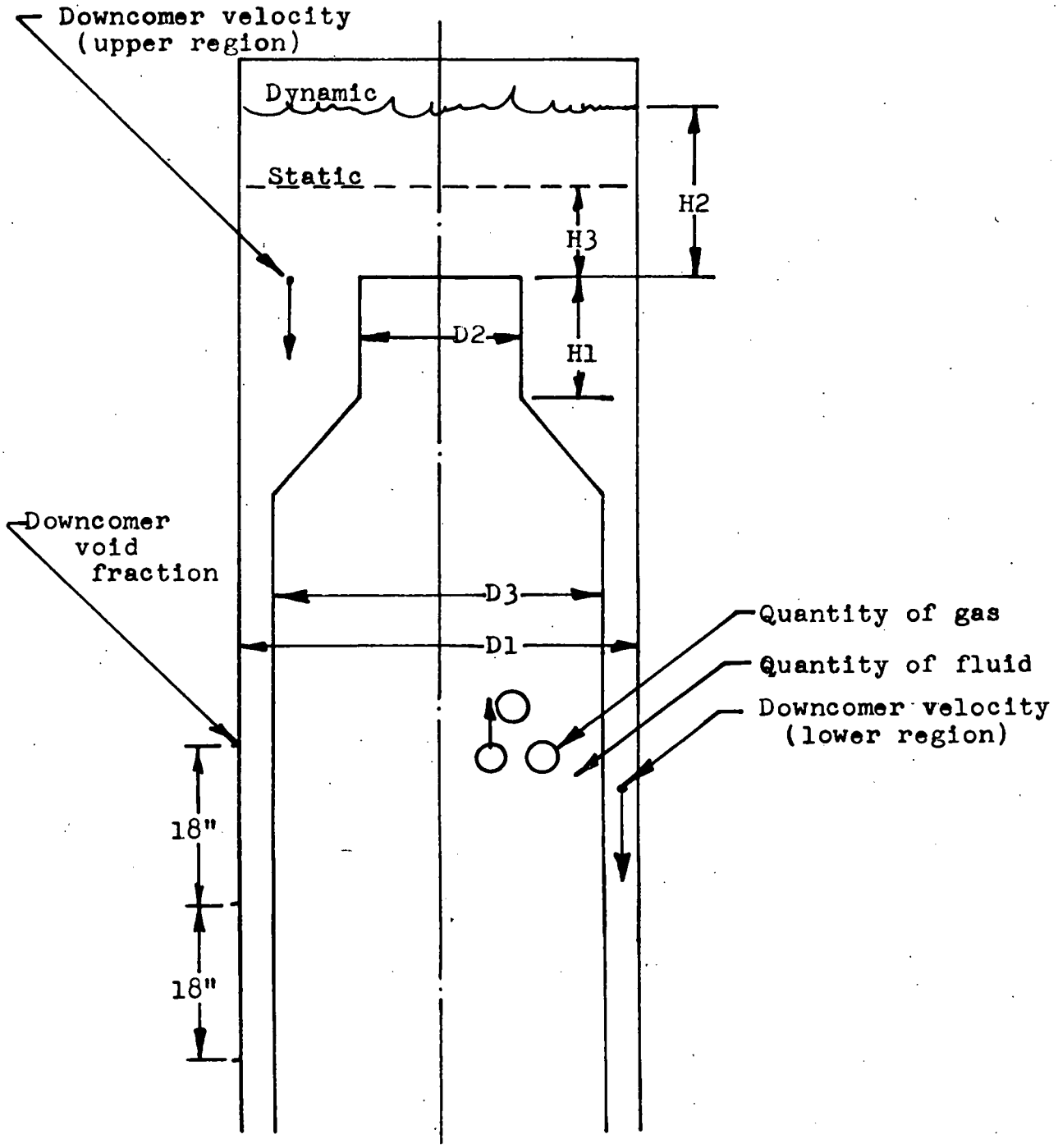

Figure 1 - Test Section Showing Parameters Under Investigation

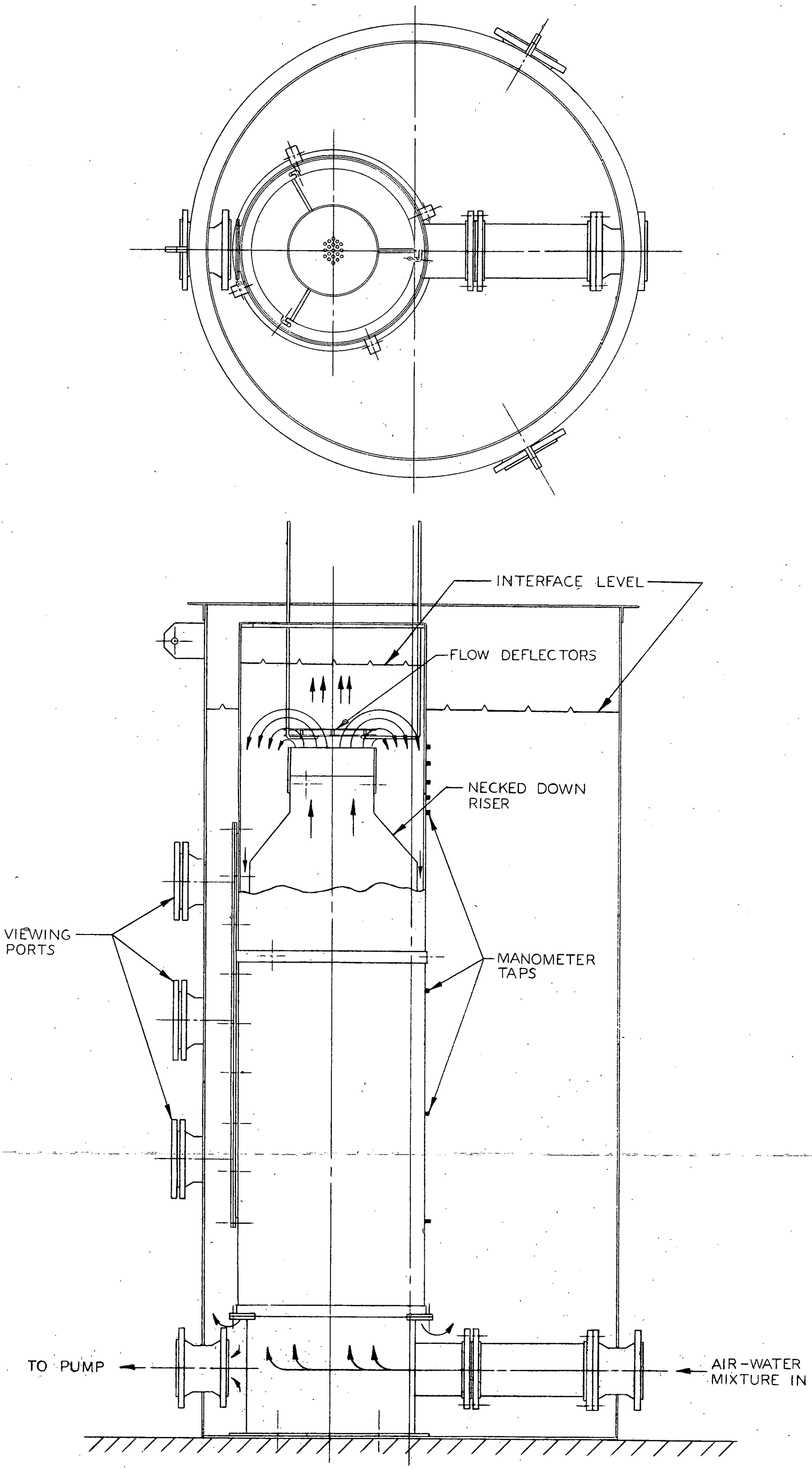

Figure I-A - Air-Water Tank Tests

```
08300 C      BASIC AIR-WATER TANK ANALYSIS    CURRIER - GRENDA
08300 C
08300 C                                                  SWITCH NO. 1-ON,SKIP PRINT
08300 C                                                  SWITCH NO. 2-ON,SKIP PUNCH
08300 C                                                  SWITCH NO. 3-ON,GO TO 60
08300 C                                                  SWITCH NO. 4-ON,FORCE EXPON.
08300 C
08300        DIMENSION E(13),P(13),TEMP(16),DF(16),FMU(16),GMU(16)
08300        READ 38,SLOPE,BINT
08336        DO 50 I=1,16
08348     50 READ 38,TEMP(I),DF(I),FMU(I),GMU(I)
08540        READ 38,DISTY
08564        READ 38,D2,D1,D3
08612        HYDIA=4.*(D1**2.-D2**2.)/(D1+D2)
08768        DO 01 I=1,13
08780     01 READ 38,E(I)
08864        TEM=0.
08888     60 IF(SENSE SWITCH 1)56,11
08908     11 CONTINUE
08908        PRINT 400
08932        PRINT 401
08956     56 CONTINUE
08956        DO 17 JJ=1,12
08968        READ 39,PSTAT,AIR
09004        READ 38,ALPHA,VELO,H1,H2,TEMPO,H3
09088        IF(TEMPO-TEM)04,06,04
09156     04 TEM=TEMPO
09180        DO 51 N=1,16
09192        TT=TEM-TEMP(N)
09252        IF(TT)52,52,51
09308     51 CONTINUE
09344     52 RHOF=DF(N)+(TT*(DF(N)-DF(N-1))/10.)
09488        FFMU=FMU(N)+(TT*(FMU(N)-FMU(N-1))/10.)
09632        GGMU=GMU(N)+(TT*(GMU(N)-GMU(N-1))/10.)
09776        VAPPR=0.203454+1.038372E-8*(TEM**3.922951)
09836        RHOG=(2.699*(14.696-VAPPR)+1.678*VAPPR)/(TEM+460.)
09980        W=0.622*VAPPR/(14.696-VAPPR)
10064        C=(TEM-32.)/1.8
10112        S =(75.68-.138*C-(3.56E-4)*C**2+(4.7E-7)*C**3)*2.205E-3
10292     06 CONTINUE
10292        DCVEL=1.460*VELO**.5
10340        ALPHA=ALPHA-SLOPE*VELO-BINT
10412        ALPHA=(ALPHA-6.0)/5.000
10460        ALPHB=ALPHA*62.4/(DISTY*(RHOF-RHOG))+0.00005
10568        ALPHA=ALPHB
10592        GPM=533.00*(VELO **.5)
10640        QF=GPM/7.481
10676        DDVEL=0.1955*DCVEL
10712        QG=3.78*(((PSTAT+14.696)*AIR)**.5)
10784        QG=(0.0764*(1.+W)*QG)/RHOG
10856        IF(SENSE SWITCH 2)57,58
10876     58 CONTINUE
10876        IF(ALPHB)05,05,07
10932     05 ALPHA=0.0001
10956     07 CONTINUE
10956        P(1)=ALPHA
```

Figure 2 - Fortran Statement for Air-Water Tank Data Reduction (Sheet 1 of 3)

```
T0980         P(2)=RHOG/(RHOF-RHOG)
T1028         P(3)=(H2-H3)/H2
T1076         P(4)=H1/H2
T1112         P(5)=D1/H2
T1148         P(6)=D2/H2
T1184         P(7)=D3/H2
T1220         P(8)=FFMU/GGMU
T1256         P(9)=(RHOF*HYDIA*DDVEL/FFMU)*300.
T1328         P(10)=(DDVEL**2./(32.2*H1))*12.
T1424         P(11)=(RHOF*DDVEL**2.)*H1/(S*12.)
T1532         P(12)=((RHOG*QG)/(H1*GGMU))*720.
T1628         P(13)=QF/QG
T1664         IF(SENSE SWITCH 4)200,57
T1684    200  DO 201 KKK=1,13
T1696         P(KKK)=P(KKK)**E(KKK)
T1804    201  CONTINUE
T1840     57  CONTINUE
T1840         IF(SENSE SWITCH 1)12,13
T1860     13  CONTINUE
T1860         PRINT 39,GPM,DCVEL,ALPHB,QG,H3,H2,TEM
T1956         PRINT 403,DDVEL
T1980         PRINT 41
T2004     12  CONTINUE
T2004         IF(SENSE SWITCH 2)14,15
T2024     15  CONTINUE
T2024         PUNCH 39
T2048         PUNCH 40,P(1),P(2),P(3),P(4),P(5)
T2120         PUNCH 40,P(6),P(7),P(8),P(9),P(10)
T2192         PUNCH 40,P(11),P(12),P(13)
T2240         PUNCH 41
T2264     14  CONTINUE
T2264         IF(SENSE SWITCH 9)10,17
T2284     17  CONTINUE
T2320         IF(SENSE SWITCH 1)60,799
T2340    799  PRINT 798
T2364         GO TO 60
T2372     10  PAUSE
T2384         IF(SENSE SWITCH 3)60,65
T2404     65  STOP
T2452    400  FORMAT(15X32HDOWNCOMER CARRYUNDER CALCULATION,//)
T2588 401FORMAT(7X3HRUN,7X3HGPM,7X3HVEL,8X2HAL,7X3HCFM,8X2HH3,8X2HH2,6X2HTE,/)
T2878    403  FORMAT(20X,F10.3)
T2948     38  FORMAT(F10.3,F10.3,F10.3,F10.3,F10.3,F10.3,F10.3,F10.3)
T3006     39  FORMAT(10H          ,F10.3,F10.3,F10.5,F10.3,F10.3,F10.3,F10.3)
T3086     40  FORMAT(F14.4,F14.4,F14.4,F14.4,F14.4)
T3128     41  FORMAT(1H-,/,1H-)
T3168    798  FORMAT(////////////)
T3246         END
```

Figure 2 - Fortran Statement for Air-Water Tank Data Reduction (Sheet 2 of 3)

NOMENCLATURE PROG. 023

Temp (I) - Temperature (From Table) F^{o}
DF (I) - Density of Water (From Table) lb/ft^{3}
FMU (I) - Viscosity of Water (From Table) lb/hr-ft
GMU (I) - Viscosity of Air (From Table) lb/hr-ft
Slope-Slope of Friction Correction Line
BINT - Intercept of Correction Line
DISTY - Distance Between Alpha Taps
D2 - Diameter of Necked-Down Riser, In.
D1 - Diameter of Outside Tank, In.
D3 - Diameter of Upcomer, In.
HYDIA - Hydraulic Diameter in Upper Region, In.
E (I) - Exponents
TEM - Internal Parameter
PSTAT - Air Line Pressure, psig
AIR - Orifice Meter Reading, Inches of Water
ALPHA - Downcomer Voids Reading from Differential Pressure Cell, Inches of Water
VELO - Water Flow Orifice Reading, Inches of Mercury
H1 - Riser Length, Inches
H2 - Dynamic Head, Inches
TEMPO - Bulk Temperature of Water, F^{o}
H3 - Static Head, Inches
TT - Internal Parameter Use in Temperature Table Search
RHOF - Density of Fluid Interpolated from Table, lb/ft^{3}
FFMU - Viscosity of Fluid Interpolated from Table, lb/hr-ft
GGMU - Viscosity of Gas Interpolated from Table, lb/hr-ft
VAPPR - Vapor Pressure of Water at Tempo, psi
RHOG - Density of Saturated Air in Loop, lb/ft^{3}
W - Specific Humidity, lb vapor per lb air
C - Temperature, C^{o}
S - Surface Tension of Liquid, lb/sec^{2}
DCVEL - Downcomer Velocity, Lower Region ft/sec
ALPHB - Void Fraction
GPM - Water flow, Gallons per Minute
QF - Water Flow, ft^{3}/min
DDVL - Downcomer Velocity, Upper Region, ft/sec
QG - (First) Air Flow Through Orifice, cfm
QG - (Second) Air Flow Through Upcomer After Saturation, cfm
P (I) - Dimensionless Parameters

FIGURE 2 - FORTRAN STATEMENT FOR AIR-WATER TANK DATA REDUCTION (SHEET 3 of 3)

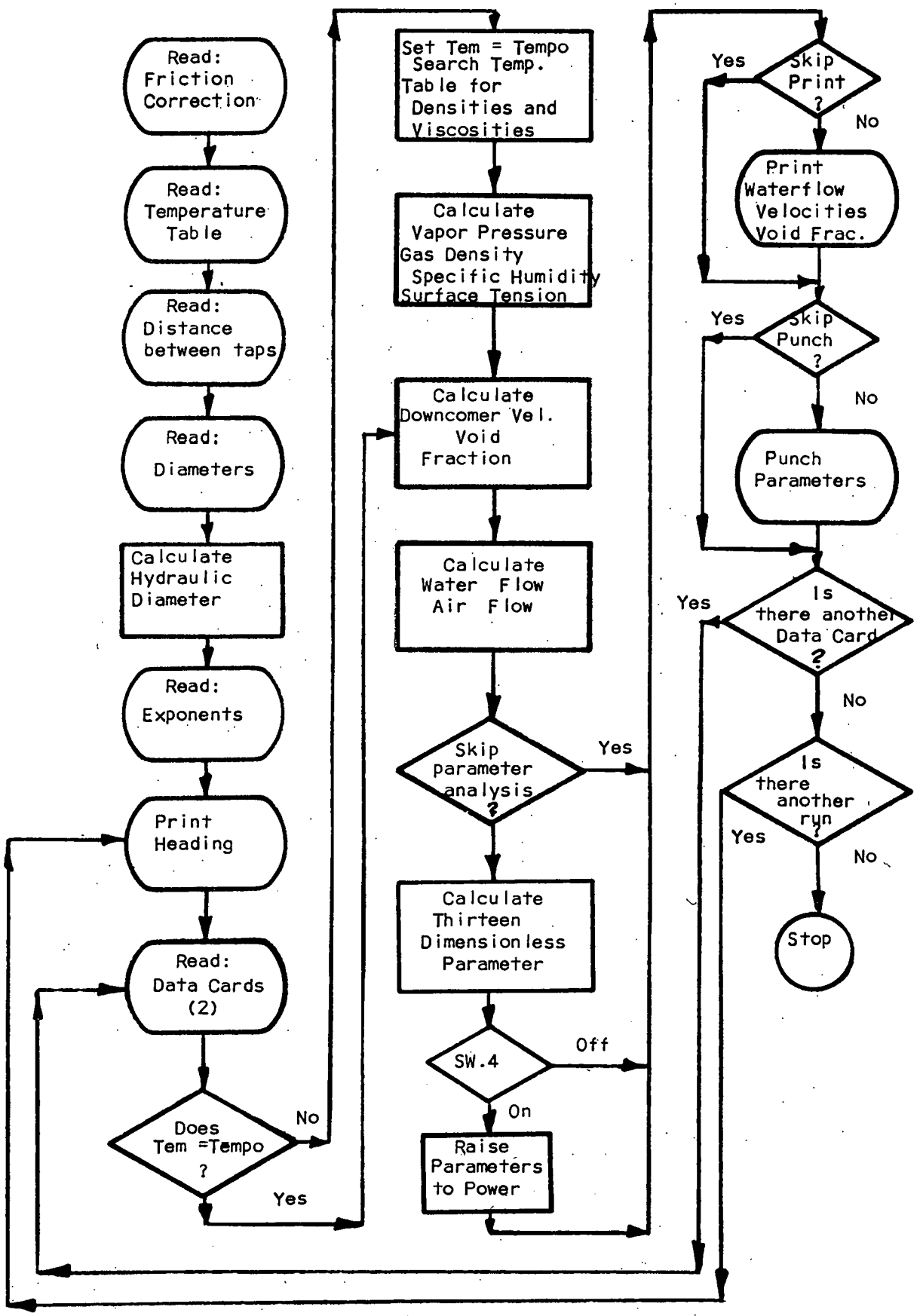

Figure 3 - Air-Water Tank Data Reduction Logic Program

DOWNCOMER CARRYUNDER CALCULATION

$H_1 = 12.0$

RUN	GPM	VEL	AL	CFM	H3	H2	TE
1AA	595.912	1.632 .319	.00000	33.757	13.000	18.500	93.000
2AA	753.775	2.064 .403	-.00046	33.757	13.000	19.500	93.000
3AA	883.880	2.421 .473	-.00093	33.757	13.000	21.500	93.000
4AA	975.550	2.672 .522	.00248	33.757	13.000	23.500	93.000
5AA	1065.999	2.919 .570	.01579	33.757	13.000	25.500	93.000
6AA	1232.832	3.376 .660	.03328	33.757	13.000	28.500	93.000
7AA	1311.006	3.591 .702	.03635	33.757	13.000	30.500	93.500
8AA	1420.222	3.890 .760	.04262	33.757	13.000	32.500	93.500
9AA	1535.558	4.206 .822	.04723	33.757	13.000	34.500	93.500
10AA	1623.682	4.447 .869	.05376	33.757	13.000	35.500	93.500
11AA	1693.900	4.639 .907	.05863	33.757	13.000	36.500	94.000
12AA	1783.759	4.886 .955	.06136	33.757	13.000	37.500	94.000

Figure 4 - Typical Data Reduction Print-Out For a Complete Run (Sheet 1 of 5)

DOWNCOMER CARRYUNDER CALCULATION

$H_1 = 12.0$

RUN	GPM	VEL	AL	CFM	H3	H2	TE
13AA	1865.500	5.110 .999	.06428	33.757	13.000	39.500	94.000
14AA	1947.456	5.334 1.042	.06479	33.757	13.000	40.500	94.500
15AA	2029.603	5.559 1.086	.06511	33.757	13.000	42.500	94.800
16AA	630.654	1.727 .337	.00058	71.611	13.000	21.500	95.000
17AA	772.390	2.115 .413	.00029	71.611	13.000	23.500	95.000
18AA	899.807	2.464 .481	-.00129	71.611	13.000	25.500	95.000
19AA	968.242	2.652 .518	.00266	71.611	13.000	26.500	95.200
20AA	1028.013	2.815 .550	.01010	71.611	13.000	28.500	95.600
21AA	1098.807	3.009 .588	.02720	71.611	13.000	30.500	95.700
22AA	1173.810	3.215 .628	.03622	71.611	13.000	33.000	95.800
23AA	1255.664	3.439 .672	.04600	71.611	13.000	35.500	95.900
24AA	1343.117	3.679 .719	.05318	71.611	13.000	37.500	96.000

Figure 4 - Typical Data Reduction Print-Out For a Complete Run (Sheet 2 of 5)

DOWNCOMER CARRYUNDER CALCULATION

$H_1 = 12.0$

RUN	GPM	VEL	AL	CFM	H3	H2	TE
25AA	1415.212	3.876 .757	.05736	71.611	13.000	38.500	96.000
26AA	1483.809	4.064 .794	.06378	71.611	13.000	40.500	96.000
27AA	1558.512	4.269 .834	.06985	71.611	13.000	41.500	96.500
28AA	1672.805	4.582 .895	.07634	71.611	13.000	43.500	96.500
29AA	1723.000	4.719 .922	.07864	71.611	13.000	44.500	96.500
30AA	1799.615	4.929 .963	.08529	71.611	13.000	45.500	97.000
31AA	1861.689	5.099 .996	.08575	71.611	13.000	47.500	97.000
32AA	1932.814	5.294 1.035	.09351	71.611	13.000	49.500	97.000
33AA	684.650	1.875 .366	.00191	123.458	13.000	25.500	98.000
34AA	794.152	2.175 .425	.00209	123.458	13.000	27.500	98.000
35AA	883.880	2.421 .473	.00130	123.458	13.000	29.500	98.000
36AA	945.981	2.591 .506	.00656	123.458	13.000	31.000	98.000

Figure 4 - Typical Data Reduction Print-Out For a Complete Run (Sheet 3 of 5)

DOWNCOMER CARRYUNDER CALCULATION

$H_1 = 12.0$

RUN	GPM	VEL	AL	CFM	H3	H2	TE
37AA	1039.008	2.846 .556	.01876	123.458	13.000	32.500	98.000
38AA	1124.364	3.079 .602	.03096	123.458	13.000	34.500	98.000
39AA	1221.256	3.345 .654	.04486	123.458	13.000	36.500	98.000
40AA	1311.006	3.591 .702	.05093	123.458	13.000	38.500	99.000
41AA	1384.774	3.793 .741	.05735	123.458	13.000	41.500	99.000
42AA	1479.015	4.051 .792	.06175	123.458	13.000	42.500	99.000
43AA	1544.780	4.231 .827	.06706	123.458	13.000	44.500	99.000
44AA	1638.487	4.488 .877	.06774	123.458	13.000	46.500	99.000
45AA	1723.000	4.719 .922	.07532	123.458	13.000	48.500	99.000
46AA	1854.043	5.078 .992	.09062	123.458	13.000	50.500	99.000
47AA	595.912	1.632 .319	.00224	203.270	13.000	29.500	99.000
48AA	790.566	2.165 .423	.00272	200.853	13.000	31.500	99.000

Figure 4 - Typical Data Reduction Print-Out For a Complete Run (Sheet 4 of 5)

DOWNCOMER CARRYUNDER CALCULATION

$H_1 = 12.0$

RUN	GPM	VEL	AL	CFM	H3	H2	TE
49AA	923.183	2.528 .494	.01047	200.853	13.000	34.500	99.500
50AA	1092.324	2.992 .584	.03523	199.476	13.000	37.500	99.500
51AA	1203.683	3.297 .644	.04429	199.476	13.000	40.500	99.500
52AA	1343.117	3.679 .719	.05433	199.476	13.000	43.500	99.500
53AA	1454.806	3.985 .779	.06042	199.476	13.000	46.500	99.500

Figure 4 - Typical Data Reduction Print-Out For a Complete Run (Sheet 5 of 5)

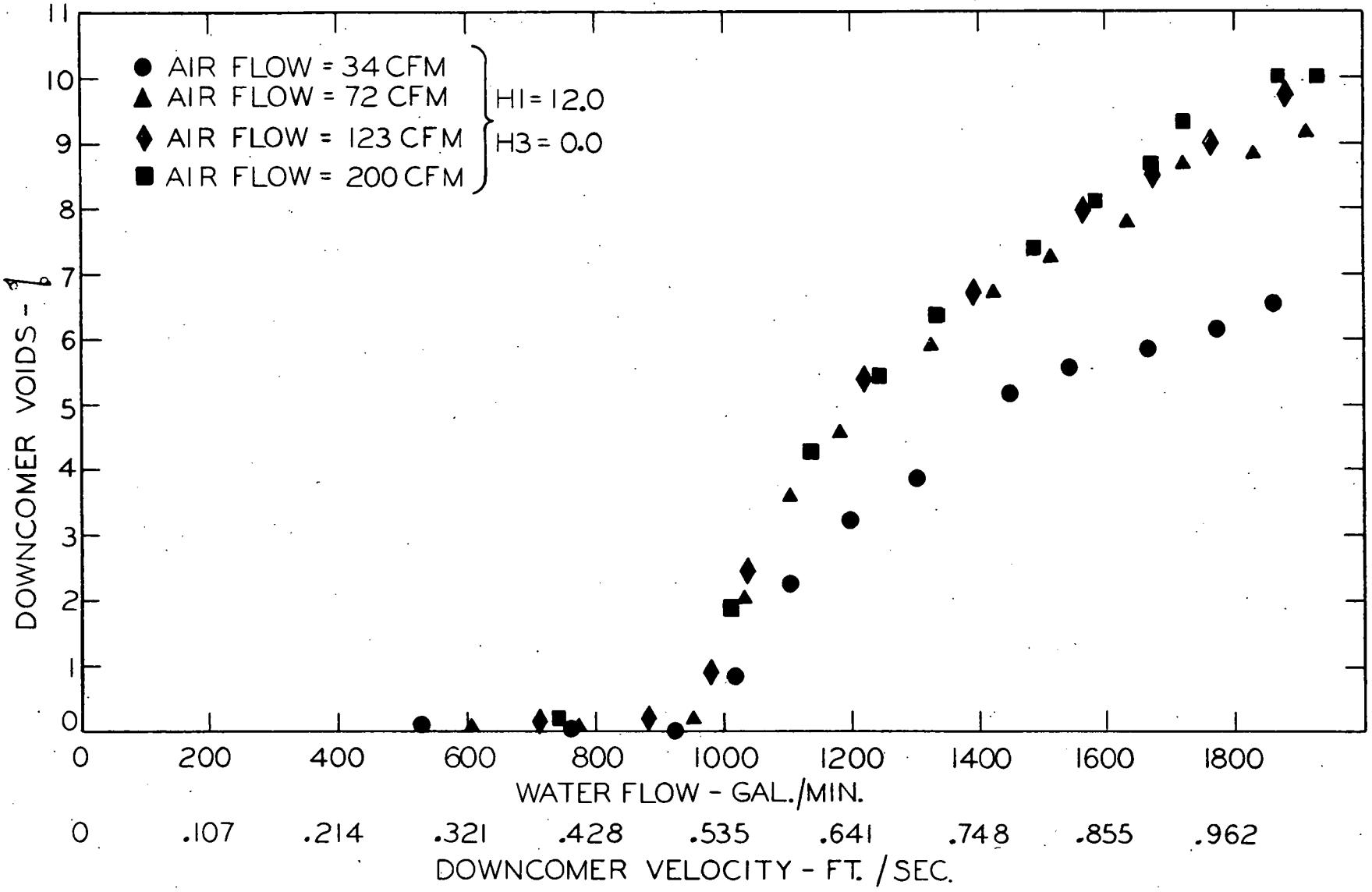

Figure 5 - Effect of Air Flow on Downcomer Voids (Loop Temp. $90^{\circ}F \pm 6^{\circ}$)

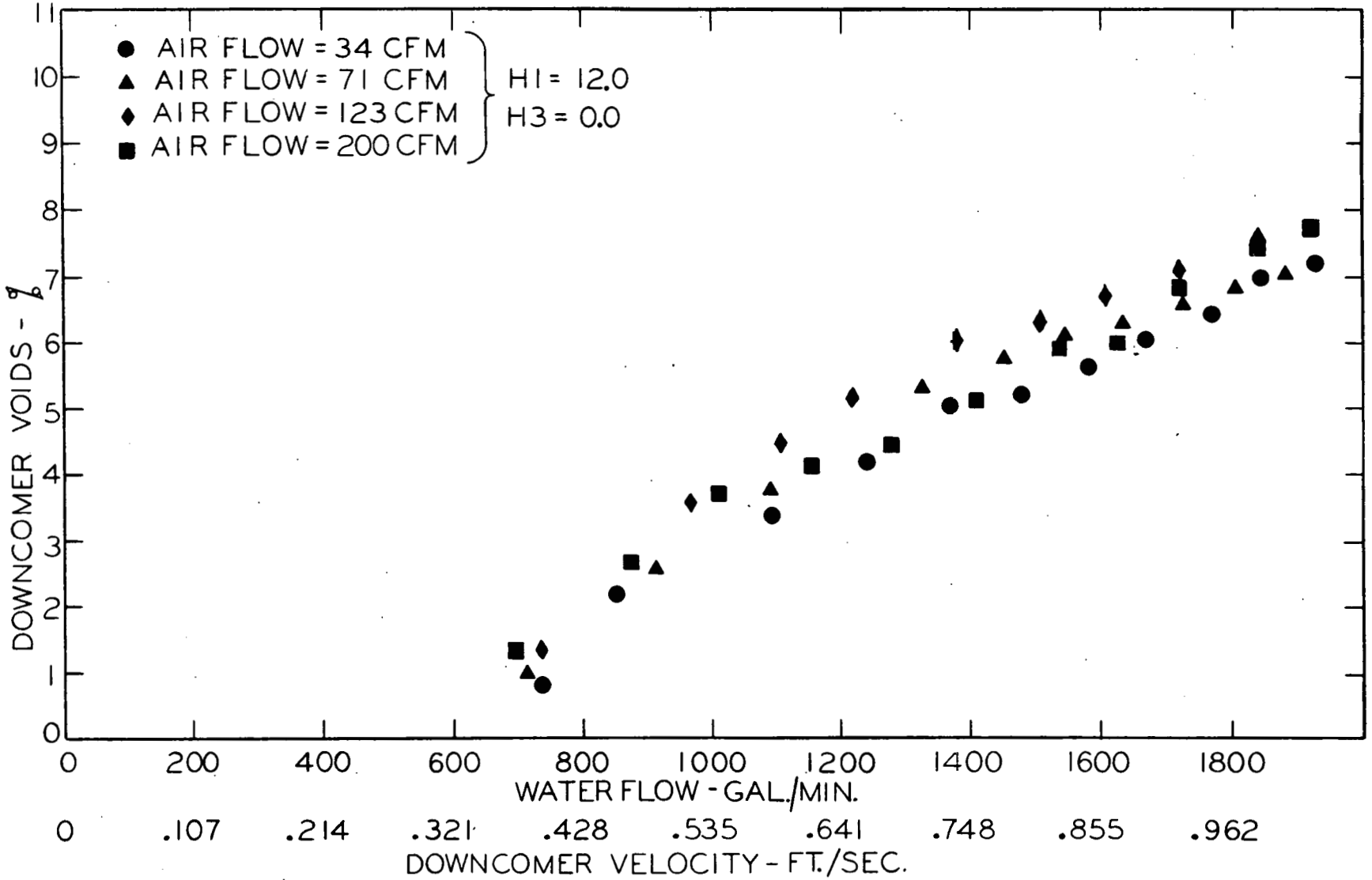

Figure 6 - Effect of Air Flow on Downcomer Voids (Loop Temp. 150°F ± 3°)

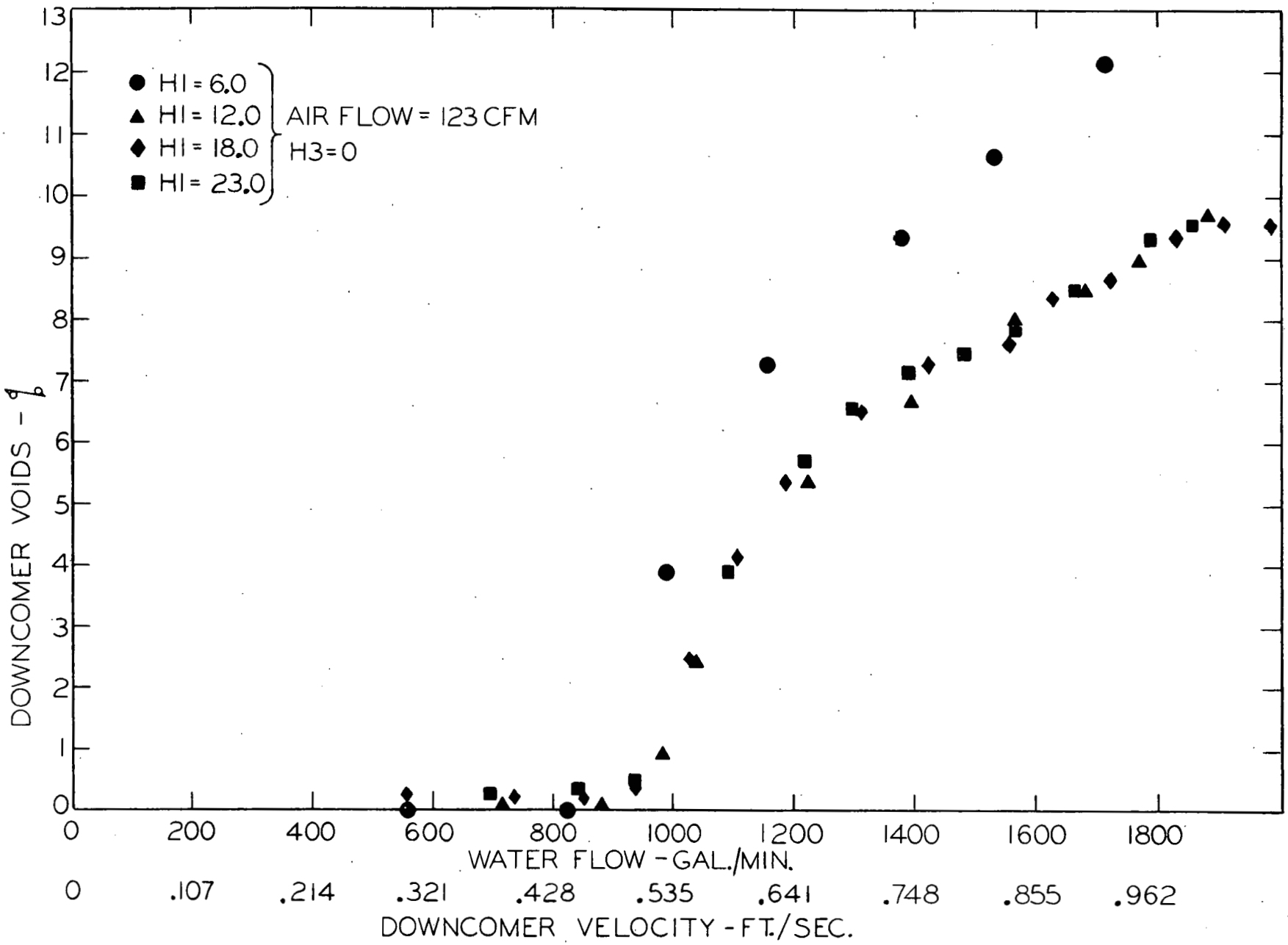

Figure 7 - Effect of Riser Length on Downcomer Voids (Loop Temp. 90°F ± 5°)

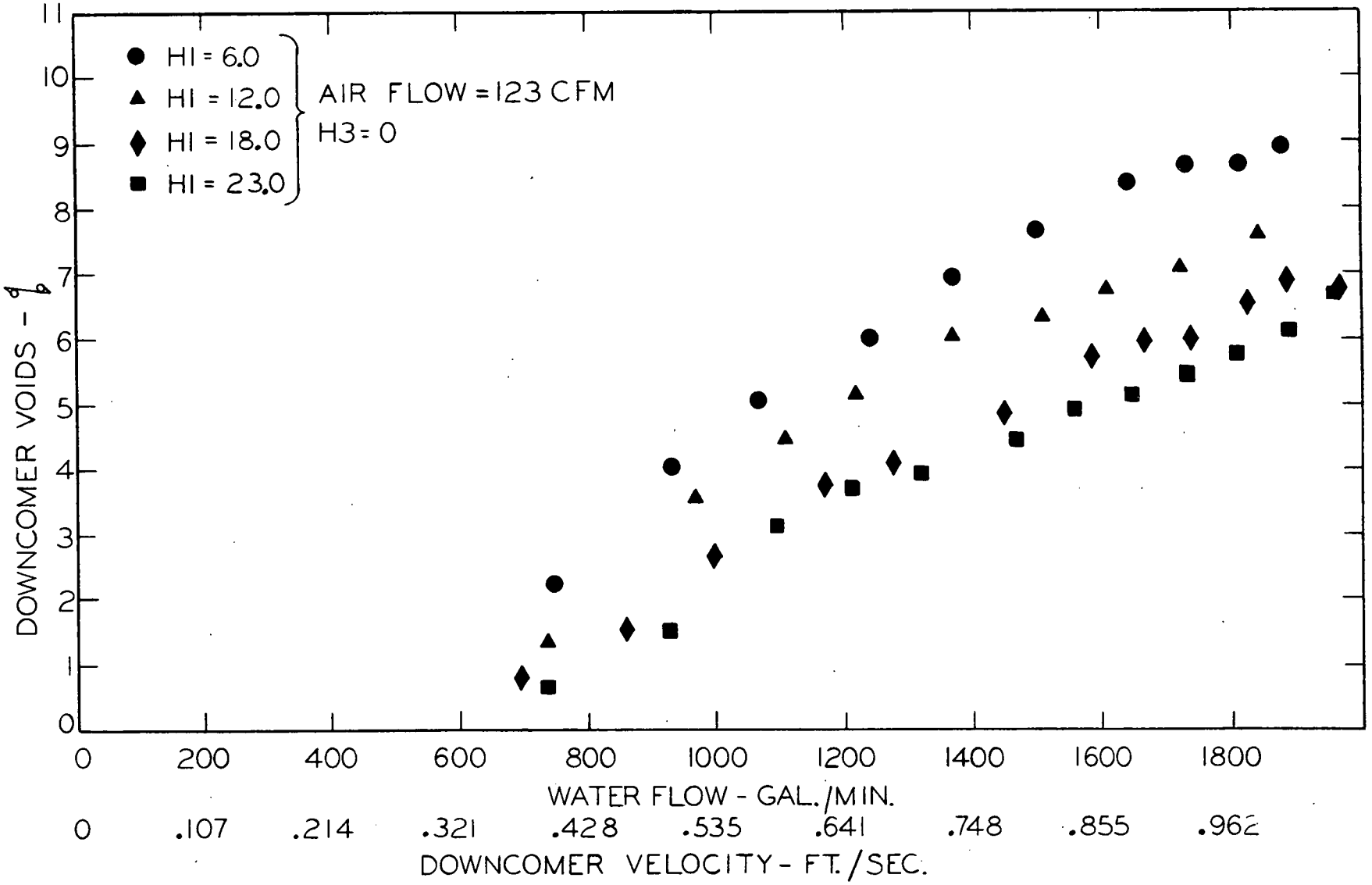

Figure 8 - Effect of Riser Length on Downcomer Voids (Loop Temp. $150^{\circ}F \pm 10^{\circ}$)

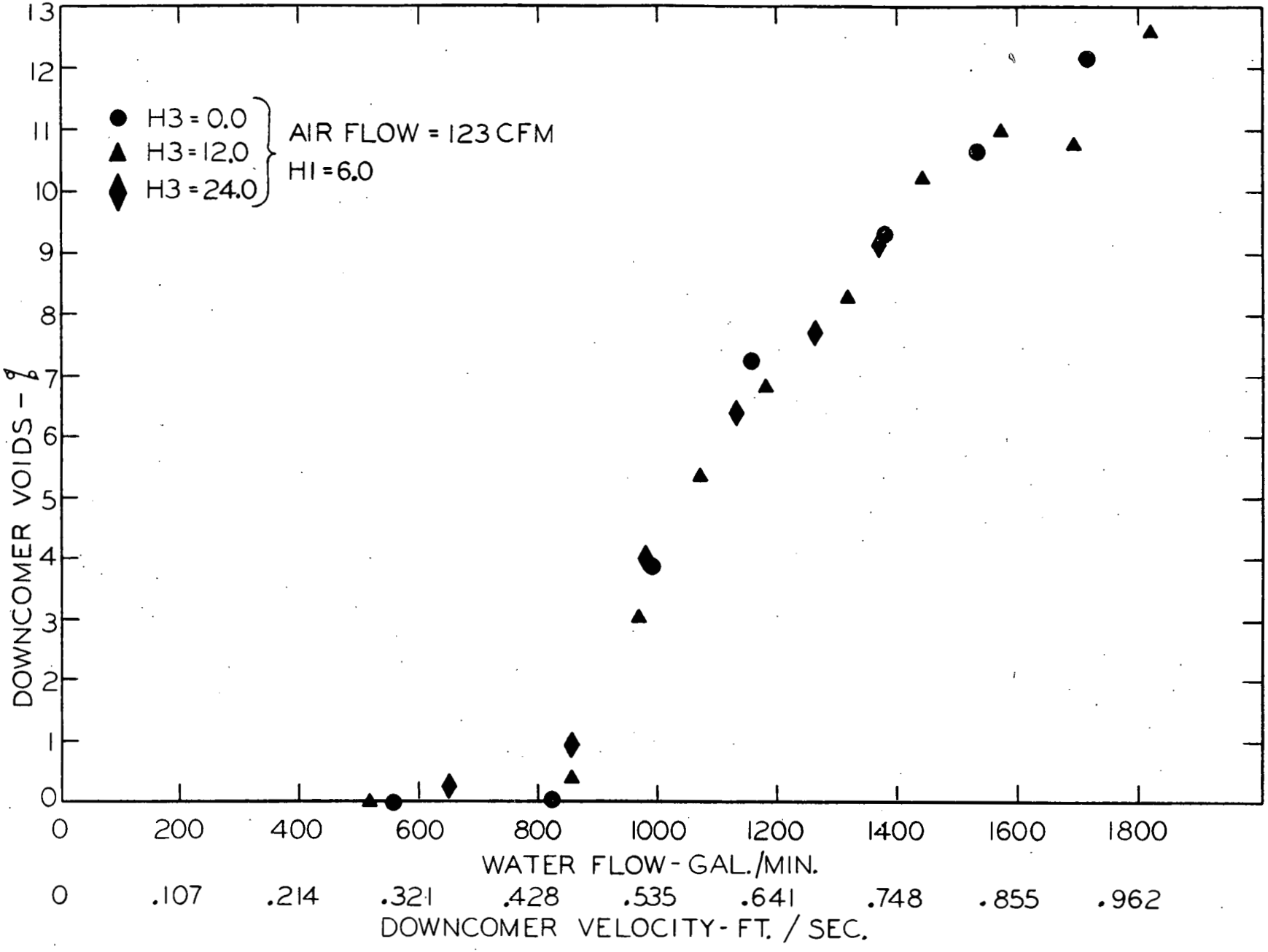

Figure 9 - Effect of Initial Water Level on Downcomer Voids (Loop Temp. $90^{\circ}F \pm 5^{\circ}$)

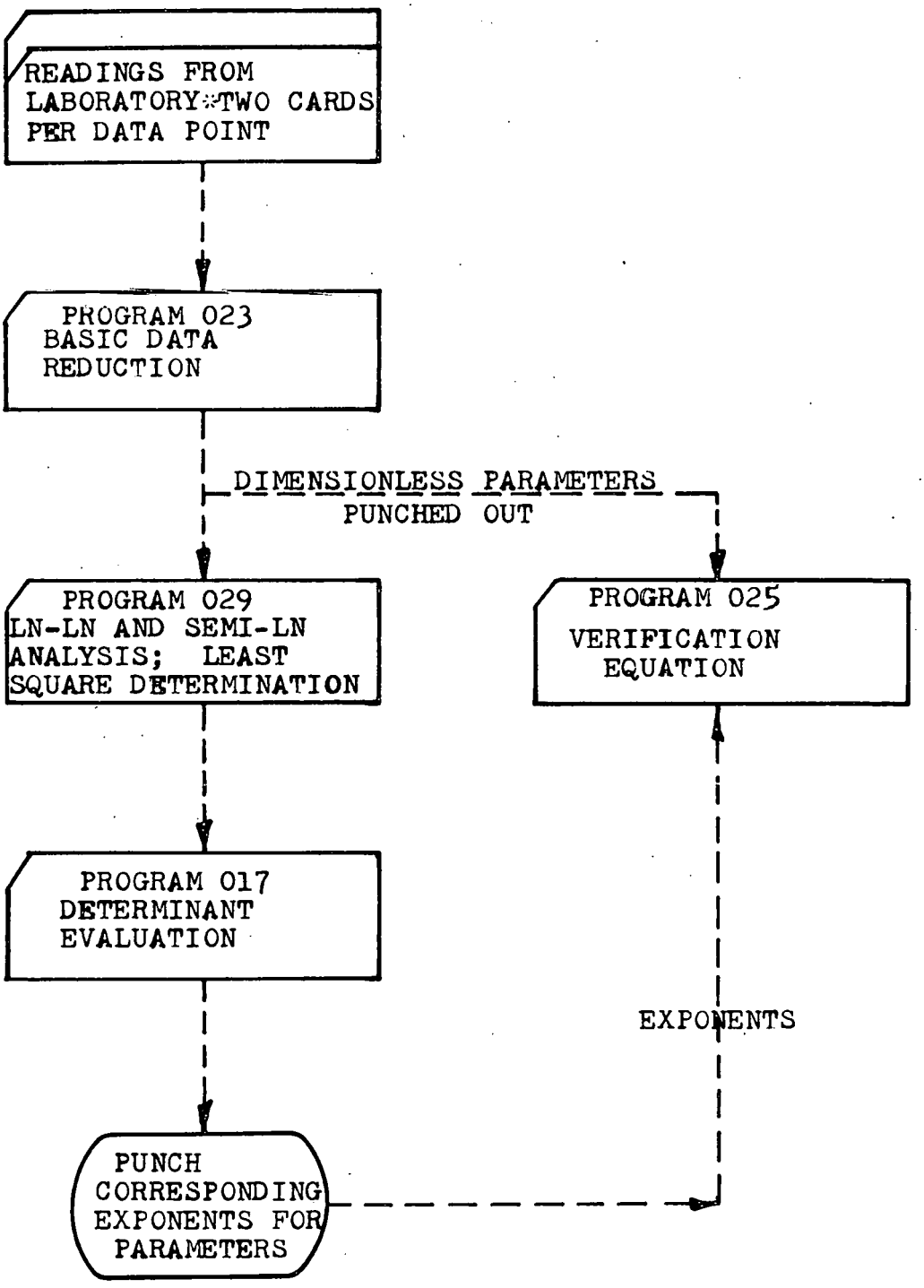

Figure 10 - Systematics of Correlation Procedure

```
08300 C      PROGRAM 029,DATA CONVERSION AND LEAST SQUARE ANALYSIS  CURRIER
08300 C
08300 C                                                  SWITCH 1 OFF,LOG-LOG
08300 C                                                  SWITCH 1 ON  ,SEMI-LOG
08300 C
08300        DIMENSION CONSK(5),E(18),P(20),B(15,20)
08300        DO 14 I=1,5
08312        READ 37,CONSK(I)
08360        CONSK(I)=LOG(CONSK(I))
08432     14 CONTINUE
08468        DO 01 I=1,18
08480        READ 37,E(I)
08528     01 CONTINUE
08564        DO 15 I=1,20
08576        P(I)=0.
08624        DO 16 J=1,15
08636        B(J,I)=0.
08720     16 CONTINUE
08756     15 CONTINUE
08792     18 READ 39
08816        DO 25 I=1,11,5
08828        READ 37,P(I),P(I+1),P(I+2),P(I+3),P(I+4)
09020     25 CONTINUE
09056        READ 41
09080        READ 41
09104        DO 02 I=1,13
09116        P(I)=E(I)*LOG(P(I))
09224     02 CONTINUE
09260        DO 05 I=1,5
09272        IF(SENSE SWITCH 1)03,04
09292     04 P(I+13)=CONSK(I)-P(1)
09376        GO TO 05
09384     03 P(I+13)=LOG(P(1)-CONSK(I))
09480     05 CONTINUE
09516        N=1
09540        DO 06 I=2,18
09552        IF(E(I)-1.)07,11,07
09644     07 IF(E(I))08,06,08
09724     08 DO 09 J=14,18
09736        P(J)=P(J)-P(I)
09844     09 CONTINUE
09880        GO TO 06
09888     11 P(N)=P(I)
09960        N=N+1
09996     06 CONTINUE
10032        N=N-1
10068        NN=N-5
10104        DO 13 J=1,NN
10116        DO 12 I=1,N
10128        B(J,I)=P(J)*P(I)+B(J,I)
10344     12 CONTINUE
10380     13 CONTINUE
10416        L=N-NN
10452        IF(SENSE SWITCH 9)17,18
10472     17 PUNCH 45,NN,L
10508        DO 19 I=1,N
10520        DO 20 J=1,NN,5
10532        PUNCH 36,B(J,I),B(J+1,I),B(J+2,I),B(J+3,I),B(J+4,I)
10904     20 CONTINUE
10940     19 CONTINUE
```

Figure 11 - Fortran Statement for Program 029 (Sheet 1 of 3)

```
T0976          STOP
T1024     45 FORMAT(I2,I2)
T1052     36 FORMAT(E14.7,E14.7,E14.7,E14.7,E14.7)
T1094     39 FORMAT(10H          )
T1138     41 FORMAT(1H )
T1164     37 FORMAT(F14.4,F14.4,F14.4,F14.4,F14.4)
T1206          END
```

Figure 11 - Fortran Statement for Program 029 (Sheet 2 of 3)

NOMENCLATURE PROG. 029

CONSK (I)	-	Constants
E (I)	-	Exponents
P (I)	-	Dimensionless Parameters
B (J,I)	-	Least Square Coefficients
L	-	Number of Constants
NN	-	Number of Unknowns

FIGURE 11 - FORTRAN STATEMENT FOR PROGRAM 029(SHEET 3 OF 3)

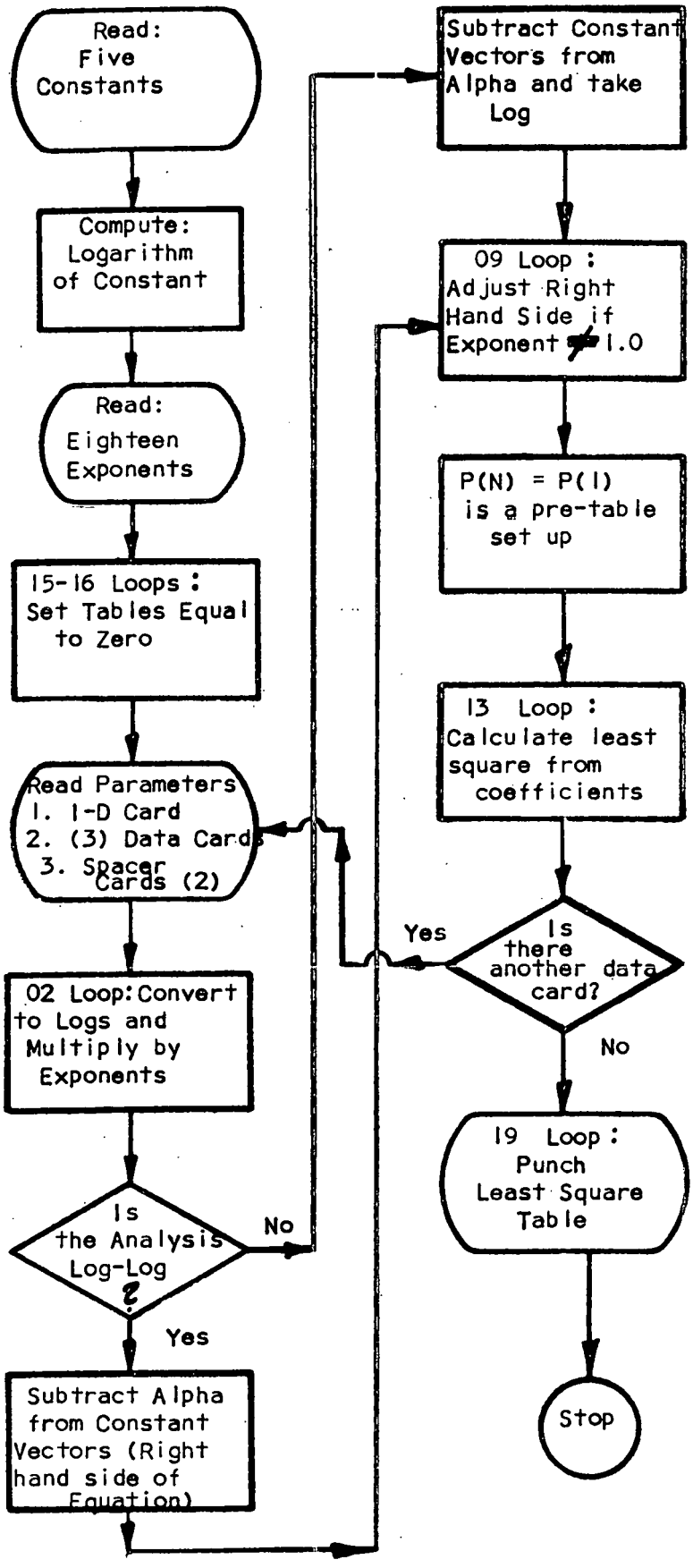

Figure 12 - Logic Diagram for Program 029

```
C  SOLUTION OF N NON-HOMOGENEOUS SIMULTANEOUS LINEAR EQUATIONS BY THE
C    JORDAN METHOD OF ELIMINATION      ** P.R. HENNINGSEN   IBM  MILW.
C  N MUST BE LESS THAN OR EQUAL TO 15
C  UP TO 5 CONSTANT VECTORS MAY BE INCLUDED PER SET OF EQUATIONS
      DIMENSION A(15,20),P(20)
      IF(SENSE SWITCH 9) 1,1
    1 IF (SENSE SWITCH 9) 999,2
C  RESET AREAS TO FLOATING ZEROS
    2 DO 25 J=1,20
      P(J)=0.
      DO 25 I=1,15
   25 A(I,J)=0.
C  READ SYSTEM SIZE,N AND NO. OF CONSTANT VECTORS,L
      READ 101,N,L
C  READ MATRIX OF COEFFICIENTS AND CONSTANT VECTORS
      NL=N+L
      DO 3 J=1,NL
      DO 3 I=1,N,5
    3 READ 102,A(I,J),A(I+1,J),A(I+2,J),A(I+3,J),A(I+4,J)
C  PRINT MATRIX + CONSTANT VECTORS UNDER CONTROL OF SENSE SWITCH 2
C     SENSE SWITCH 2 ON -BYPASS    ** SENSE SWITCH 2 OFF -PRINT
      IF(SENSE SWITCH 2) 9,4
    4 PRINT 111, N,N
      DO 6  I=1,N
      DO 5  J=1,N,5
    5 PRINT 112, A(I,J),A(I,J+1),A(I,J+2),A(I,J+3),A(I,J+4)
    6 PRINT 113
      PRINT 114,L
      DO 8 J=1,L
      PRINT 115, J
      JN=J+N
      DO 7 I=1,N,5
    7 PRINT 112, A(I,JN),A(I+1,JN),A(I+2,JN),A(I+3,JN),A(I+4,JN)
    8 PRINT 113
C  REDUCE COEFFICIENT MATRIX TO UNIT MATRIX
    9 DO 10 K=1,N
C  REARRANGE ROWS SO THAT A(K,K) IS LARGEST (ABSOLUTELY) OF THE A(J,K)
      KK=K
      TEST= ABS(A(K,K))
      DO 11 I=K,N
      IF(TEST-ABS(A(I,K))) 12,11,11
   11 CONTINUE
      GO TO 13
   12 TEST = ABS(A(I,K))
      KK=I
      GO TO 11
   13 DO 14 J=1,NL
      P(J) = A(KK,J)
      A(KK,J)=A(K,J)
   14 A(K,J)=P(J)
C  DIVIDE ROW K BY A(K,K) SO THAT A(K,K) WILL BE UNITY
      AKK=A(K,K)
      DO 15 J=1,NL
   15 A(K,J)=A(K,J)/AKK
```

Figure 13 - Fortran Statement for Program 17 (Sheet 1 of 2)

```
C  DEVELOP PIVOTAL ROW AND REDUCE KTH COLUMN
      KM1=K-1
      K1=K+1
      IF (KM1)999,47,46
   46 DO 16 I=1,KM1
      AIK=A(I,K)
      DO 16 J=1,NL
      P(J)=A(K,J)*AIK
   16 A(I,J)=A(I,J)-P(J)
      IF (K1-N) 47,47,10
   47 DO 17 I=K1,N
      AIK=A(I,K)
      DO 17 J=1,NL
      P(J)=A(K,J)*AIK
   17 A(I,J)=A(I,J)-P(J)
   10 CONTINUE
C  REDUCTION COMPLETE, TYPE(SW 3 OFF) OR PUNCH(SW 3 ON) SOLUTIONS
      IF(SENSE SWITCH 3) 20,30
   30 DO 31 J=1,L
      PRINT 117,J
      JN=J+N
      DO 32 I=1,N,5
   32 PRINT 112, A(I,JN),A(I+1,JN),A(I+2,JN),A(I+3,JN),A(I+4,JN)
   31 PRINT 113
      GO TO 1
   20 DO 21 J=1,L
      PUNCH 117,J
      JN=J+N
      DO 21 I=1,N,5
   21 PUNCH 102, A(I,JN),A(I+1,JN),A(I+2,JN),A(I+3,JN),A(I+4,JN)
      GO TO 1
  999 STOP
  101 FORMAT(I2,I2)
  102 FORMAT(E14.7,E14.7,E14.7,E14.7,E14.7)
  111 FORMAT(////14X13,3H X ,I3,4X22HMATRIX OF COEFFICIENTS,///)
  112 FORMAT(E12.5,5XE12.5,5XE12.5,5XE12.5,5XE12.5)
  113 FORMAT(/)
  114 FORMAT(//20X,I2,4X18HCONSTANT   VECTORS,//)
  115 FORMAT(20HCONSTANT VECTOR NO. ,I2)
  117 FORMAT(33HSOLUTION FOR CONSTANT VECTOR NO. ,I2)
      END
```

Figure 13 - Fortran Statement for Program 17 (Sheet 2 of 2)

```
9 X  9    MATRIX OF COEFFICIENTS

 2.22913E+04    8.04053E+02    3.23993E+03   -1.08930E+04   -4.34956E+04
 1.24344E+04   -1.81773E+04   -2.90218E+04   -2.33726E+03    2.29268E+04

 8.04053E+02    6.16091E+01    1.54358E+02   -3.90032E+02   -1.56675E+03
 4.38078E+02   -6.33421E+02   -1.04388E+03   -9.87124E+01    8.16540E+02


SOLUTION FOR CONSTANT VECTOR NO.  1
 3.79717E-01   -6.92048E-01    5.04683E-01    6.02576E-01    7.30338E-01
 5.20100E-01   -7.29847E-01   -1.02053E-00   -1.01076E-00    .00000E-99

SOLUTION FOR CONSTANT VECTOR NO.  2
 1.43143E-01   -6.82285E-01    5.22780E-01   -1.52342E-01    2.46820E-01
-1.75778E-01   -3.42278E-01    9.82646E-02    1.05343E-01    .00000E-99

SOLUTION FOR CONSTANT VECTOR NO.  3
 3.74025E-01   -6.88955E-01    5.07129E-01    9.33028E-01    1.19662E-00
 2.90124E-01   -8.09763E-01   -8.65386E-01   -8.55775E-01    .00000E-99

SOLUTION FOR CONSTANT VECTOR NO.  4
 1.29497E-01   -6.80943E-01    5.10426E-01    5.12447E-01    8.03600E-01
 6.81072E-02   -6.08131E-01   -4.28592E-01   -4.19330E-01    .00000E-99

SOLUTION FOR CONSTANT VECTOR NO.  5
 8.12224E-02   -6.77020E-01    5.18068E-01    1.52013E-02    4.24212E-01
-2.17584E-01   -3.88507E-01    9.05856E-02    9.87230E-02    .00000E-99

STOP
```

Figure 14 - Sample Print-Out for Program 17

```
08300 C      DOWNCOMER CARRYUNDER VERIFICATION    1-21-63  GRENDA-CURRIER
08300 C
08300 C                                          SWITCH 1 ON,SEMI-LOG
08300 C                                          SWITCH 1 OFF,LOG-LOG
08300 C
08300        DIMENSION E(13),P(15)
08300        READ 38,CONSK
08324        DO 03 L=1,13
08336     03 READ 38,E(L)
08420        PRINT 398
08444        PRINT 399
08468        PAUSE
08480     22 PRINT 400
08504        IF(SENSE SWITCH 1)200,201
08524    200 PRINT 401
08548        GO TO 18
08556    201 PRINT 403
08580     18 PRINT 01
08604        DO 444 NIN=1,50
08616        READ 39
08640        DO 25 K=1,11,5
08652        READ 37,P(K),P(K+1),P(K+2),P(K+3),P(K+4)
08844     25 CONTINUE
08880        READ 41
08904        READ 41
08928        X=1.
08952        DO 02 J=2,13
08964        X=(P(J)**E(J))*X
09060     02 CONTINUE
09096        IF(SENSE SWITCH 1)300,301
09116    300 Y=CONSK*EXP(X)
09152        GO TO 302
09160    301 Y=CONSK*(X**(-E(1)))
09208    302 PRINT 39,P(1),Y,X
09256        IF(SENSE SWITCH 9)83,444
09276    444 CONTINUE
09312        PRINT 445
09336        GO TO 22
09344     83 STOP
09392     37 FORMAT(F14.4,F14.4,F14.4,F14.4,F14.4)
09434     38 FORMAT(F10.3)
09456     39 FORMAT(10H          ,F14.4,F14.4,F15.5)
09516     41 FORMAT(1H )
09542     01 FORMAT(5X3HRUN,9X11HALPHA MEAS.,3X26HALPHA CALC.    X COORDINATE,/)
09720    398 FORMAT(10X39HADVANCE PAPER,SW1 ON-SEMILOG,OFF-LN-LN.)
09850    399 FORMAT(10X10HPUSH START)
09922    400 FORMAT(15X,33HDOWNCOMER CARRYUNDER VERIFICATION,/)
10054    401 FORMAT(20X17HSEMI-LOG ANALYSIS,//)
10170    403 FORMAT(20X16HLOG-LOG ANALYSIS,//)
10284    445 FORMAT(////////)
10342        END
```

Figure 15 - Fortran Statement for Program 025(Sheet 1 of 2)

NOMENCLATURE PROG. 025

CONSK	-	Constant
E (L)	-	Exponent
P (K)	-	Dimensionless Parameters
X	-	X Coordinate
Y	-	Alpha Calculated

FIGURE 15 - FORTRAN STATEMENT FOR PROGRAM 025
(SHEET 2 of 2)

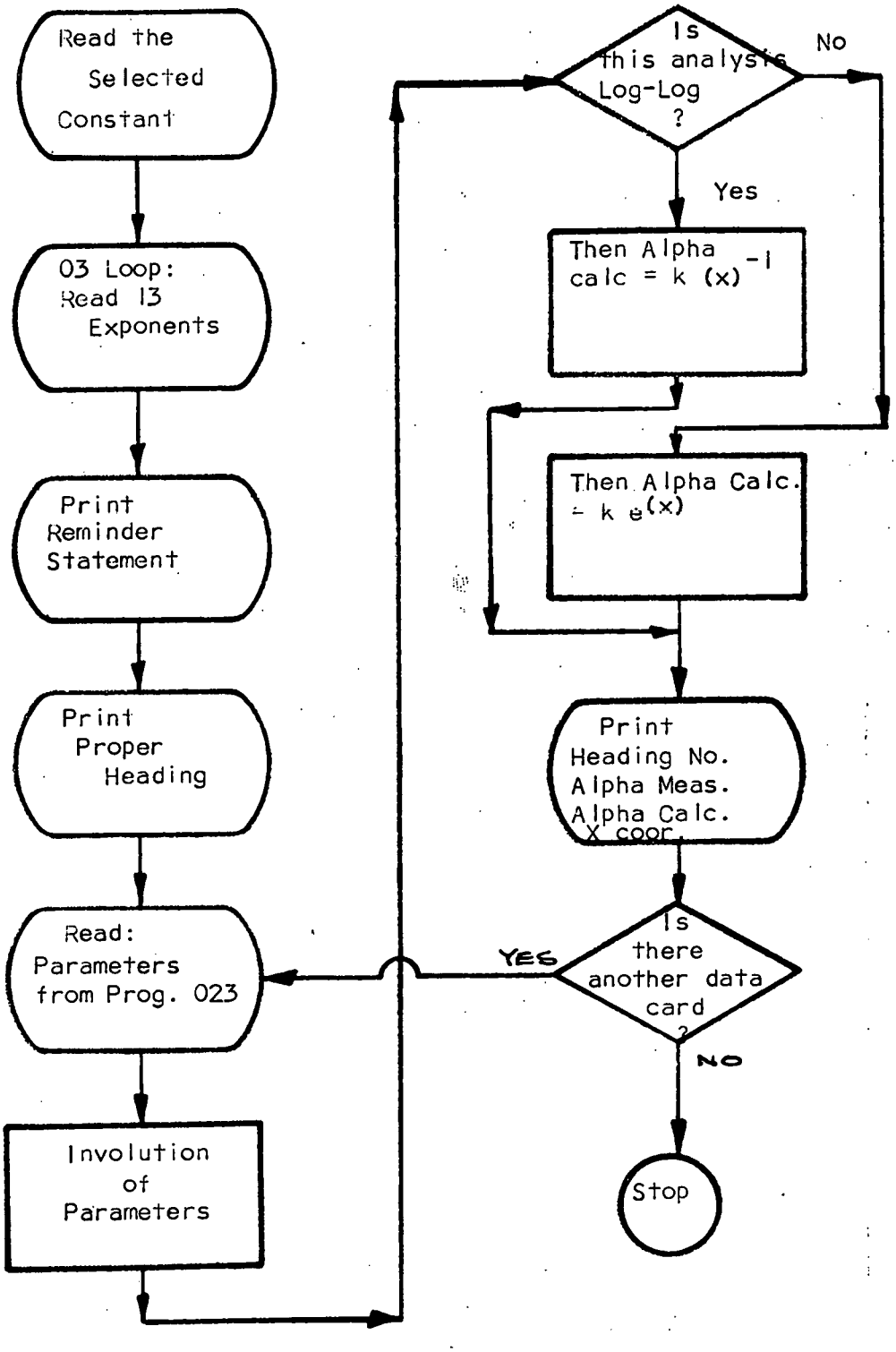

Figure 16 - Logic Diagram for Program 25

DOWNCOMER CARRYUNDER VERIFICATION

LOG-LOG ANALYSIS

RUN	ALPHA MEAS.	ALPHA CALC.	X COORDINATE
7Z	.0387	.0504	.00099
8Z	.0515	.0589	.00084
9Z	.0557	.0647	.00077
10Z	.0585	.0713	.00070
11Z	.0616	.0761	.00065
12Z	.0655	.0816	.00061
18Z	.0459	.0502	.00099
19Z	.0592	.0585	.00085
20Z	.0670	.0640	.00078
21Z	.0727	.0694	.00072
22Z	.0779	.0760	.00065
23Z	.0864	.0815	.00061
24Z	.0882	.0878	.00056
25Z	.0911	.0932	.00053
30Z	.0537	.0563	.00088
31Z	0670	.0643	.00077
32Z	.0795	.0752	.00066
33Z	.0850	.0839	.00059
34Z	.0900	.0883	.00056
35Z	.0971	.0953	.00052
39Z	.0541	.0593	.00084
40Z	.0636	.0668	.00074
41Z	.0736	.0782	.00063
42Z	.0810	.0830	.00060
43Z	.0864	.0885	.00056
44Z	.0932	.0946	.00052
45Z	.0999	.1007	.00049
46Z	.1003	.1054	.00047
6AA	.0332	.0406	.00123
7AA	.0363	.0454	.00110
8AA	.0426	.0512	.00097
9AA	.0472	.0571	.00087
10AA	.0537	.0611	.00081
11AA	.0586	.0644	.00077
12AA	.0613	.0683	.00073
13AA	.0642	.0738	.00067
14AA	.0647	.0775	.00064
15AA	.0651	.0829	.00060
22AA	.0362	.0455	.00109
23AA	.0460	.0509	.00098
24AA	.0531	.0561	.00089
25AA	.0573	.0594	.00084
26AA	.0637	.0641	.00077
27AA	.0698	.0676	.00073
28AA	.0763	.0738	.00067
29AA	.0786	.0767	.00065
30AA	.0852	.0803	.00062
31AA	.0857	.0851	.00058
32AA	.0935	.0901	.00055
39AA	.0448	.0511	.00097
40AA	.0509	.0559	.00089
41AA	.0573	.0620	.00080

Figure 17 - Sample Print-Out for Program 25(Sheet 1 of 2)

DOWNCOMER CARRYUNDER VERIFICATION

LOG-LOG ANALYSIS

RUN	ALPHA MEAS.	ALPHA CALC.	X COORDINATE
42AA	.0617	.0662	.00075
43AA	.0670	.0708	.00070
44AA	.0677	.0763	.00065
45AA	.0753	.0816	.00061
46AA	.0906	.0886	.00056
51AA	.0442	.0551	.00090
52AA	.0543	.0632	.00078
53AA	.0604	.0704	.00070
6BB	.0239	.0358	.00139
7BB	.0365	.0439	.00113
8BB	.0411	.0490	.00101
9BB	.0459	.0526	.00094
10BB	.0522	.0564	.00088
11BB	.0540	.0617	.00080
12BB	.0584	.0652	.00076
13BB	.0630	.0709	.00070
19BB	.0518	.0484	.00103
20BB	.0640	.0555	.00090
21BB	.0733	.0639	.00078
22BB	.0822	.0703	.00071
23BB	.0846	.0762	.00065
29BB	.0520	.0499	.00100
30BB	.0569	.0541	.00092
31BB	.0646	.0590	.00084
32BB	.0703	.0642	.00077
7CC	.0418	.0486	.00102
8CC	.0454	.0537	.00093
9CC	.0540	.0598	.00083
10CC	.0632	.0634	.00078
11CC	.0650	.0685	.00072
12CC	.0681	.0722	.00069
13CC	.0729	.0773	.00064
14CC	.0757	.0803	.00062
15CC	.0785	.0841	.00059
23CC	.0637	.0545	.00091
24CC	.0702	.0589	.00084
25CC	.0799	.0645	.00077
26CC	.0838	.0712	.00070
27CC	.0855	.0744	.00067
28CC	.0928	.0778	.00064
29CC	.0947	.0828	.00060
30CC	.0959	.0863	.00057
31CC	.1028	.0937	.00053
32CC	.1079	.0974	.00051
40CC	.0653	.0601	.00083
41CC	.0727	.0660	.00075
42CC	.0766	.0725	.00068
43CC	.0839	.0768	.00065
44CC	.0865	.0813	.00061
45CC	.0937	.0873	.00057
46CC	.0957	.0924	.00054

Figure 17 - Sample Print-Out for Program 25(Sheet 2 of 2)

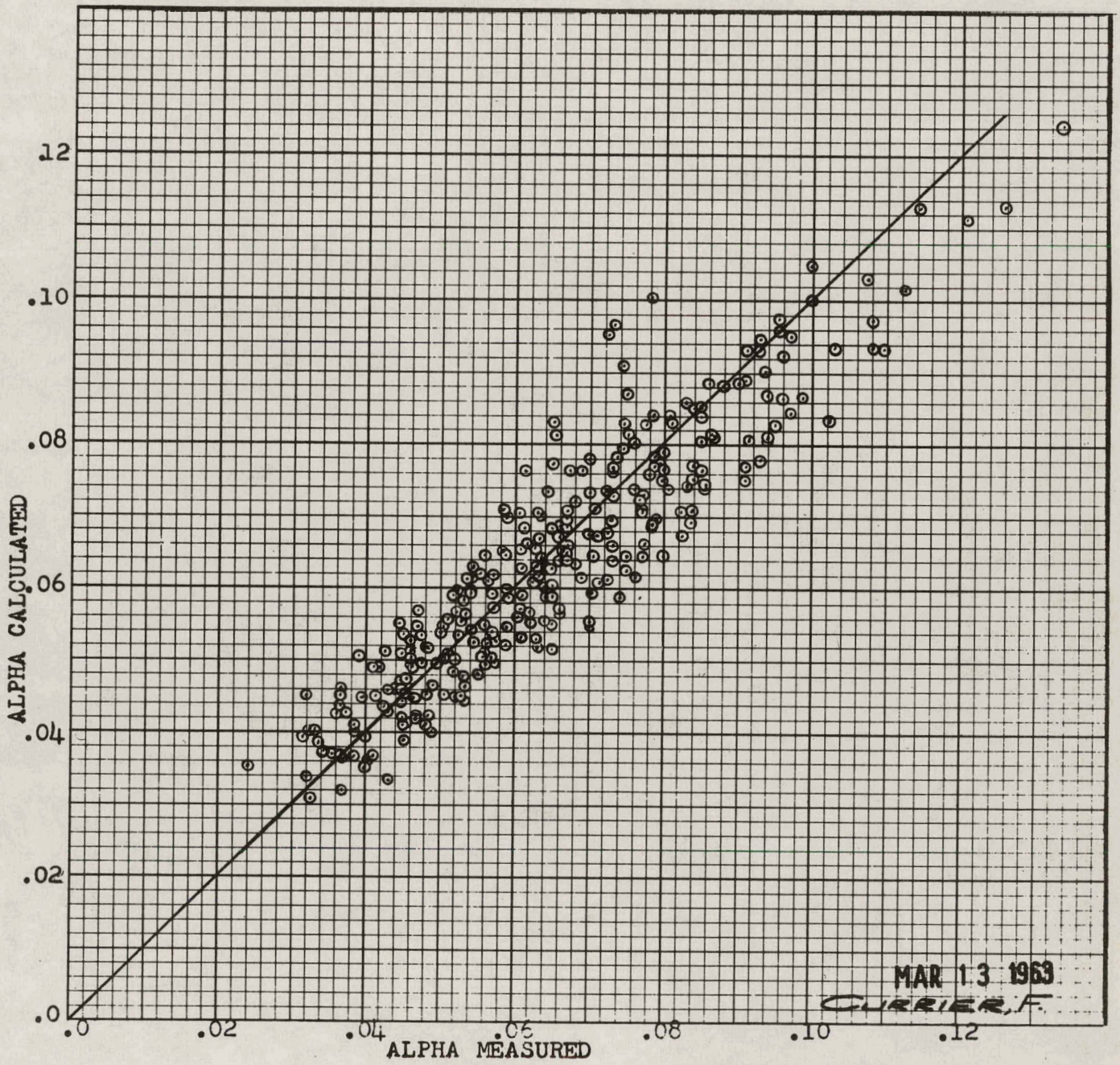

Figure 18 - Error Plot for Carryunder Prediction

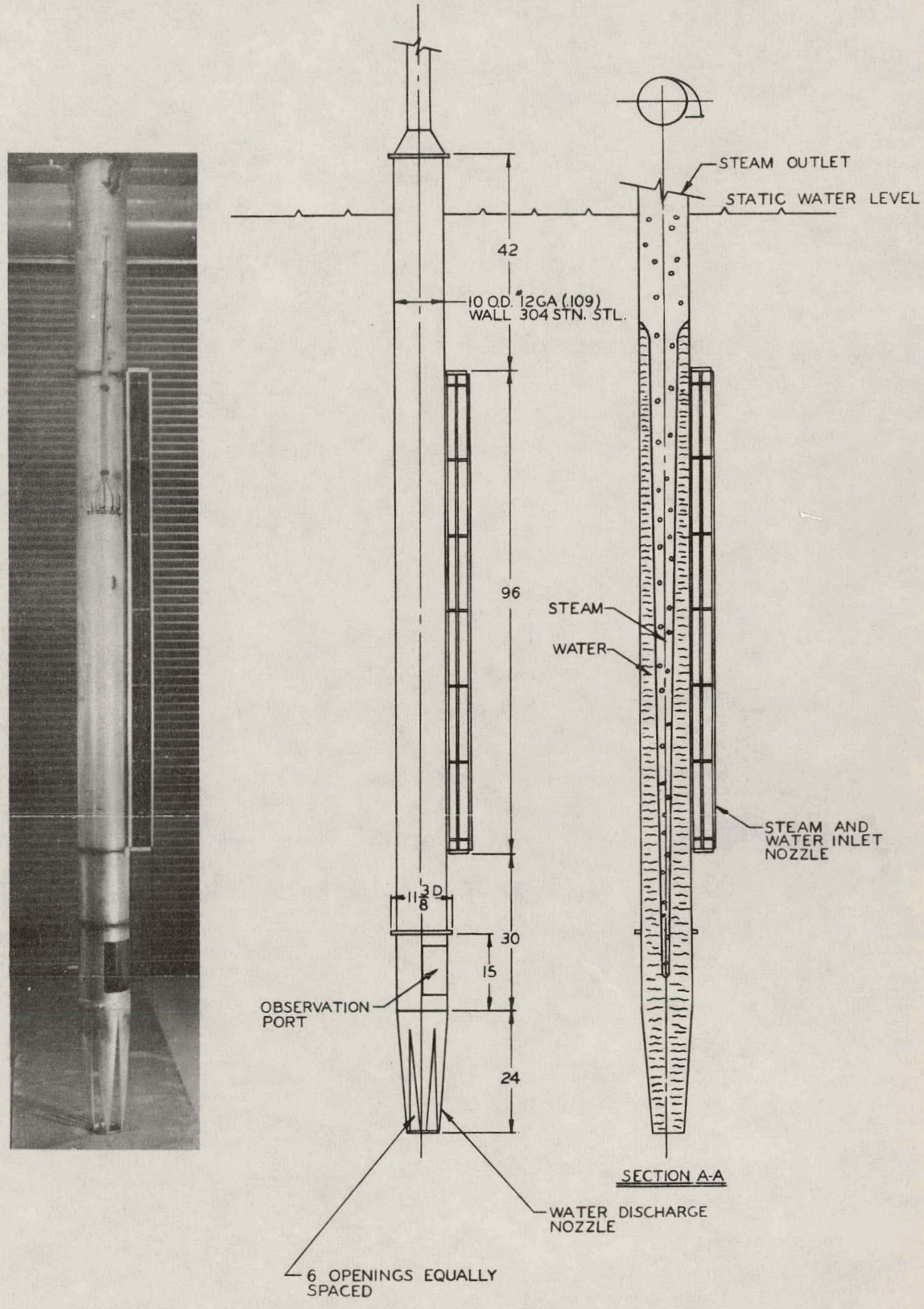

Figure 19 - Ten Inch Diameter Centrifugal Steam Separator Model

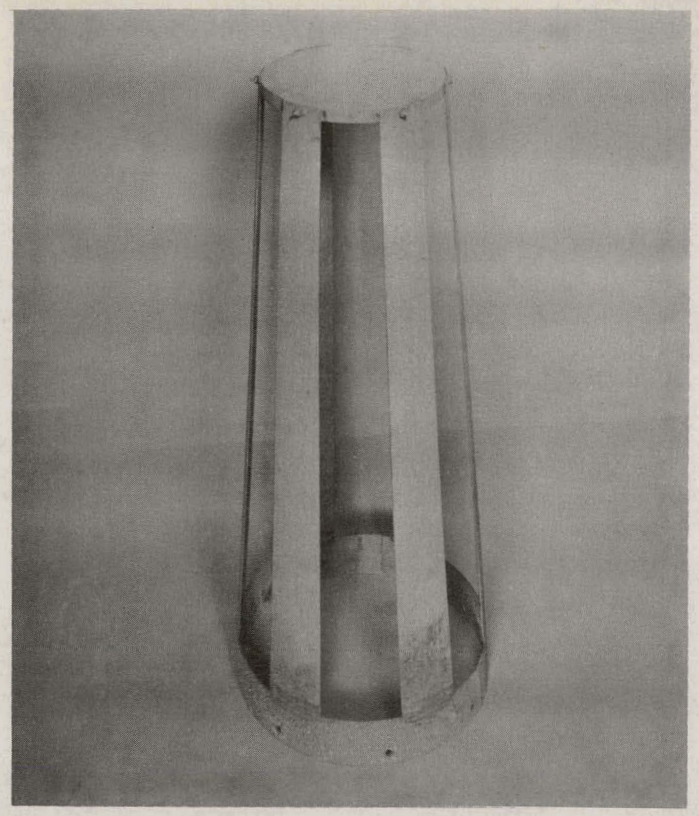

Outlet Nozzle Model 27

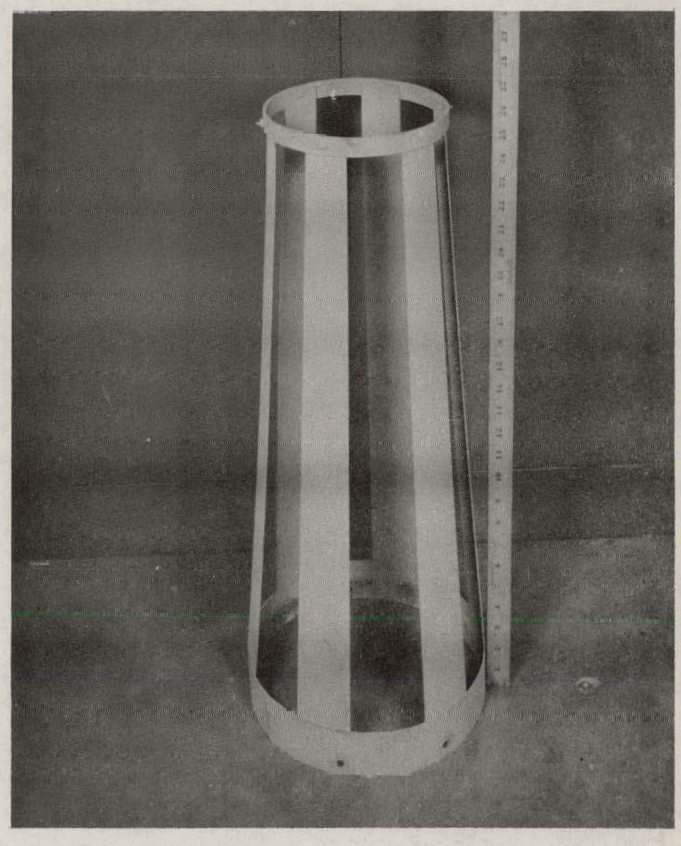

Outlet Nozzle Model 30

Figure 20 - Twenty-four Inch Outlet Nozzles

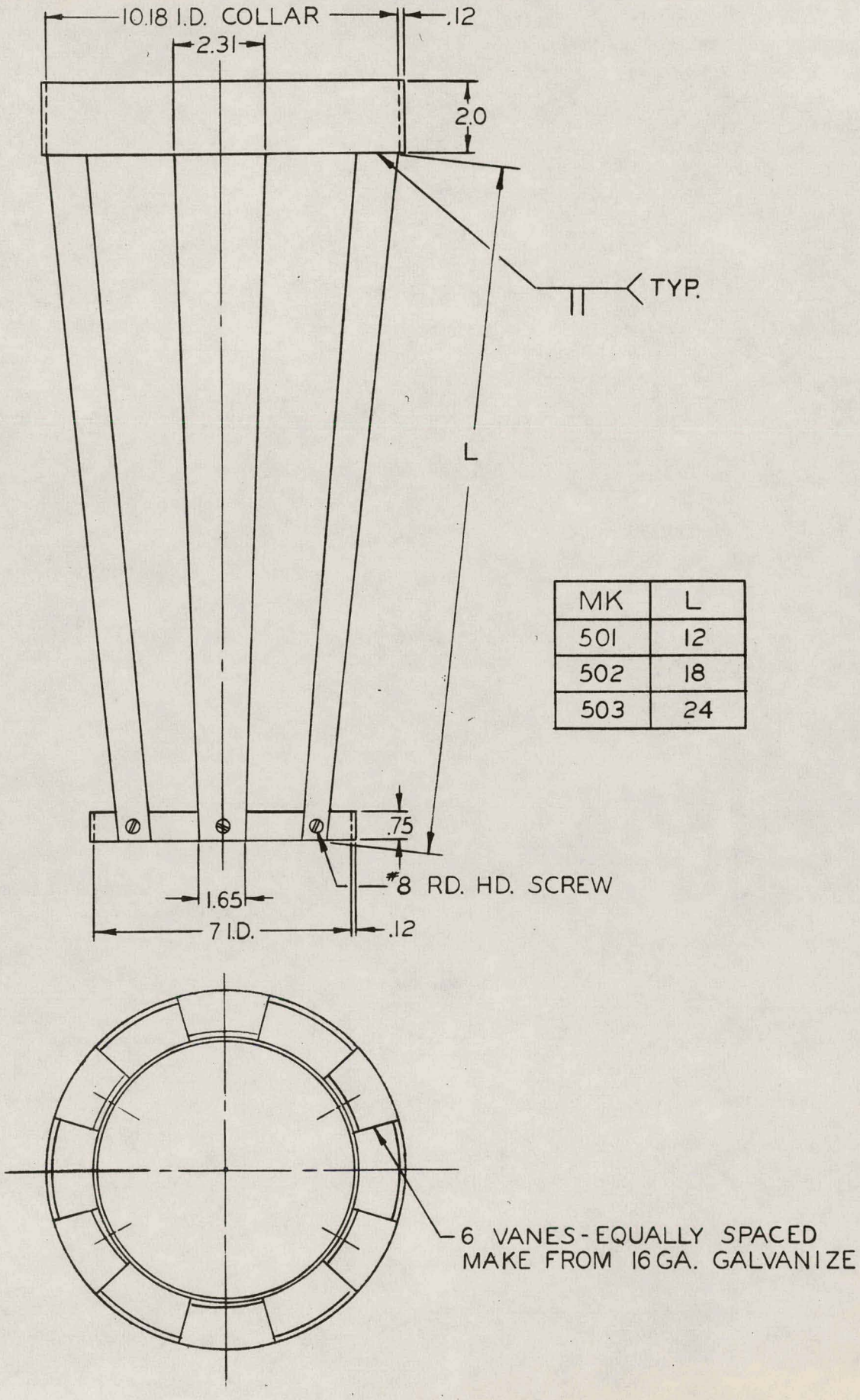

MK	L
501	12
502	18
503	24

Figure 21 - Outlet Nozzle

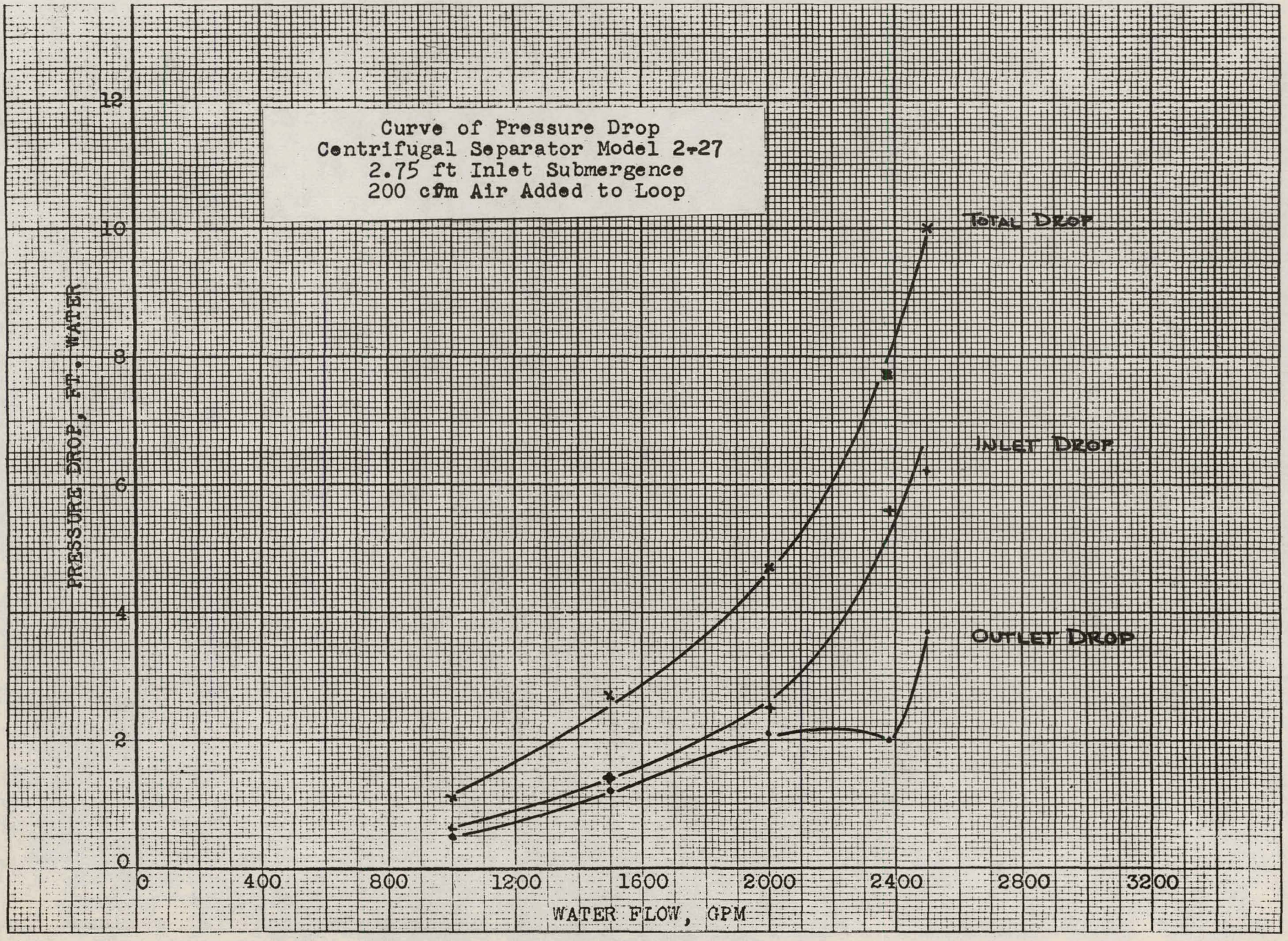

Figure 22 - Performance Curves for Separator Model 2-27

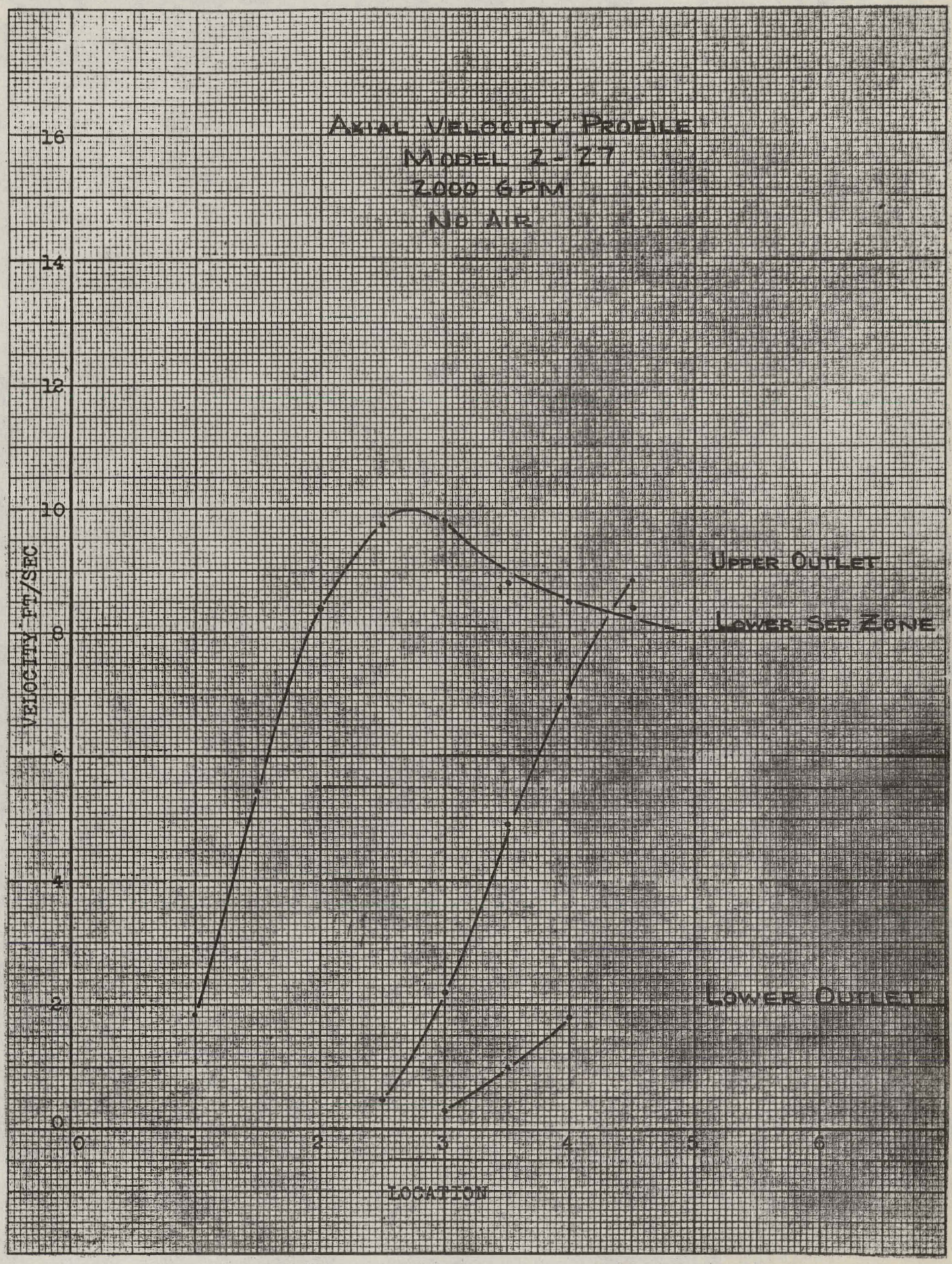

Figure 23 - Axial Velocity Profile of Outlet Model 27

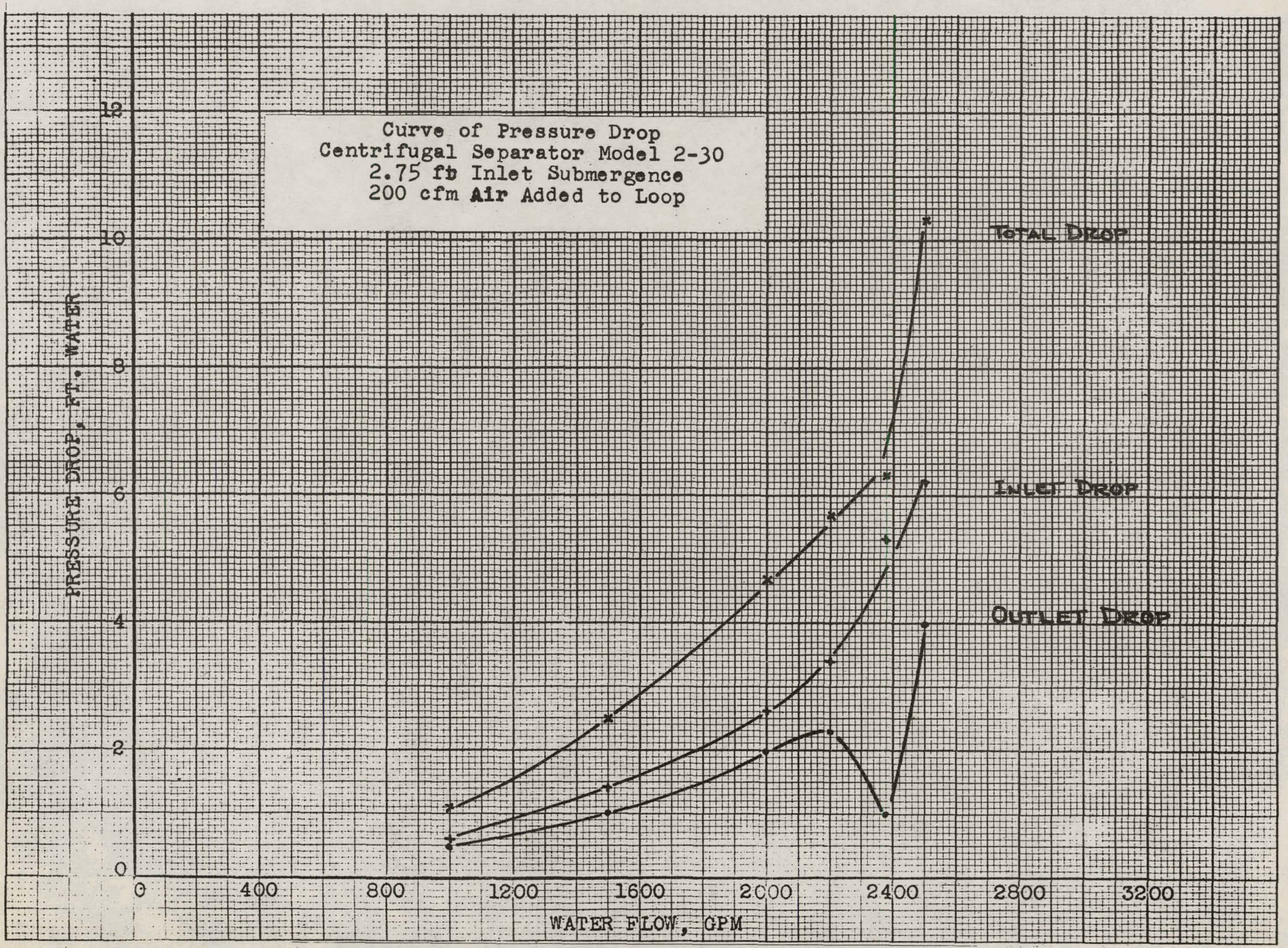

Figure 24 - Performance Curves for Separator Model 2-30

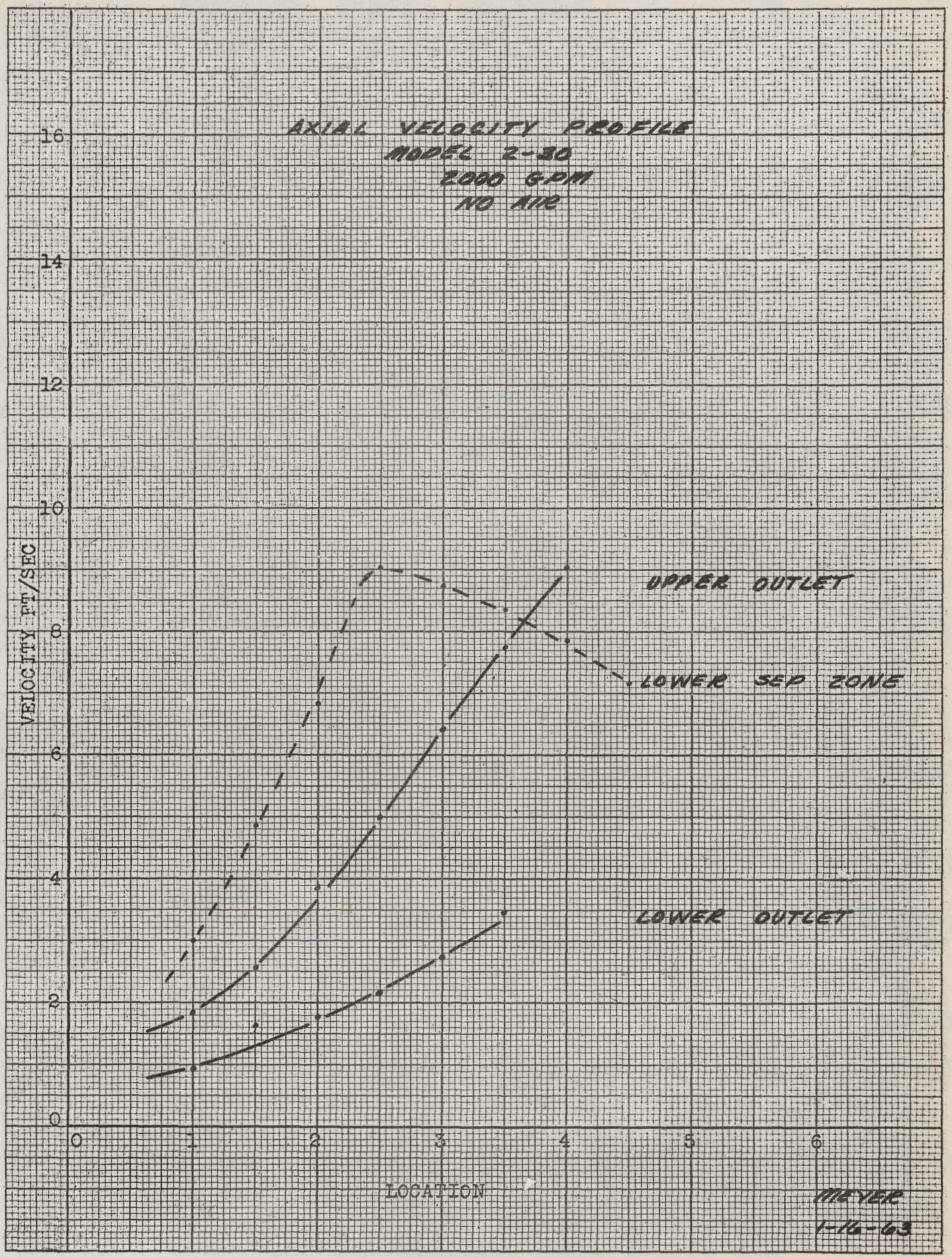

Figure 25 - Axial Velocity Profile of Outlet Model 30

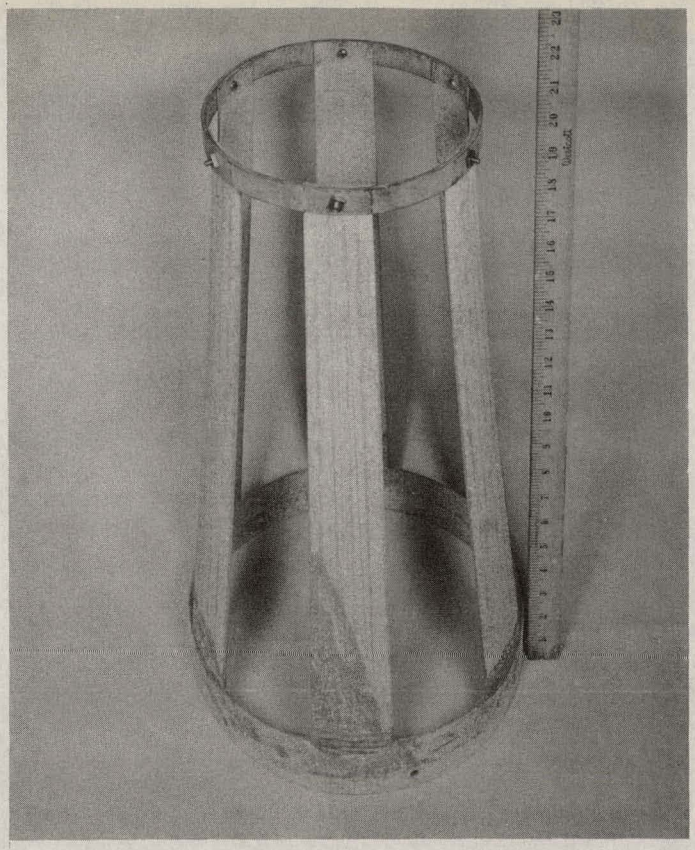

Outlet Nozzle Model 36

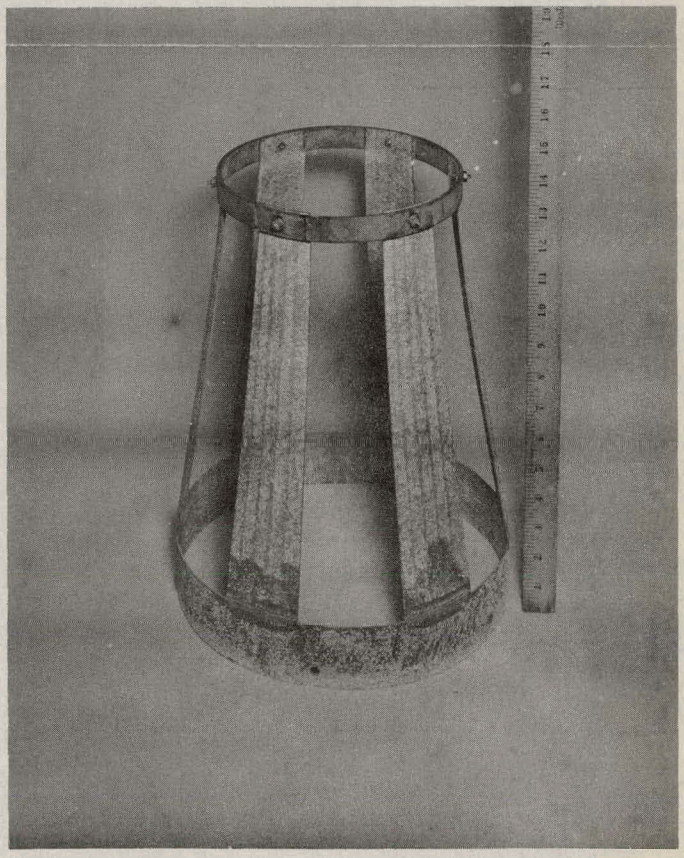

Outlet Nozzle Model 40

Figure 26 - Short Outlet Nozzles

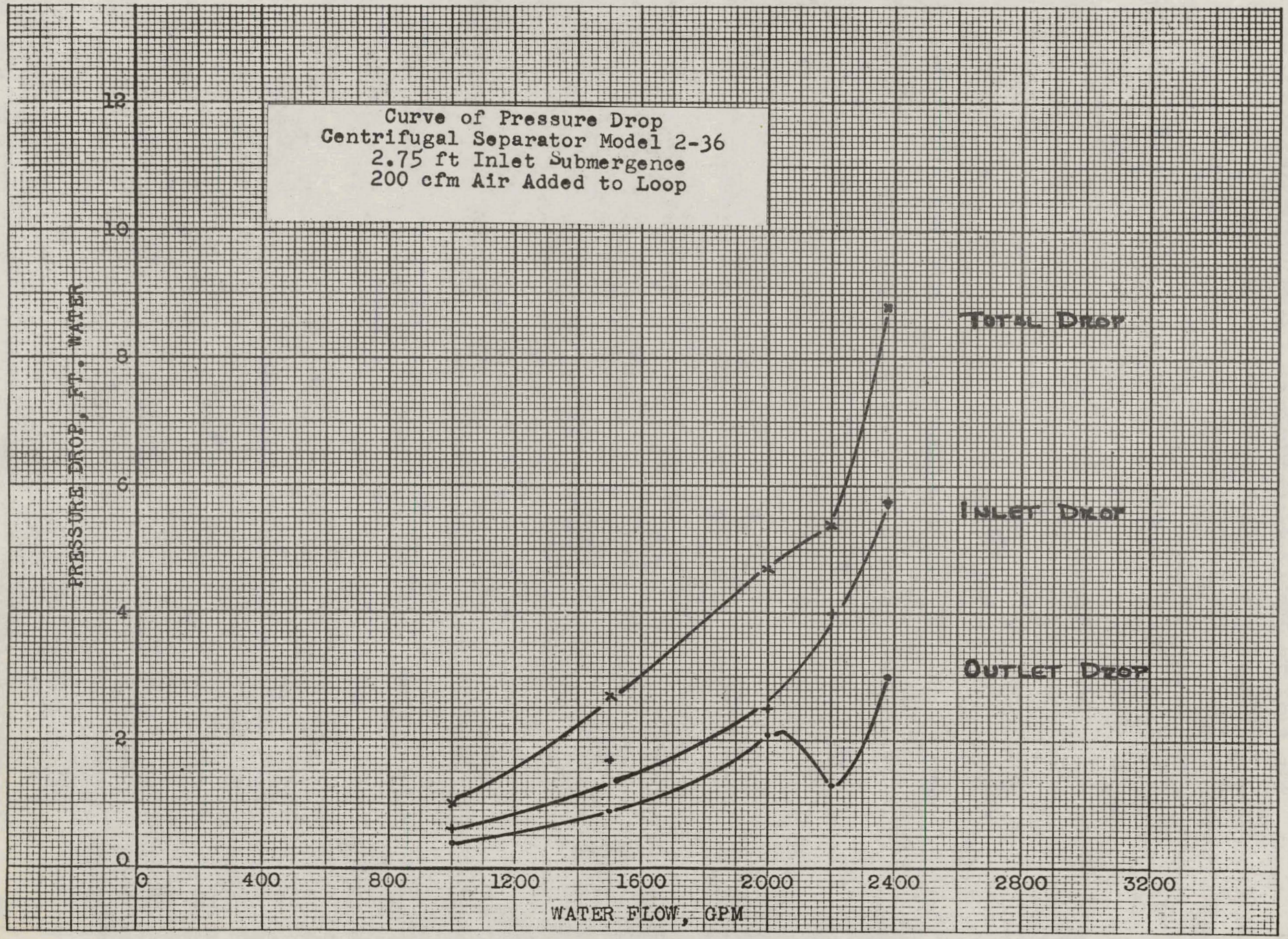

Figure 27 - Performance Curves for Separator Model 2-36

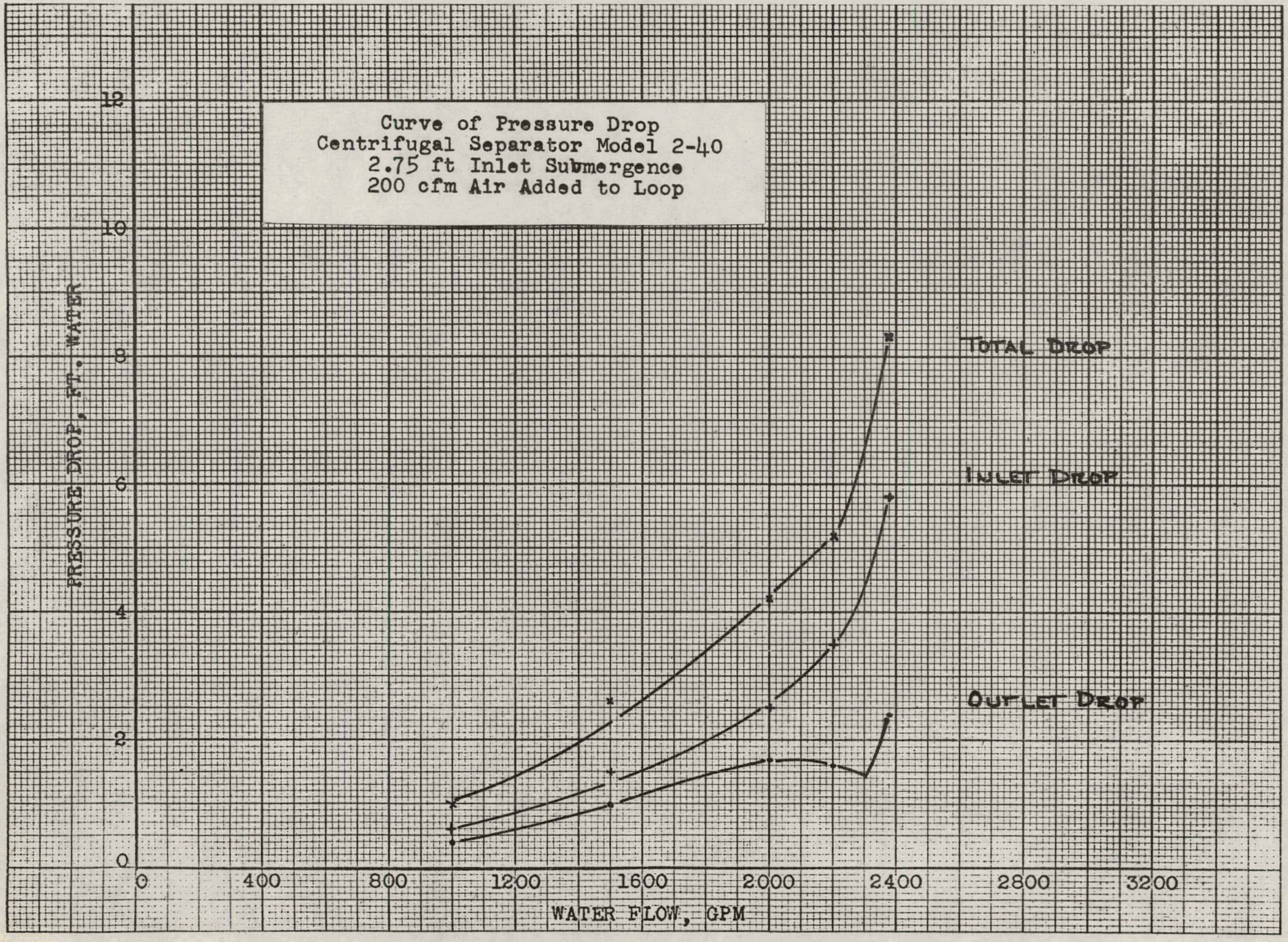

Figure 28 - Performance Curves for Separator Model 2-40

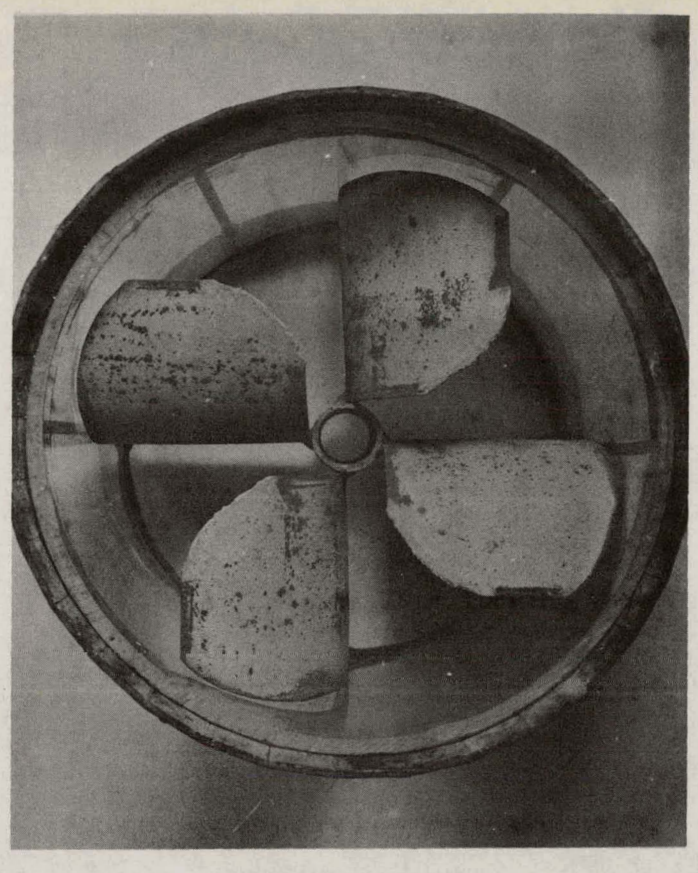

Outlet Nozzle Model 32
Top View

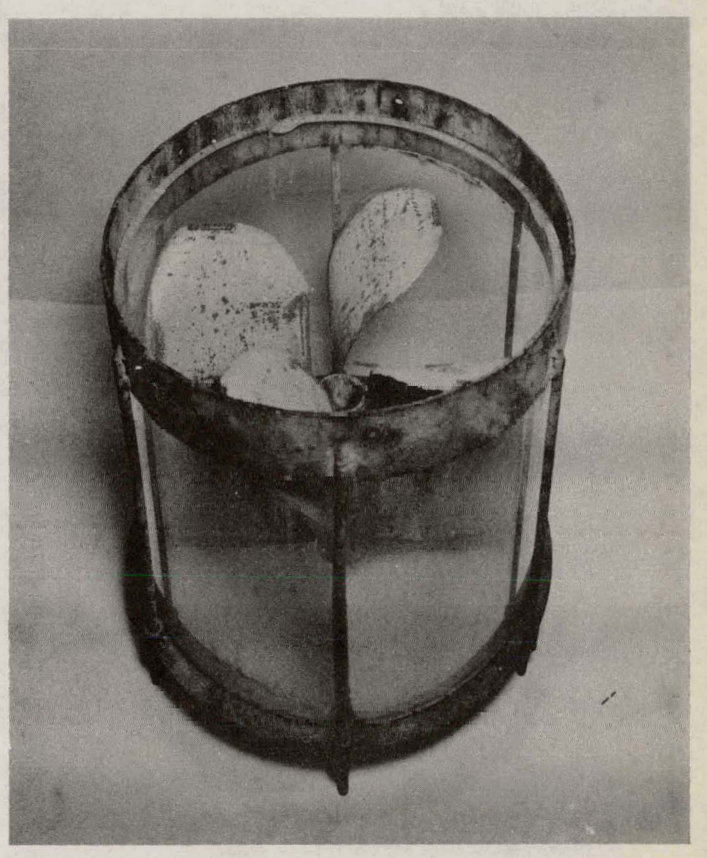

Outlet Nozzle Model 32
Side View

Figure 29 - Turning Vane Outlet Nozzle

```
      STOP
      CORE CLEAR                    PAGE  1

C     CENTRIFUGAL SEPARATOR-SEPARATING LENGTH  III-IIII  YANT GREENDALE
C     GPM = GALLONS PER MINUTE
C     DS = DIAMETER OF SEPARATOR (INCHES)
C     DV = DIAMETER OF VORTEX (INCHES)
C     N = NUMBER OF ITERATIONS = (RS-RV) X 4
C     E = EXPONENT IN EQUATION C= VIN*(R**E)
C     PW = DENSITY OF WATER (LB/CUBIC FT)
C     PV = DENSITY OF VAPOR (LB/CUBIC FT)
C     GAMMA = SURFACE TENSION (LB FORCE/FT)
C     TEMP = TEMPERATURE (DEGREES F)
C     VIN = INLET VELOCITY (FT/SEC)
C     RB=BUBBLE RADIUS (FT)
C     VAX = AXIAL VELOCITY (FT /SEC)
C     AREA = SEPARATOR X-SECTION     (FT SQUARED)
C     R = SEPARATOR RADIUS (FT)
C     VTAN = AVERAGE TANGENTIAL VELOCITY (FT/SEC)
C     RAV = AVERAGE BUBBLE PATH RADIUS (FT)
C     ENG = N SUB G - PEEBLES
C     VB4=BUBBLE VELOCITY - REGION 4  (FT/SEC)
C     VB3=BUBBLE VELOCITY - REGION 3  (FT/SEC)
C     VB4M=MINIMUM BUBBLE VELOCITY - REGION 4  (FT/SEC)
C     T = TRANSIT TIME (SECONDS)
C     SAX = AXIAL TRAVEL DISTANCE (FT)
C     STAN = TANGENTIAL TRAVEL DISTANCE (FT)
    1 READ2,GPM,DS,DV,N,E,PW,PV,GAMMA,TEMP,VIN,RB
      PRINT3,GPM,DS,DV
      PRINT4,N,E,PW
      PRINT5,PV,GAMMA,TEMP
      PRINT6,VIN,RB
      ASEP=(3.1416*((DS**2)-(DV**2)))/((4.*144.))
      VAX=(GPM)/(449.*ASEP)
      R=(DS/24.)
      C=VIN*((R)**E)
      VTAV=0
      A=1.
      S=N
      DO10J=1,N
      V=C/(R-(.0208*A))**E
      VTAV=VTAV+(V/S)
   10 A=A+1.
      PRINT9,ASEP,VAX,VTAV
      RAV=(DS+DV)/48.
      ENG=8.*((VTAV**2)*(PW-PV))/((3.*(RAV)*PW))
      VB4=.825*(((ENG**4)/32.2)**.083)*(((GAMMA*32.2)/PW)**.25)
      PRINT19,VB4
      VB3=1.146*(((ENG/32.2)**.167))*(((GAMMA*32.2)/(RB*PW))**.50)
      PRINT18,VB3
      VB4M=.663*(((GAMMA*32.2)/(PW))**.75)*(1./RB)
      PRINT17,VB4M
      IF(VB4-VB4M)11,12,12
   11 PRINT13,RAV,ENG,VB3
      VB=VB3
      GOTO15
   12 PRINT14,RAV,ENG,VB4
```

Figure 30-A - Listing of Computer Program for Separating Length

```
      VB=VB4
   15 T=((DS-DV)/24.)/(VB)
      SAX=(VAX*T)
      STAN=VTAV*T
      PRINT16,T,SAX,STAN
    2 FORMAT(F6.0,F6.2,F6.2,I3,F6.2,F6.1,F6.1,F6.4,F6.0,F6.2,F7.5)
    3 FORMAT(5X,6HGPM = ,F6.0,9X,6HDS  = ,F6.2,9X,6HDV  = ,F6.2)
    4 FORMAT(5X,9HN    =   ,I3,9X,6HE   = ,F6.2,9X,6HPW   = ,F6.1)
    5 FORMAT(5X,6HPS  = ,F6.1,9X,6HGAMMA=,F6.4,9X,6HTEMP =,F6.0)
    6 FORMAT(5X,6HVIN = ,F6.2,9X,5HRB  =,F7.5)
    9 FORMAT(5X,6HASEP= ,F6.3,9X,6HVAX = ,F6.2,9X,6HVTAV= ,F6.2)
   13 FORMAT(5X,6HRAV = ,F6.2,9X,6HENG = ,F6.0,9X,6HVB3 = ,F6.2)
   14 FORMAT(5X,6HRAV = ,F6.2,9X,6HENG = ,F6.0,9X,6HVB4 = ,F6.2)
   16 FORMAT(5X,6HTIME= ,F6.2,9X,6HSAX = ,F6.2,9X,6HSTAN= ,F6.2//)
   17 FORMAT(10X,6HVB4M =,F6.2)
   18 FORMAT(10X,6HVB3  =,F6.2)
   19 FORMAT(10X,6HVB4  =,F6.2)
      IF(SENSE SWITCH 9)20,1
   20 STOP
      END
```

END OF LISTING

Figure 30-B - Listing of Computer Program for Separating Length (Continued)

```
GPM =  2000.          DS  =  10.00          DV  =  3.00
N   =    14           E   =    .30          PW  =  60.6
PS  =    .1           GAMMA=  .0043         TEMP=  175.
VIN =  9.75           RB  =  .00278
ASEP=  .496           VAX =   8.97          VTAV=  11.48
     VB4  =  1.46
     VB3  =  1.92
     VB4M =  2.49
RAV =    .27          ENG =  1295.          VB3 =  1.92
TIME=    .15          SAX =   1.35          STAN=  1.73


GPM =  2000.          DS  =  10.00          DV  =  3.00
N   =    14           E   =    .30          PW  =  60.6
PS  =    .1           GAMMA=  .0043         TEMP=  175.
VIN =  9.75           RB  =  .00347
ASEP=  .496           VAX =   8.97          VTAV=  11.48
     VB4  =  1.46
     VB3  =  1.72
     VB4M =  1.99
RAV =    .27          ENG =  1295.          VB3 =  1.72
TIME=    .16          SAX =   1.51          STAN=  1.94


GPM =  2000.          DS  =  10.00          DV  =  3.00
N   =    14           E   =    .30          PW  =  60.6
PS  =    .1           GAMMA=  .0043         TEMP=  175.
VIN =  9.75           RB  =  .00417
ASEP=  .496           VAX =   8.97          VTAV=  11.48
     VB4  =  1.46
     VB3  =  1.57
     VB4M =  1.66
RAV =    .27          ENG =  1295.          VB3 =  1.57
TIME=    .18          SAX =   1.66          STAN=  2.12


GPM =  2000.          DS  =  10.00          DV  =  3.00
N   =    14           E   =    .30          PW  =  60.6
PS  =    .1           GAMMA=  .0043         TEMP=  175.
VIN =  9.75           RB  =  .00487
ASEP=  .496           VAX =   8.97          VTAV=  11.48
     VB4  =  1.46
     VB3  =  1.45
     VB4M =  1.42
RAV =    .27          ENG =  1295.          VB4 =  1.46
TIME=    .19          SAX =   1.79          STAN=  2.29


GPM =  2000.          DS  =  10.00          DV  =  3.00
N   =    14           E   =    .30          PW  =  60.6
PS  =    .1           GAMMA=  .0043         TEMP=  175.
VIN =  9.75           RB  =  .00556
ASEP=  .496           VAX =   8.97          VTAV=  11.48
     VB4  =  1.46
     VB3  =  1.36
     VB4M =  1.24
RAV =    .27          ENG =  1295.          VB4 =  1.46
TIME=    .19          SAX =   1.79          STAN=  2.29
```

Figure 31-A - Computer Print-Out; Separating Length; VIN=9.75 Varying RB

```
GPM =  2000.          DS  =  10.00          DV  =  3.00
N   =    14           E   =   .30          PW  =  60.6
PS  =    .1           GAMMA=  .0043         TEMP=  175.
VIN =   8.00          RB  =  .00278
ASEP=    .496         VAX =   8.97          VTAV=  9.42
     VB4  =  1.28
     VB3  =  1.80
     VB4M =  2.49
RAV =    .27          ENG =   872.          VB3 =  1.80
TIME=    .16          SAX =   1.45          STAN=  1.52


GPM =  2000.          DS  =  10.00          DV  =  3.00
N   =    14           E   =   .30          PW  =  60.6
PS  =    .1           GAMMA=  .0043         TEMP=  175.
VIN =   8.00          RB  =  .00347
ASEP=    .496         VAX =   8.97          VTAV=  9.42
     VB4  =  1.28
     VB3  =  1.61
     VB4M =  1.99
RAV =    .27          ENG =   872.          VB3 =  1.61
TIME=    .18          SAX =   1.62          STAN=  1.70


GPM =  2000.          DS  =  10.00          DV  =  3.00
N   =    14           E   =   .30          PW  =  60.6
PS  =    .1           GAMMA=  .0043         TEMP=  175.
VIN =   8.00          RB  =  .00417
ASEP=    .496         VAX =   8.97          VTAV=  9.42
     VB4  =  1.28
     VB3  =  1.47
     VB4M =  1.66
RAV =    .27          ENG =   872.          VB3 =  1.47
TIME=    .19          SAX =   1.77          STAN=  1.86


GPM =  2000.          DS  =  10.00          DV  =  3.00
N   =    14           E   =   .30          PW  =  60.6
PS  =    .1           GAMMA=  .0043         TEMP=  175.
VIN =   8.00          RB  =  .00487
ASEP=    .496         VAX =   8.97          VTAV=  9.42
     VB4  =  1.28
     VB3  =  1.36
     VB4M =  1.42
RAV =    .27          ENG =   872.          VB3 =  1.36
TIME=    .21          SAX =   1.92          STAN=  2.01


GPM =  2000.          DS  =  10.00          DV  =  3.00
N   =    14           E   =   .30          PW  =  60.6
PS  =    .1           GAMMA=  .0043         TEMP=  175.
VIN =   8.00          RB  =  .00556
ASEP=    .496         VAX =   8.97          VTAV=  9.42
     VB4  =  1.28
     VB3  =  1.27
     VB4M =  1.24
RAV =    .27          ENG =   872.          VB4 =  1.28
TIME=    .22          SAX =   2.04          STAN=  2.14
```

Figure 31-B - Computer Print-Out; Separating Length: VIN = 8.00, Varying RB

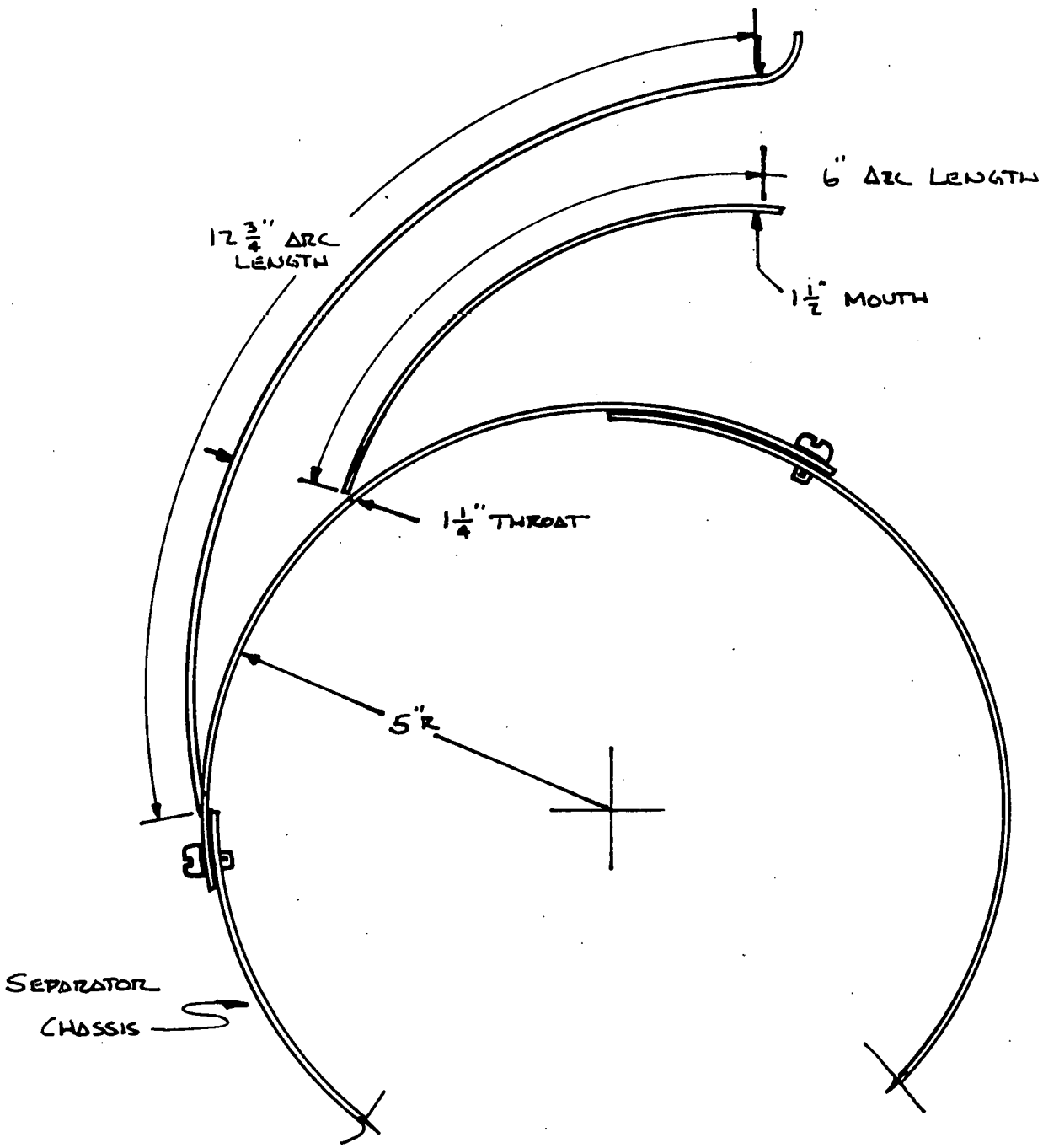

Figure 32 - Inlet Nozzle Model 2

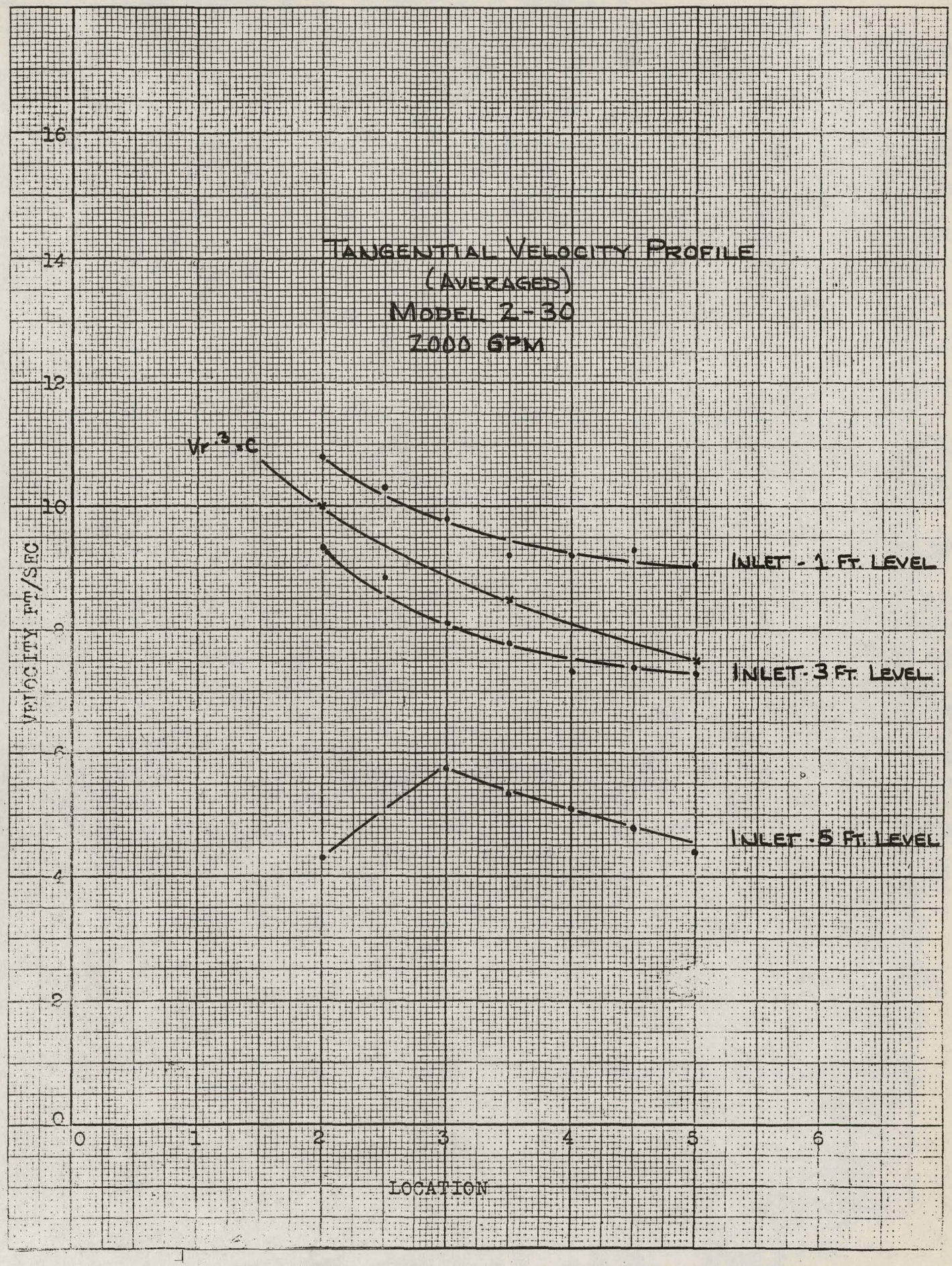

Figure 33 - Velocity Profile of Model 2 Inlet Nozzle

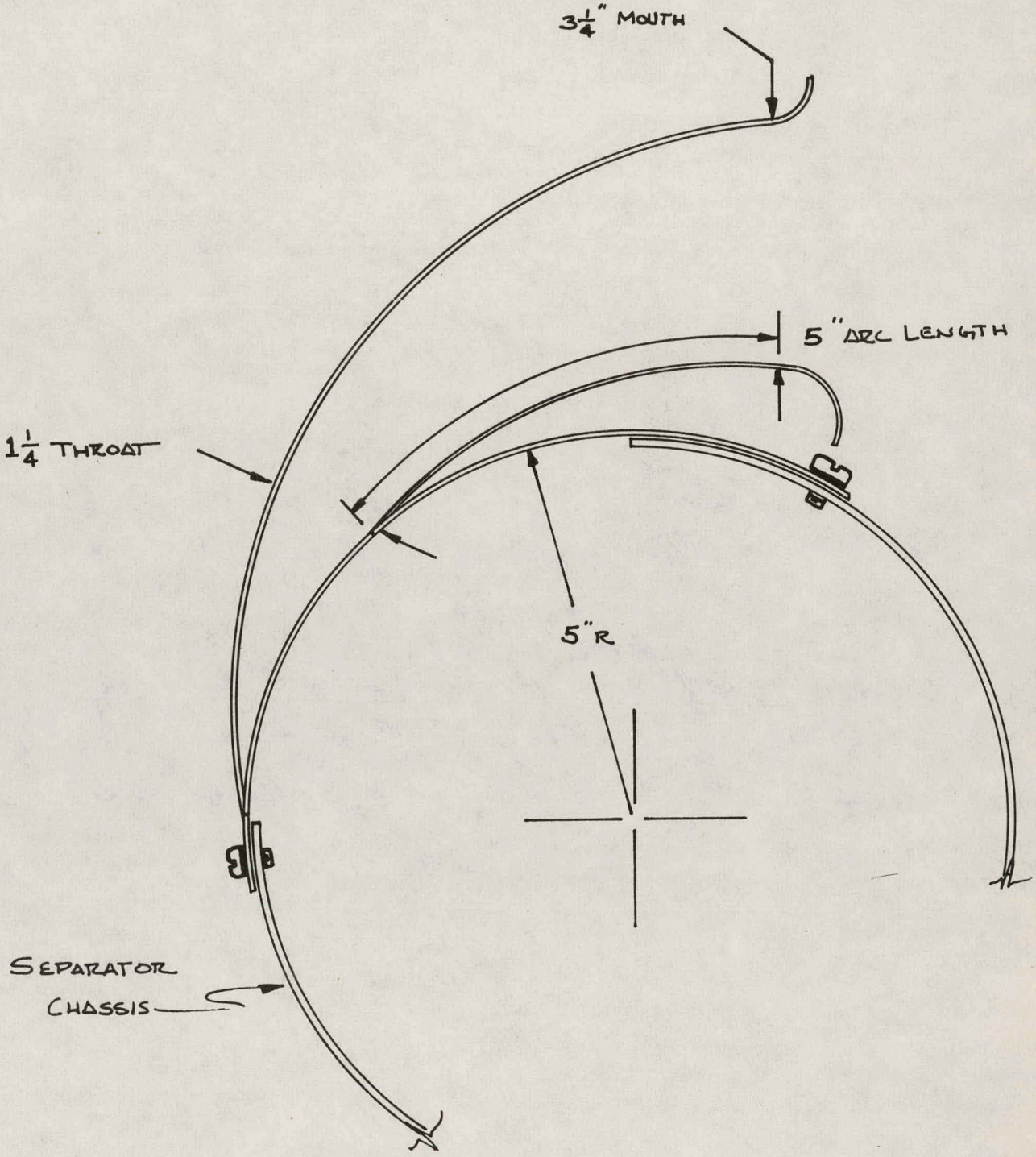

Figure 34 - Inlet Nozzle Model 3

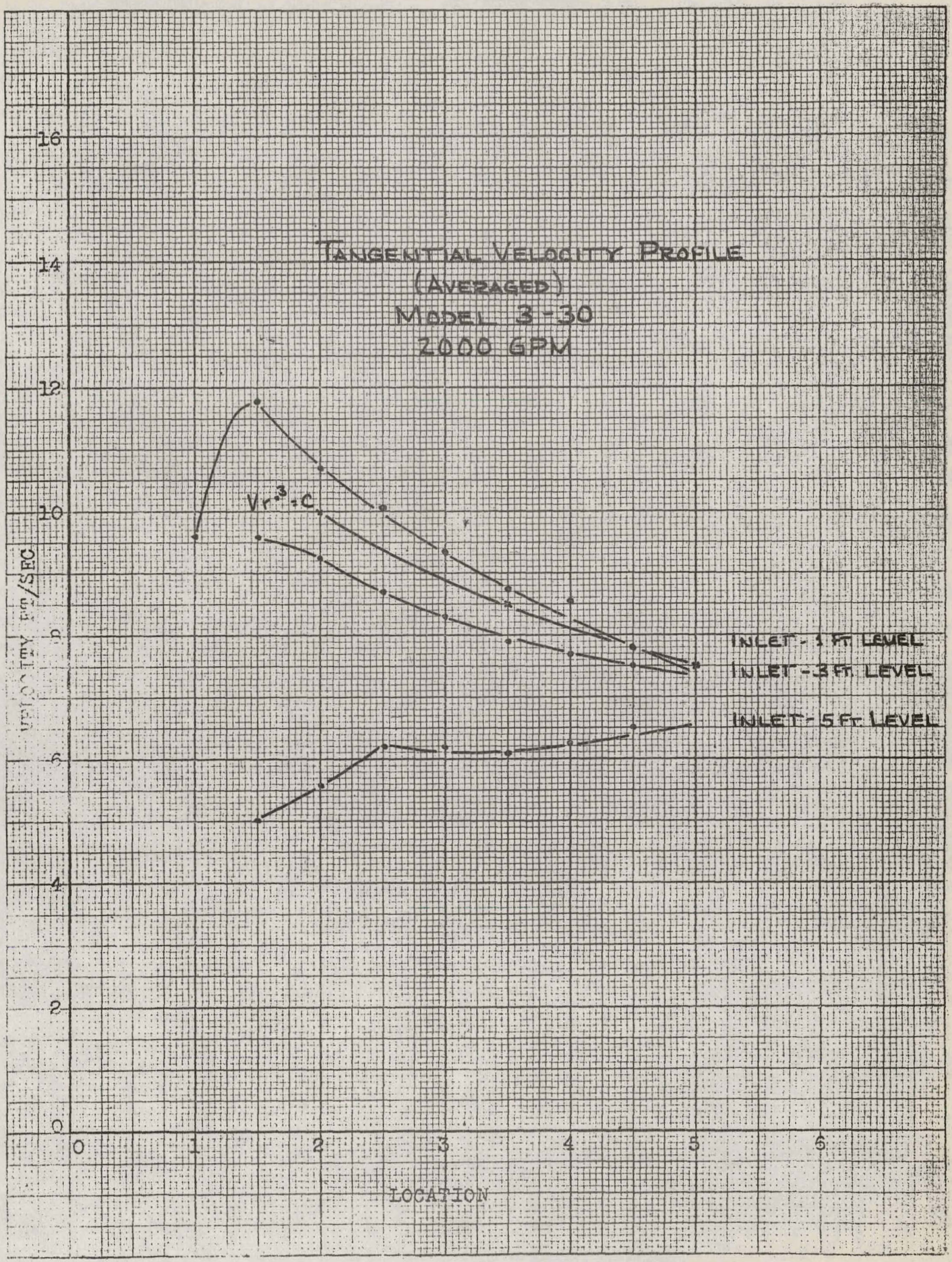

Figure 35 - Velocity Profile of Model 3 Inlet Nozzle

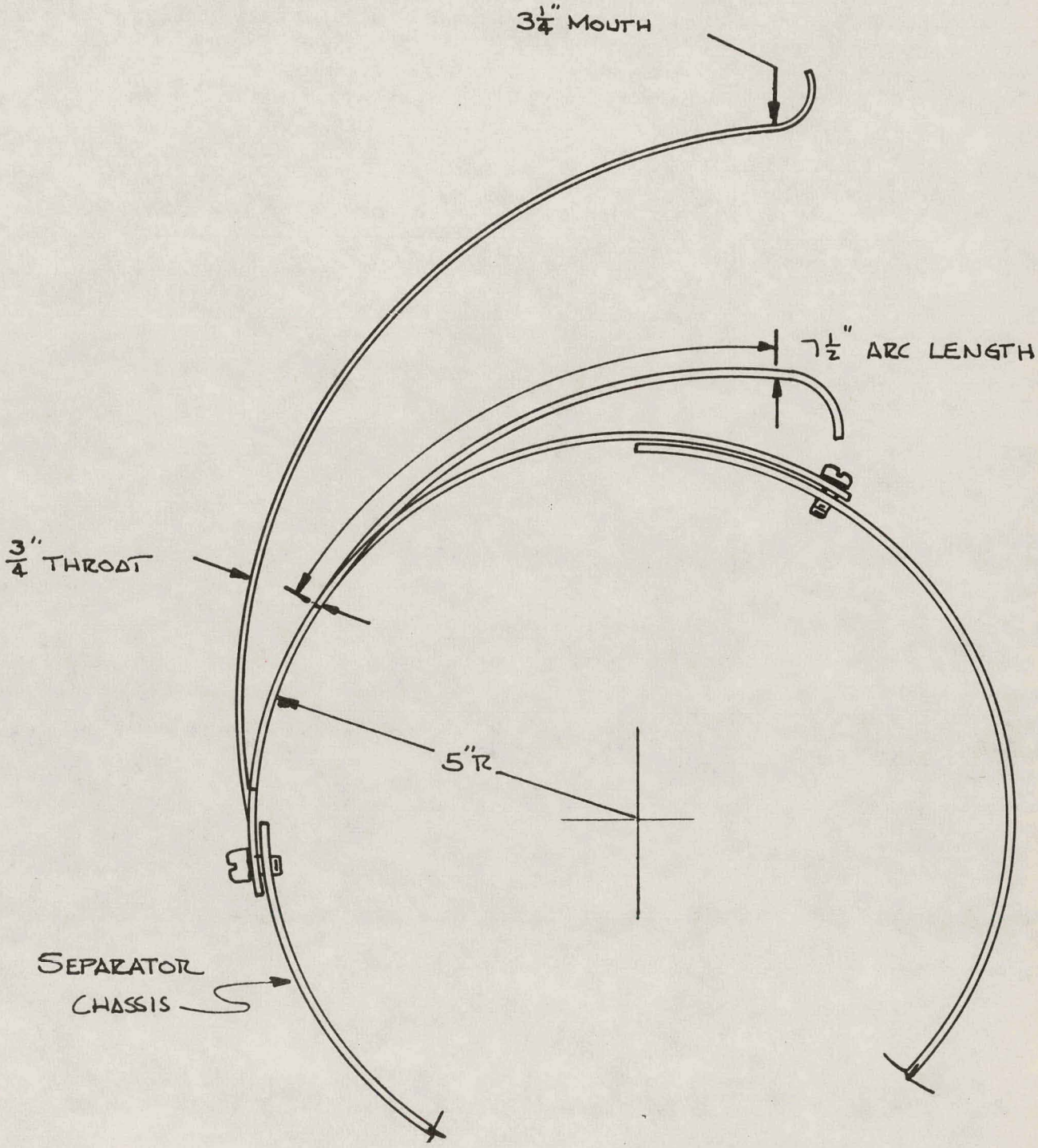

Figure 36 - Inlet Nozzle Model 4

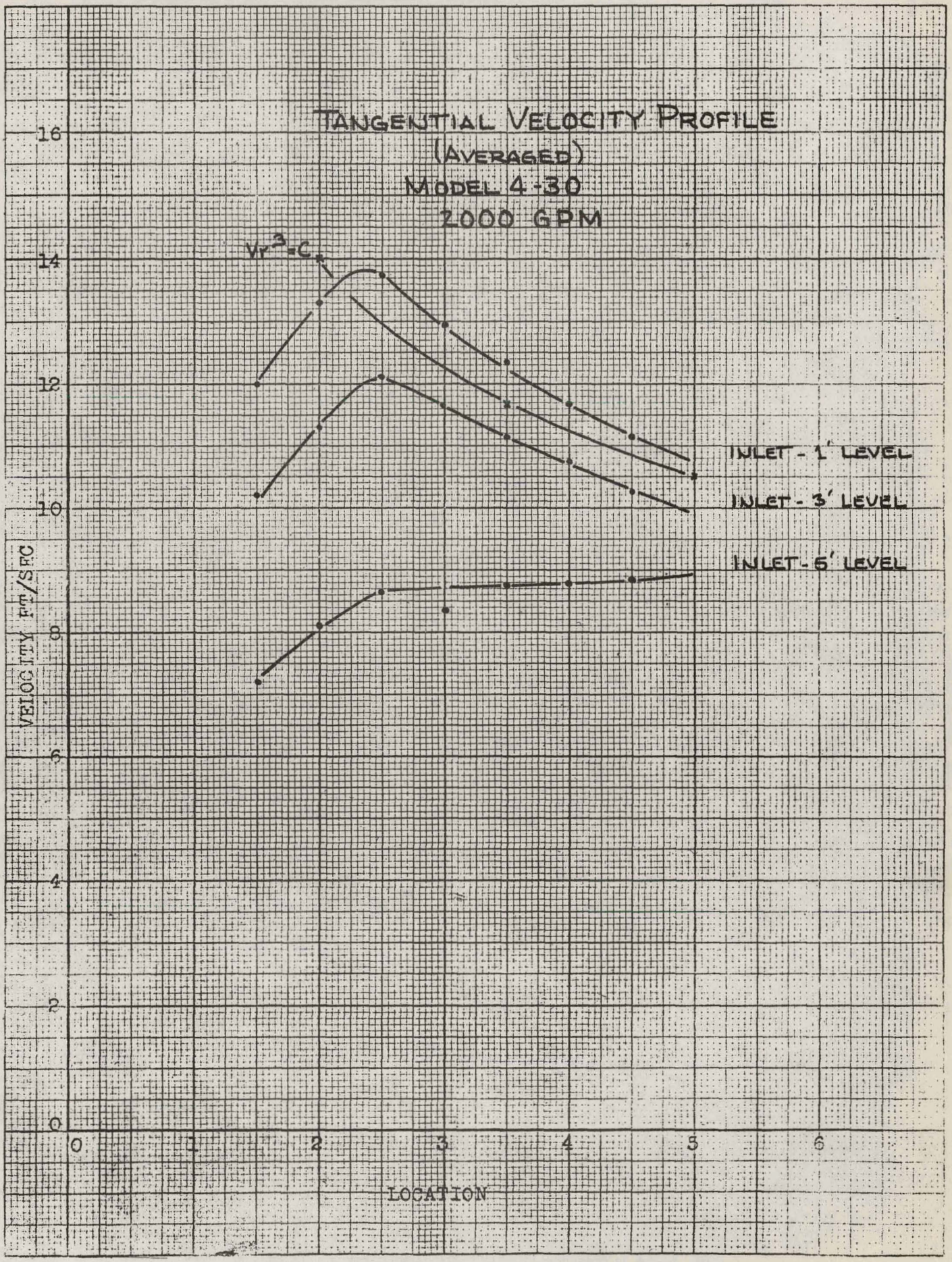

Figure 37 - Velocity Profile of Model 4 Inlet Nozzle

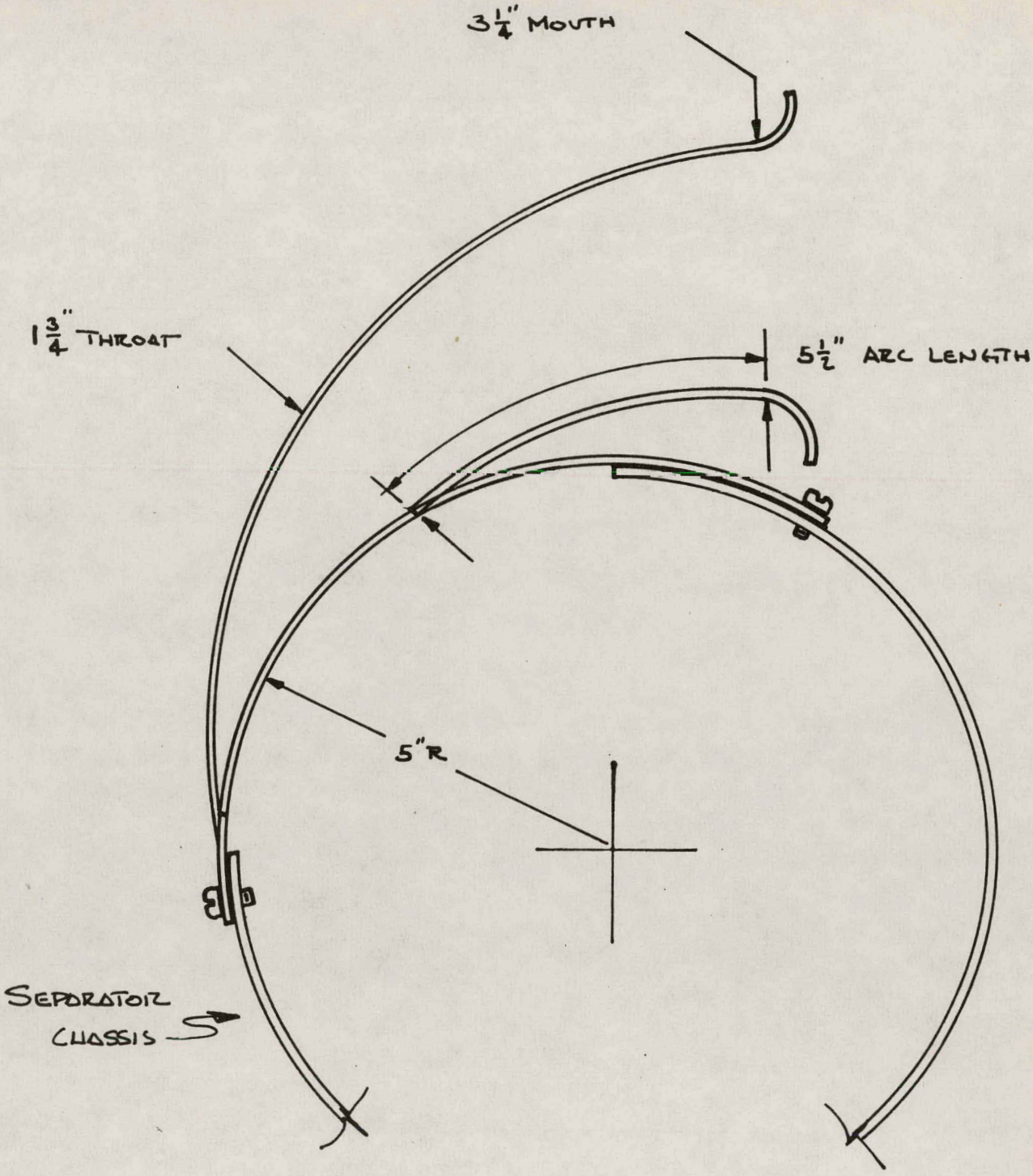

Figure 38 - Inlet Nozzle Model 5

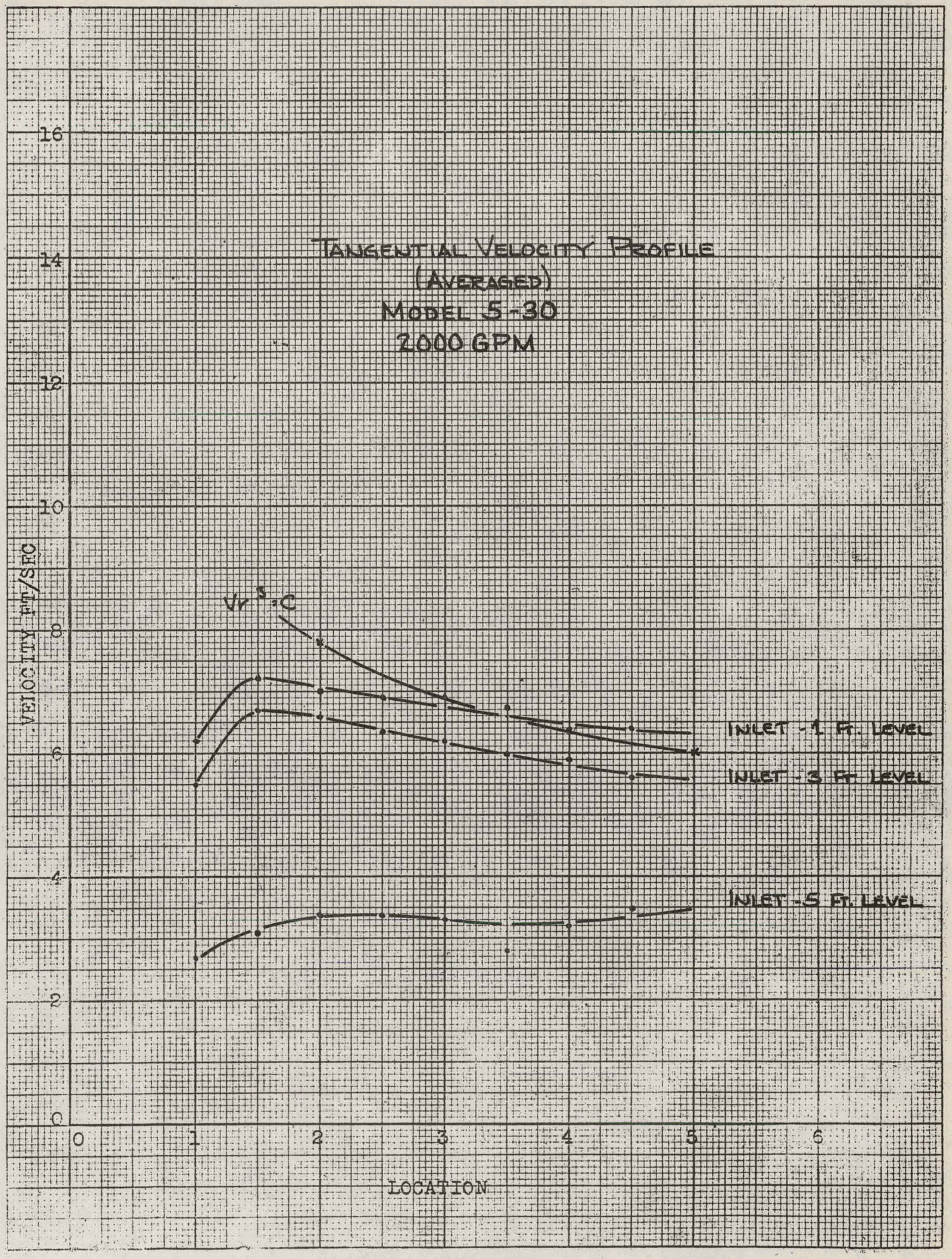

Figure 39 - Velocity Profile of Model 5 Inlet Nozzle

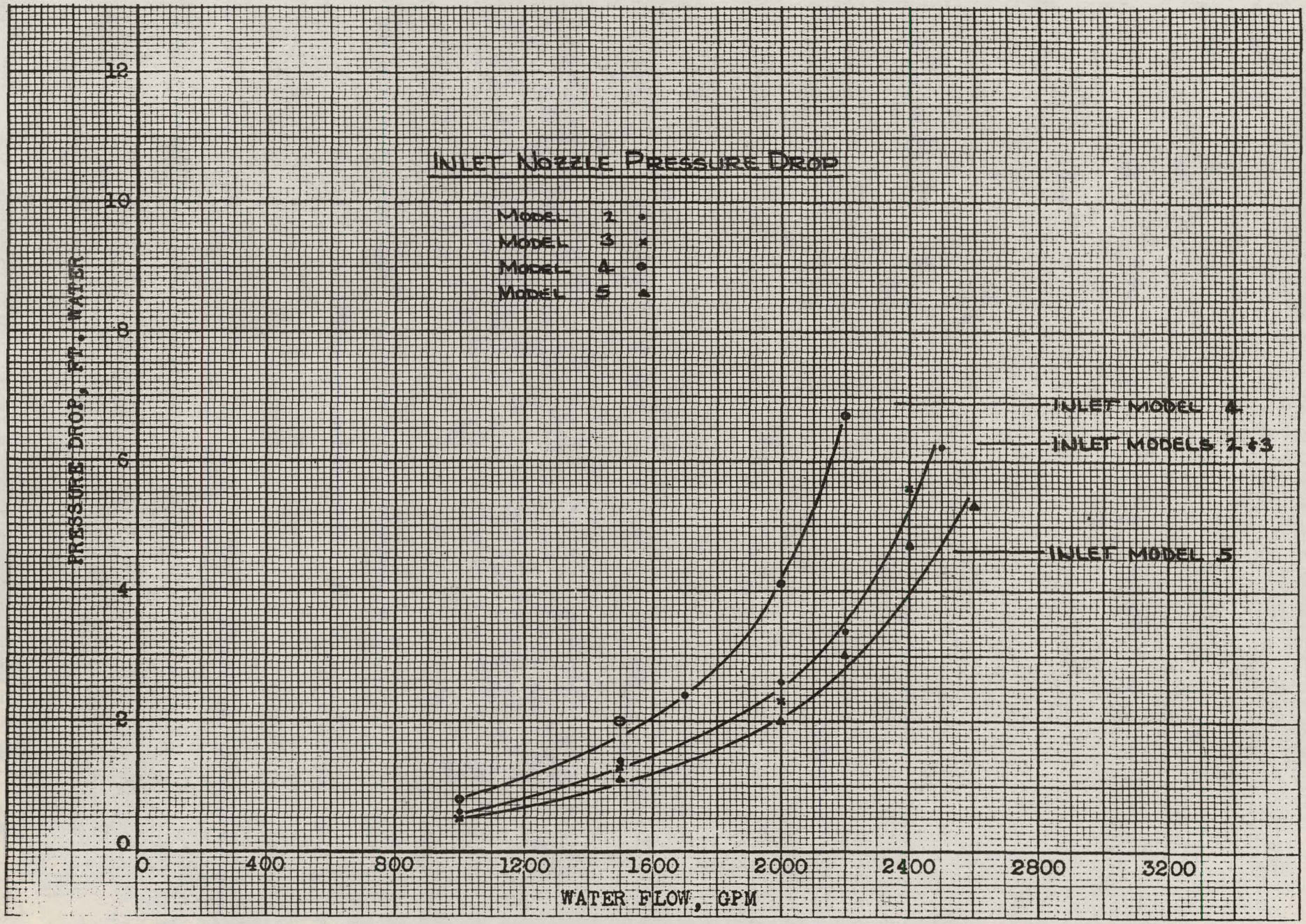

Figure 40 - Relative Performance of Inlet Nozzle

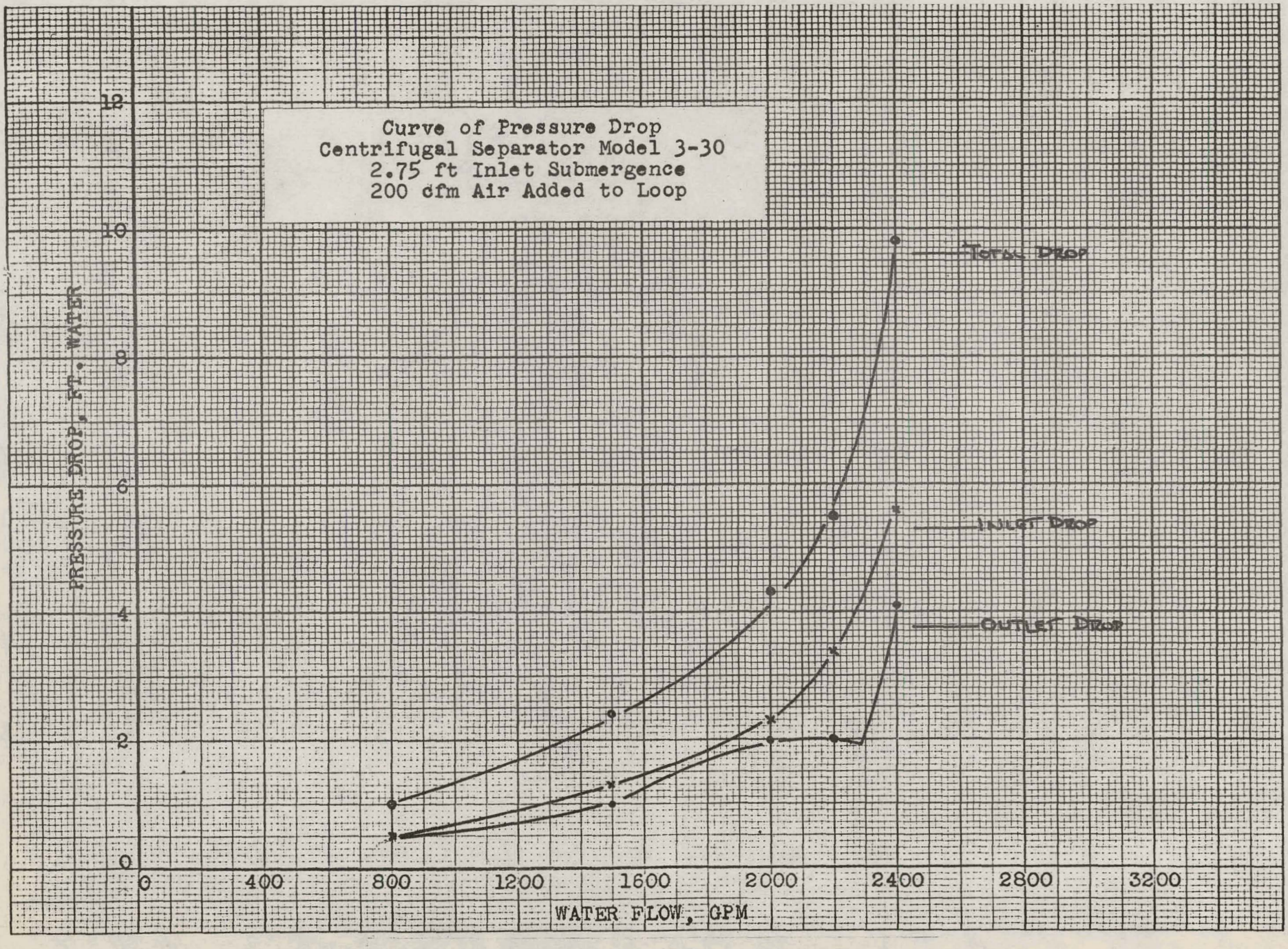

Figure 41 - Performance of Separator Model 3-30

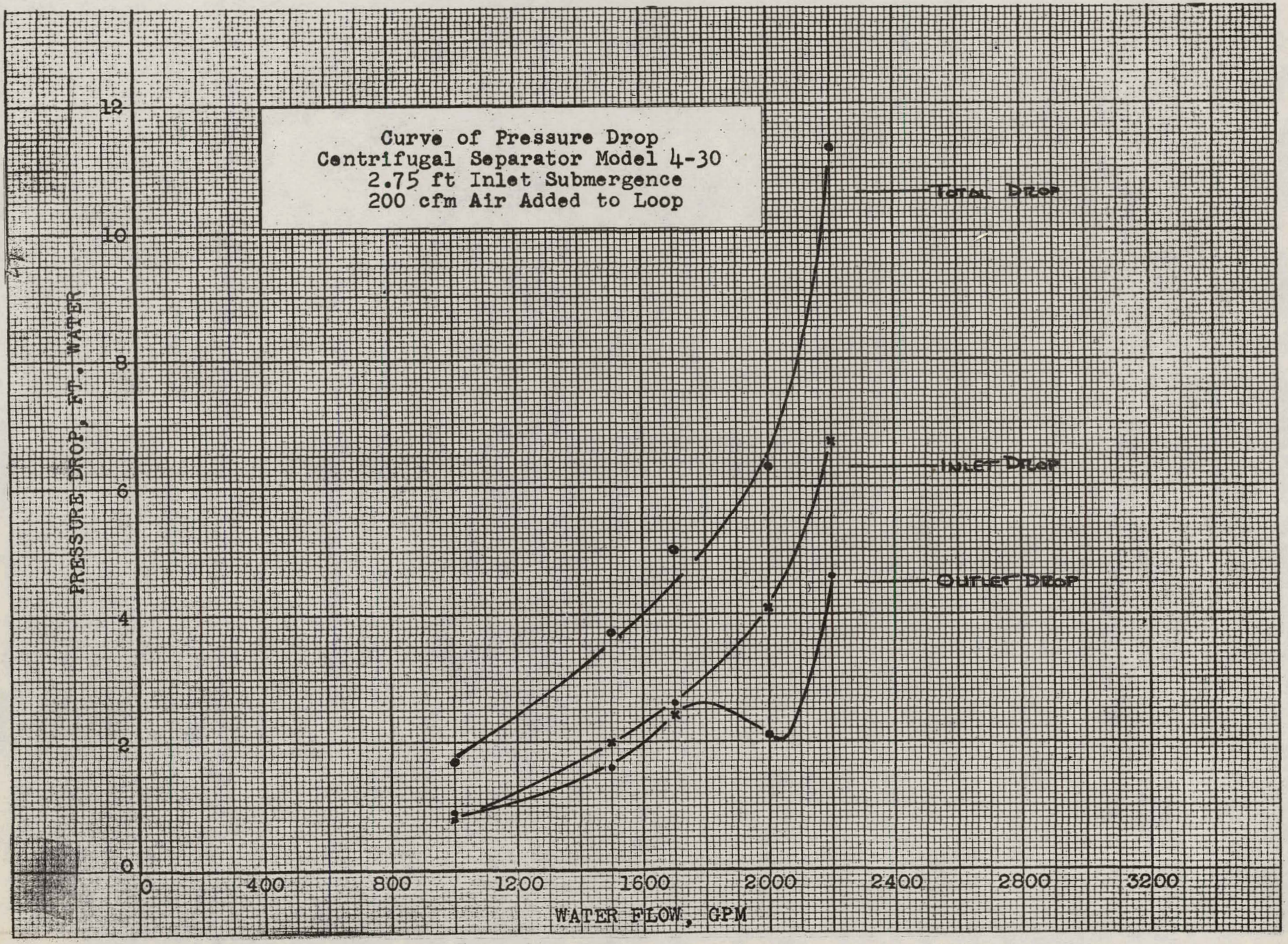

Figure 42 - Performance of Separator Model 4-30

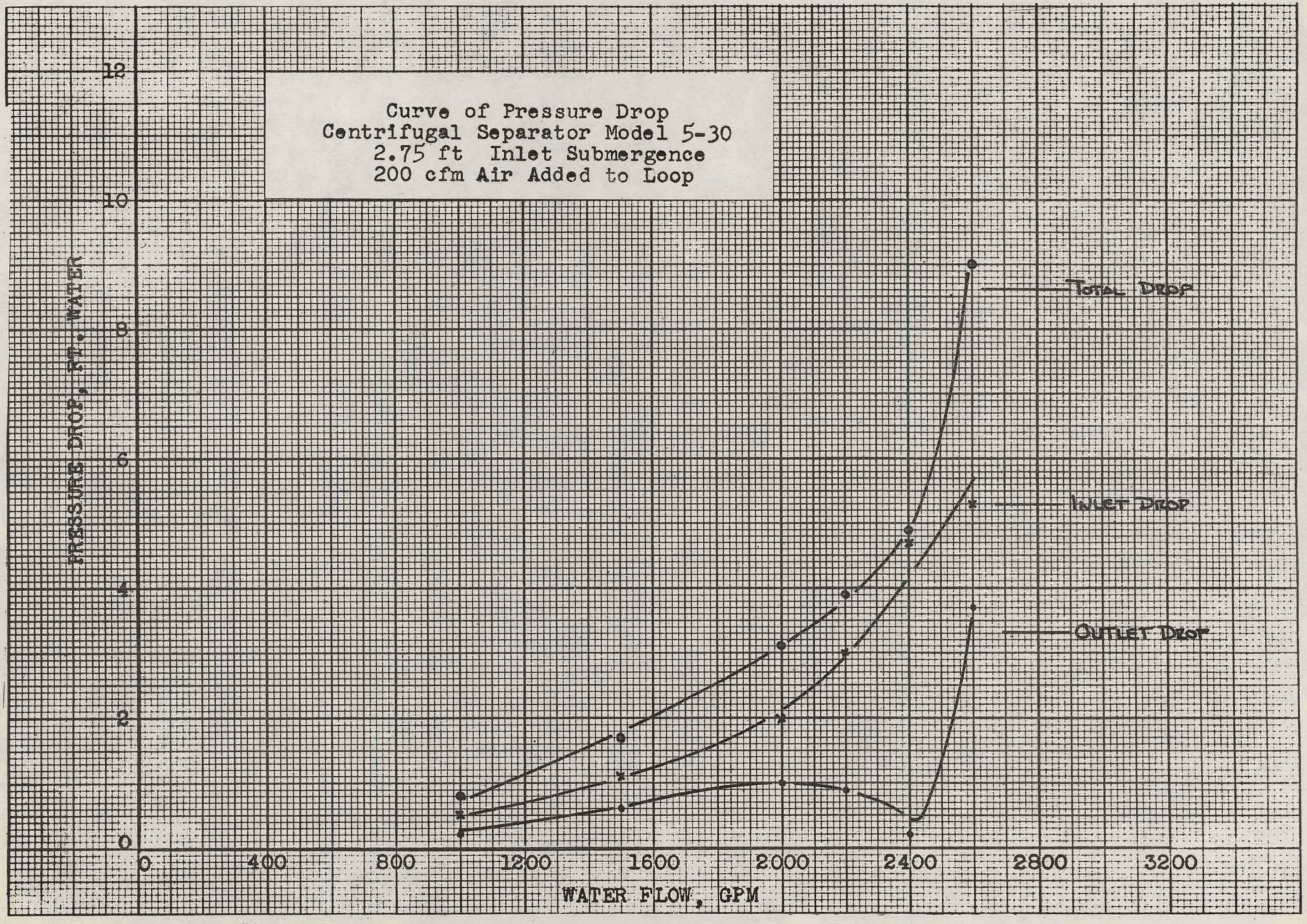

Figure 43 - Performance of Separator Model 5-30

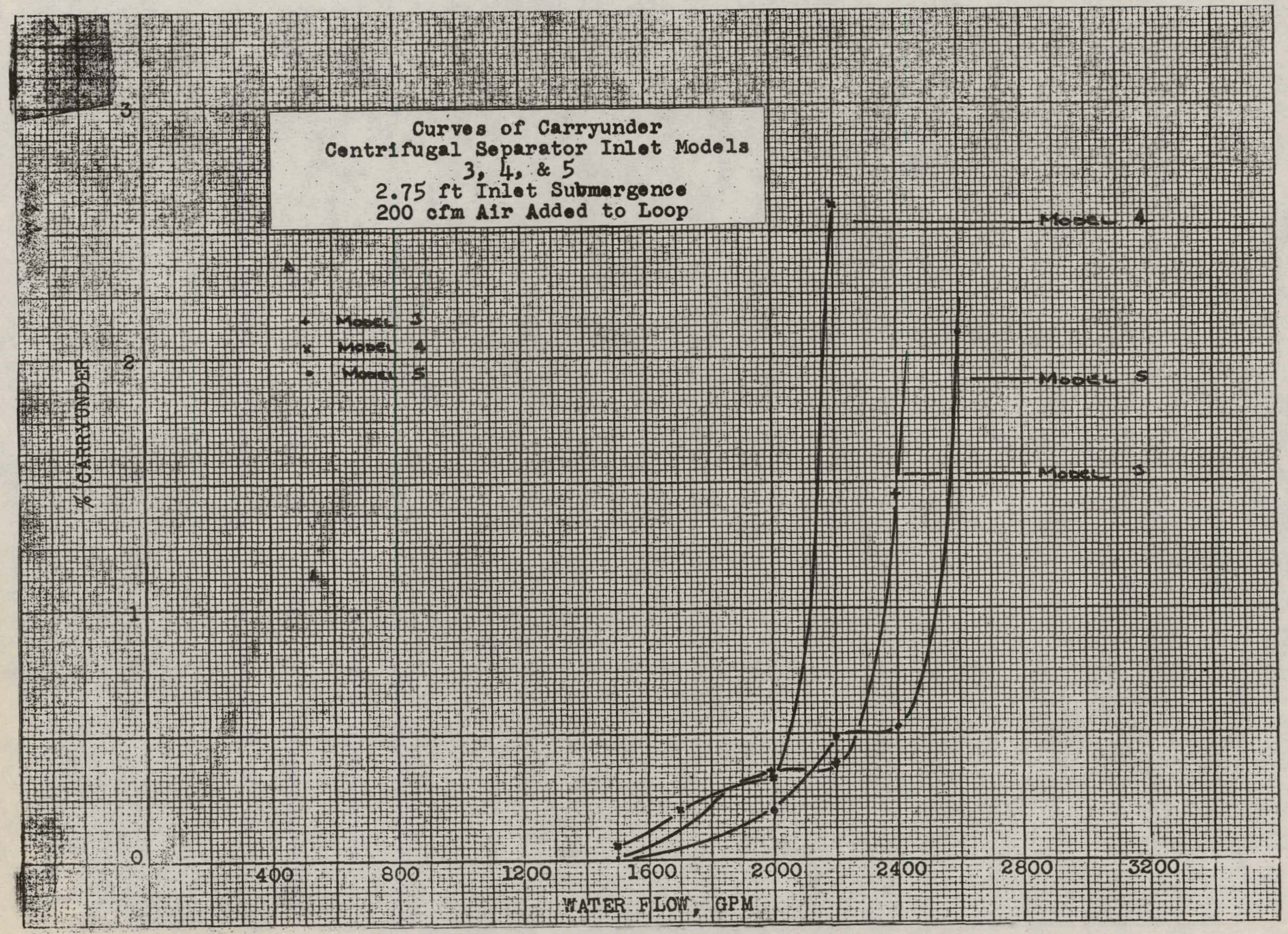

Figure 44 - Carryunder for Separator Inlets 3, 4 and 5

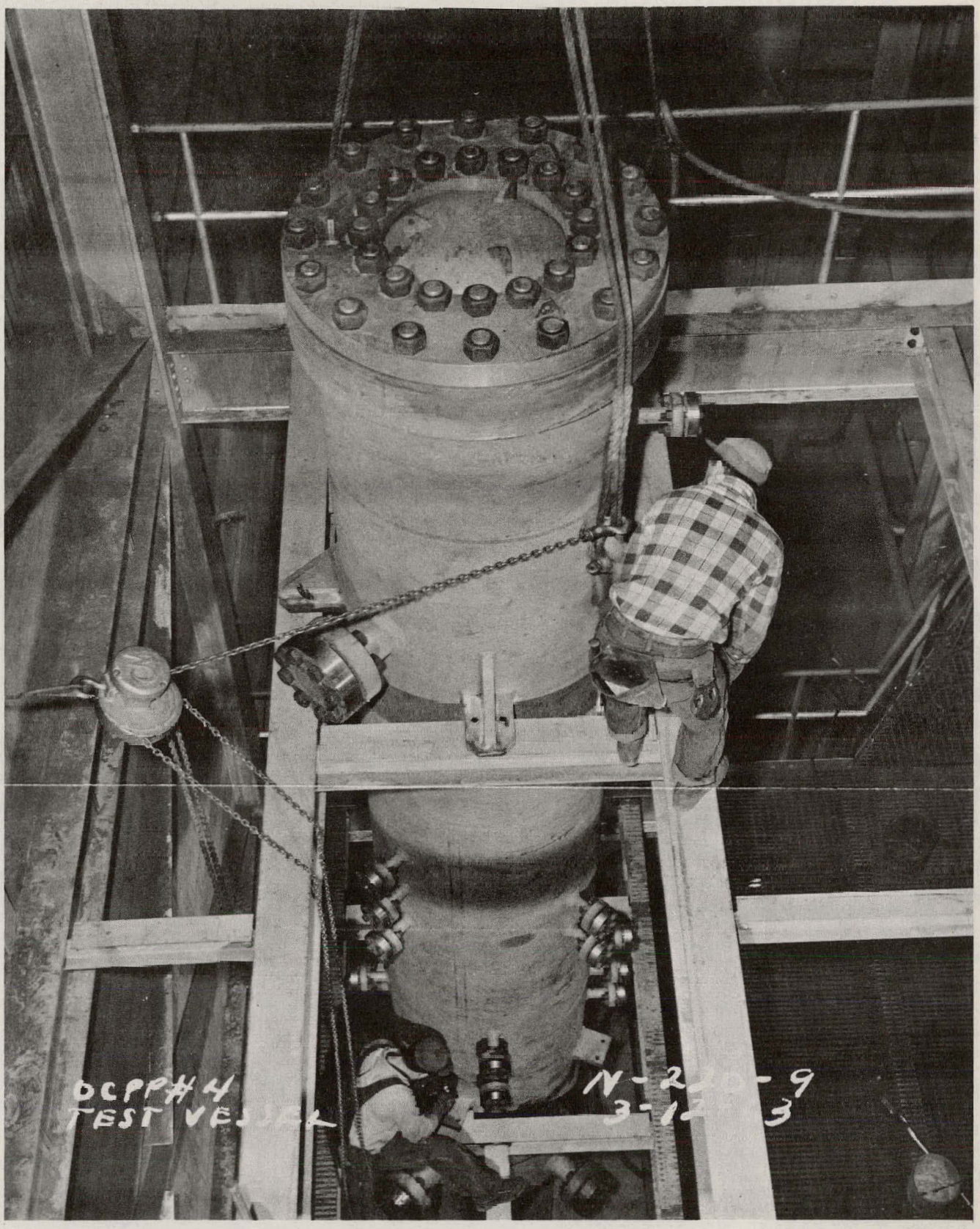

Figure 45 - Pressure Vessel Installation

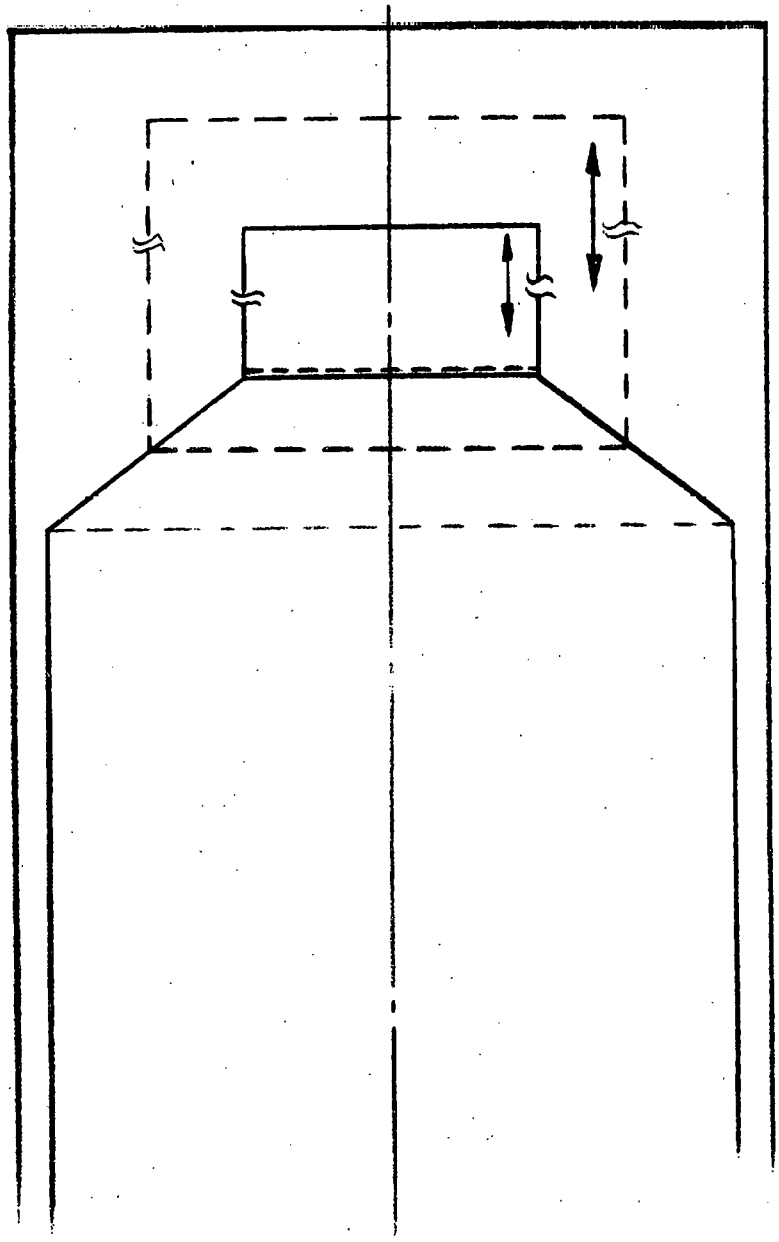

Present Design

Future Geometries to be studied

Figure 46 - Future Geometry Changes for Reduced Flow Area Riser Studies

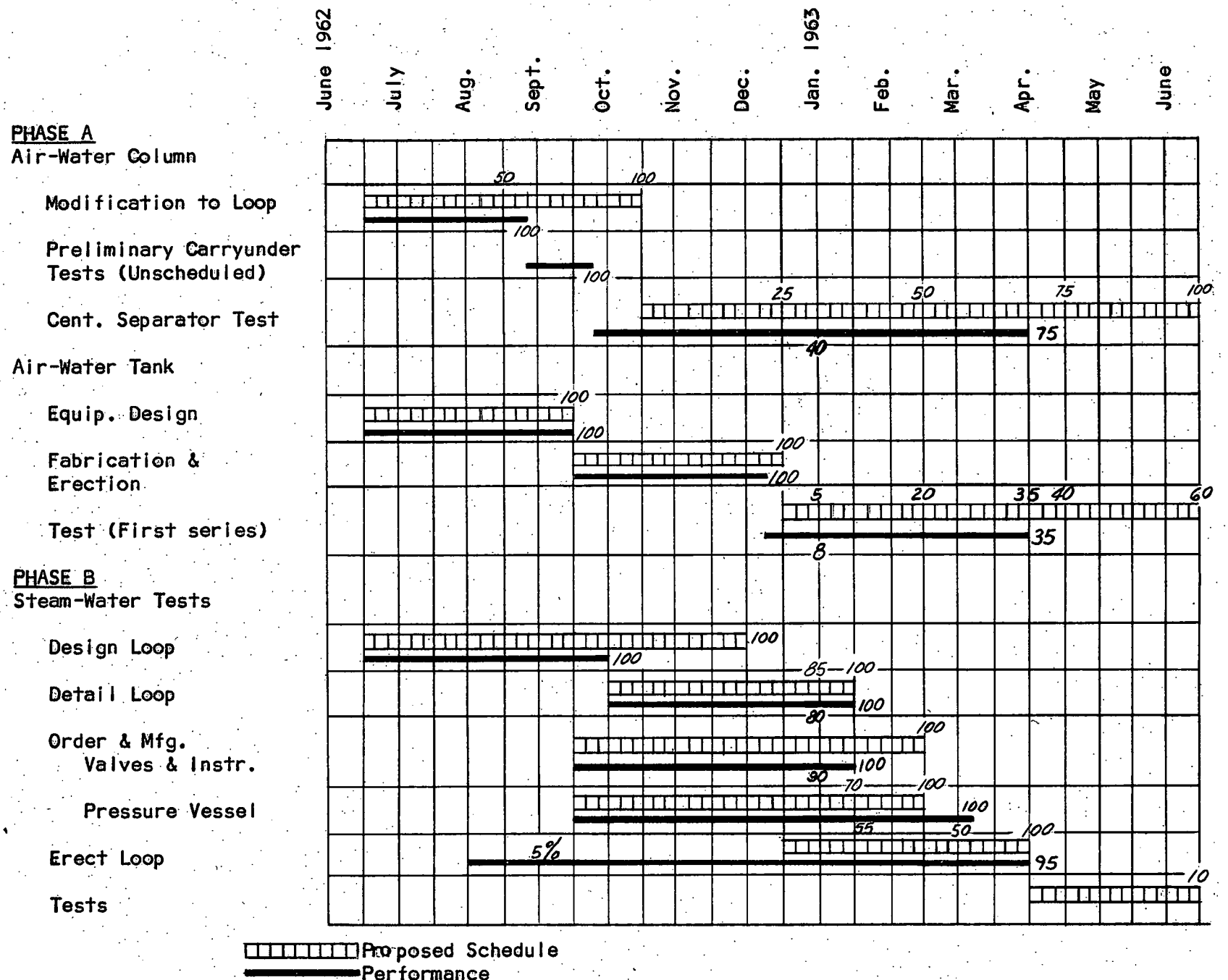

Figure 47 - Schedule of Progress Chart